

**Investigation of the Role of Polyploidization in Glial Cells During the
Development of the Drosophila Nervous System**

by

Laura E. Frawley

B.A. Biological Sciences
Connecticut College, 2010

SUBMITTED TO THE DEPARTMENT OF BIOLOGY IN PARTIAL
FULFILLMENT OF THE REQUIREMENTS FOR THE DEGREE OF

DOCTOR OF PHILOSOPHY IN BIOLOGY
AT THE
MASSACHUSETTS INSTITUTE OF TECHNOLOGY

JUNE 2018

© 2018 Laura E. Frawley. All rights reserved.

The author hereby grants to MIT permission to reproduce
and to distribute publicly paper and electronic
copies of this thesis document in whole or in part
in any medium now known or hereafter created.

Signature of Author:
Department of Biology
May 24, 2018

Signature redacted

Certified by:
Terry L. Orr-Weaver
Professor of Biology
Thesis Supervisor

Signature redacted

Accepted by:
Amy E. Keating
Professor of Biology
Co-Chair, Biology Graduate Committee

Signature redacted



Investigation of the Role of Polyploidization in Glial Cells During the Development of the *Drosophila* Nervous System

by

Laura E. Frawley

Submitted to the Department of Biology on May 24, 2018
in Partial Fulfillment of the Requirements for the Degree of
Doctor of Philosophy in Biology

ABSTRACT

Organogenesis is a complex process encompassing cell determination, cell differentiation, cell proliferation, and cell size regulation. The proper orchestration of these events ensures that each organ is scaled correctly and can function properly. Polyploidization is a process by which cells increase their DNA content and is used across species to generate large cells. Our lab had previously determined that subperineurial glia (SPG) of the *Drosophila melanogaster* nervous system become polyploid by both the endocycle and endomitosis. These are two cell cycle variants employed to produce polyploid cells that differ in the latter undergoing some aspects of mitosis but not cytokinesis. Polyploidization of the SPG is critical for blood-brain barrier (BBB) function. Here, we determined that the developmental switch from endocycling to endomitotic SPG occurs in about 70% of SPG in the brain lobes by the second larval instar. The SPG in the ventral nerve cord and peripheral nervous system solely endocycle. We demonstrated that both the Notch signaling pathway and the String Cdc25 phosphatase are critical in determining whether SPG endocycle or endomitose. Experiments manipulating the percentage of cells that are endocycling versus endomitotic highlight key differences between endocycling and endomitotic SPG. We find that endomitotic SPG cells are capable of achieving higher ploidy and cell area values than endocycling cells and are essential to the integrity of the BBB. Strikingly, we find that endocycling SPG within the ventral nerve cord retain the ability to undergo endomitosis when the Notch signaling pathway or the String Cdc25 phosphatase are altered. Further, we showed that a second glial cell type in the peripheral nervous system, wrapping glia (WG), is polyploid and determined that total WG ploidy correlates with nerve length. Interestingly, when WG ploidy was reduced, we found that axonal ensheathment is defective. We also established that the three WG per peripheral nerve differentially contribute to overall ploidy. Axonal ensheathment throughout the entire nerve seems to be dependent on position along the anterior-posterior larval body axis. Finally, we find that reduction of DNA replication components causes reduced WG ploidy only in longer peripheral nerves.

Thesis supervisor: Terry L. Orr-Weaver
Title: Professor of Biology

*Dedicated to my sister Kimberly Frawley.
A beautiful soul gone too soon.*

August 3, 1981- November 24, 2016

Acknowledgements

I would like to thank my thesis advisor Terry Orr-Weaver. I first met Terry as a student in her Development class during which her love of and dedication to teaching was immediately evident. My first lab rotation was in her lab. While I am normally someone who takes a lot of time to weigh the pros and cons of every situation, after only a few days I knew I wanted to join her lab. One of the things I am most grateful for is how she challenged me as a scientist and writer. She always ensured I had a complete understanding of the rationale behind a scientific question and could contemplate broader implications. I am most impressed by her ability to create and sustain a lab culture for over thirty years that not only promotes scientific excellence but also fosters personal and professional growth. I know I have personally benefited from this, and I believe everyone who has worked in Terry's lab has as well.

My thesis committee members Richard Hynes and Troy Littleton have provided me with thoughtful discussion and feedback on my research throughout the years. They have both helped me prioritize my research as well as bring in outside perspectives. I am honored to have had them guide me throughout my graduate career.

I cannot thank Frank Solomon enough for his support and mentorship throughout my graduate career. He is one of the most caring individuals I have encountered. Frank's support extends to the entirety of the Biology graduate students and I know firsthand he has made an immense impact on many of us. I feel truly grateful for his constant support and advice over the last several years.

I must also acknowledge the bioREFS (Resources for Easing Friction and Stress), a peer support program at MIT I have had the privilege to be a member of since 2013. Through my time as a bioREFS, I have refined my listening, mediation, and conflict resolution skills and have worked with some truly amazing people.

I am thankful for Mandana Sassanfar and MIT's Summer Research Program (MSRP) for introducing me to the MIT Biology community as an undergraduate. I would also like to thank Tyler Jacks and his lab for hosting me as a summer intern, especially Kim Mercer, Anne Deconinck, and Judy Teixeira.

The members of the Orr-Weaver lab are a group of incredible scientists as well as friends I have had the privilege of working with over the last several years. I would especially like to thank Jessica Von Stetina for her mentorship, Boryana Petrova, Emir Aviles Pagan, Brian Hua, Yingdee Unhavaithaya, and Helena Kashevsky.

Finally, I would like to thank my biggest supporters, my family. My grandmother Lee Wade lived her life by setting an example. She taught me you can always overcome your failures and you should never give up on something you truly believe in. My grandmother R. Elaine Frawley, an accomplished poet and author, has also inspired me to pursue what I love. My late sister Kimberly Frawley was the definition of determination and perseverance. It was an honor to grow up with her and experience her magnificent personality. My parents have shown me their unwavering support throughout my life. They have always allowed me to make my own decisions but also provided guidance when I needed it. I have especially valued my mom's strength and sense of humor and my dad's inquisitiveness and moral sense. My husband Brian Knowles has always been very supportive of me as well as my aspirations. Throughout my graduate career he has helped keep me balanced and levelheaded. I feel very lucky to have him as my life partner. Brian and I have undertaken many adventures in the last several years, our biggest being welcoming our son, Will, into the world. Will has an infectious smile, is extremely curious, and has brought me more joy than I ever could have imagined.

TABLE OF CONTENTS

Chapter One:

Introduction	11
Polyploidy overview	12
Why cells become polyploid	15
Polyploidy as a means to increase cell size	15
Specialized functions of polyploid cells	20
Polyploidization as a response to injury	21
Polyploidy as a strategy for increased gene expression or metabolism	23
Cell cycle regulation	24
Endocycling onset	24
Endocycle cycling	26
Endocycling versus endomitotic cells	30
Upstream signaling pathways controlling polyploidy	31
Differential DNA replication	32
The Drosophila nervous system	34
Drosophila nervous system anatomy	34
Glial subtypes and functions	37
Surface glia and the blood-brain barrier	38
Wrapping glia of the PNS	41
Outlook	44
Summary of thesis	45
References	46

Chapter Two:

Variant Cell Cycles Regulated by Notch Signaling Control Cell Size and Ensure a Functional Blood-Brain Barrier	55
Abstract	56
Introduction	57
Results	59
Developmental cell cycle control in the SPG	59
Notch signaling inhibits endomitosis	82
Ablation of the Notch signaling pathway perturbs mitotic divisions during endomitosis	83
SPG in the VNC but not salivary gland cells are capable of endomitosis	84
The presence of both endocycling and endomitotic SPG is required for the blood-brain barrier	95
The relationship between ploidy, nuclear number and cell size in the endocycle versus endomitosis	101
Discussion	107
The role and regulation of endomitosis in the SPG	108
Ensuring a functional BBB	110

Developmental control of the cell cycle	111
Materials and Methods	112
Acknowledgements	119
References	120
Chapter Three:	
The Role of Polyploidy in Wrapping Glia of the Peripheral Nervous System	123
Abstract	124
Introduction	125
Results	127
Wrapping glia are polyploid and total wrapping glia ploidy per nerve correlates with nerve length	127
Reduction of WG ploidy correlates with defective axonal ensheathment	128
WG1 is the main contributor to total increased wrapping glia ploidy in the longer peripheral nerves	133
Axonal ensheathment in the distal NER and MFA is less than in the proximal NER	138
Reduction of DNA replication components causes significant reduction of WG ploidy in longer nerves	139
Discussion	144
Materials and Methods	147
Acknowledgments	150
References	150
Chapter Four:	
Conclusions, Perspectives, and Future Directions	153
Differential properties of endocycling and endomitotic SPG	154
Identification of other polyploid central nervous system glial subtypes	157
Polyploidization in wrapping glia of the peripheral nervous system	158
Growth coordination among the glial layers of the peripheral nerves	160
Conclusion	162
Acknowledgements	162
References	162
Appendix One:	
Generation of a Direct Subperineurial Glia Reporter	165
Acknowledgements	176
References	176
Appendix Two:	
Endomitosis in the Peripheral Nerve SPG	177
References	181

Chapter One:

Introduction

Sections of this chapter and Figures 1-3 were originally published in Frawley, L. E. and Orr-Weaver, T. L. 2015. Polyploidy. *Curr. Biol.* 25, R353-R358.

The development of an organ relies on the coordinated growth among different cell types within given tissues. Throughout the plant and animal kingdoms polyploidization is utilized as a means to increase cell size. The study of polyploidy in *Drosophila melanogaster* has led to a greater understanding of the breadth of cell types that are polyploid, why cells become polyploid, and how polyploidy is regulated. Here I review key findings that have shed light upon cell types that are polyploid, regulation of the variant cell cycles the endocycle and endomitosis, and review polyploidy, particularly in the context of the *Drosophila* nervous system development.

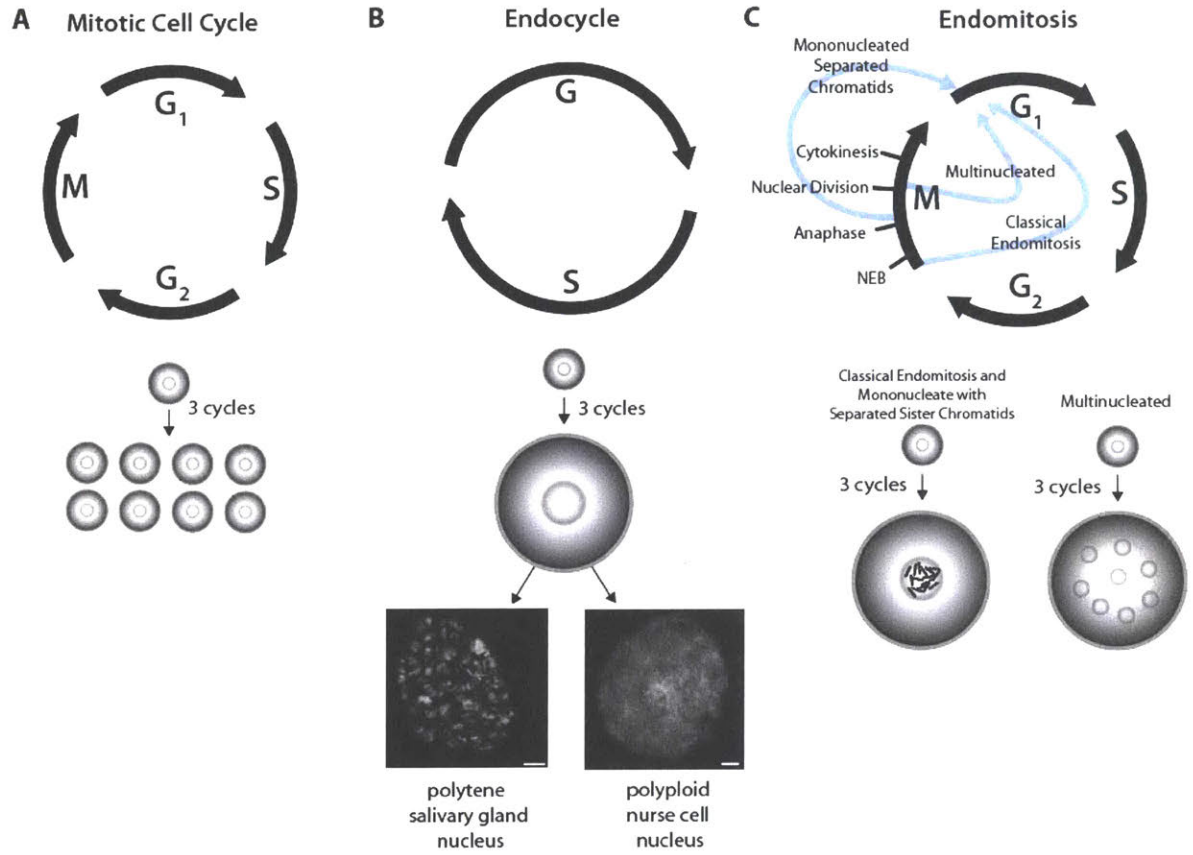
Polyploidy Overview

Polyploidization is defined as an increase in genomic content and is measured in C values, where C is the haploid genome content (Edgar and Orr-Weaver, 2001). Two variant cell cycles that produce polyploid cells are the endocycle and endomitosis. The endocycle is utilized as a developmental strategy by a number of organisms including mammals, chordates, insects, gastropods, and angiosperms (Fox and Duronio, 2013; Orr-Weaver, 2015). Originally termed endoreduplication, ‘endocycle’ is now widely used throughout the field (Fox and Duronio, 2013; Edgar et al., 2014). Unlike the mitotic cell cycle, the endocycle is driven only by repeated S and G phases resulting in a mononucleate cell (Figure 1-1A,B) (Smith and Orr-Weaver, 1991). Endocycling cells lack all features of mitosis and thus do not undergo chromosome condensation, nuclear envelope breakdown, or stain positively for phospho-Histone H3. In contrast, endomitosis is a process by which cells become polyploid by utilizing some aspects of mitosis (Figure 1-1A,C). Originally described as mitosis within an intact nuclear envelope (Nagl, 1978), the field has broadened the term significantly. For example, endomitosis now includes cells that undergo anaphase A but not anaphase B, as well as cells that undergo

Figure 1-1. Cell cycles producing polyploid cells.

(A) The mitotic cycle contains four distinct phases that produce two identical daughter cells. G1 and G2 are growth phases during which gene expression and growth occur, DNA replication takes place during S phase, and mitosis occurs during M phase. (B) The endocycle is driven by repeated S–G cycles that lead to polyploid or polytene cells. A distinct banding pattern can be seen in the image of *Drosophila* polytene salivary glands, which can reach 2048C, where C is the haploid genome content for the organism. This banding pattern is reflective of the replicated sister chromatids being tightly aligned. Scale bar, 5 μ m (image from Jessica Von Stetina, Whitehead Institute). In contrast, nurse cells have no distinct banding pattern in late oogenesis and can reach 512C. Scale bar, 20 μ m (image from Boryana Petrova, Whitehead Institute). (C) Endomitotic cells enter mitosis, but differ in which mitotic steps they complete. Endomitosis was initially defined as a process in which a spindle assembled to segregate sister chromatids within an intact nucleus (classical endomitosis). Additional variants now also are termed endomitosis, such as in cell types in which nuclear envelope breakdown and some aspects of chromosome segregation occur but nuclear division does not. This, like classical endomitosis, produces mononucleate cells. Completion of mitotic events through nuclear division in the absence of cytokinesis leads to multinucleate endomitotic cells. (D) During polyploidization, integral doublings of the genome do not necessarily occur. As schematized here, repression of replication can lead to underreplication and reduced copy number of specific regions relative to overall ploidy. Less commonly, overreplication can produce domains of amplified gene copy number (not shown). This figure and figure legend were originally published in Frawley and Orr-Weaver, 2015.

Figure 1-1



nuclear division but not cytokinesis to produce multinucleate cells (Fox and Duronio, 2013; Orr-Weaver, 2015). Polyploid cells in which sister chromatids remain attached are referred to as polytene and have a distinct banding pattern as in the *Drosophila* larval salivary glands (Figure 1-1B) (Zhimulev, 1974). Polyploidy differs from aneuploidy, an increase or decrease in copy number of at least one chromosome, because it includes whole or near whole genome increases. Cell fusion is another mechanism by which cells can become polyploid. Cell fusion is employed by a number of cell types including *C. elegans* hypodermal cells and rodent syncytiotrophoblasts of the placenta, but will not be discussed further here (Flemming et al., 2000; Zybina and Zybina, 2005). *Drosophila* serves as a powerful model to study polyploidization, as nearly all of larval tissues are polyploid. In fact, the massive organismal growth observed between the three larval stages is a consequence of increased cell size via ploidy rather than by increased cell number via proliferation (Gatti and Baker, 1989).

Why cells become polyploid

The clearest general use of somatic polyploidy appears to be as a mechanism to produce large cells. This is exploited in some developmental contexts in which fewer, larger cells have functional advantages over a similar total mass of an increased number of smaller cells.

Polyploidy additionally may aid in injury repair or regeneration and to augment gene expression or metabolism.

Polyploidy as a means to increase cell size

One use of polyploidy is to generate large cells, such as mammalian megakaryocytes or the giant cells that contribute to the structure of organs such as *Arabidopsis* sepals (Nagata et al.,

1997; Ravid et al., 2002; Roeder et al., 2010; Roeder et al., 2012). It has been appreciated since late in the 19th century that cell size is proportional to nuclear size, and this was subsequently shown to reflect DNA content (Huber and Gerace, 2007; Neumann and Nurse, 2007; Chevalier et al., 2013; Cho and Nijhout, 2013; Orr-Weaver, 2015). Thus, both polyploid and polytene cells are of increased size, some attaining sizes orders of magnitude larger than diploid cells, with corresponding increases in genomic DNA (Figure 1-2). Although increased DNA content is consistently associated with increased cell size, there is not an absolute ratio between nuclear size and cell size (the karyoplasmic ratio) across cell types (Cavalier-Smith, 1985). Cell-size increases associated with increased DNA content can be dramatic, producing cells visible to the naked eye, such as giant neurons in slugs (diameter of 1mm) and the polyploid trichome cells of *Arabidopsis* (1mm in length) (Lasek and Dower, 1971; Breuer et al., 2014). Even in bacteria, cell size is coordinated with DNA content (Mendell et al., 2008).

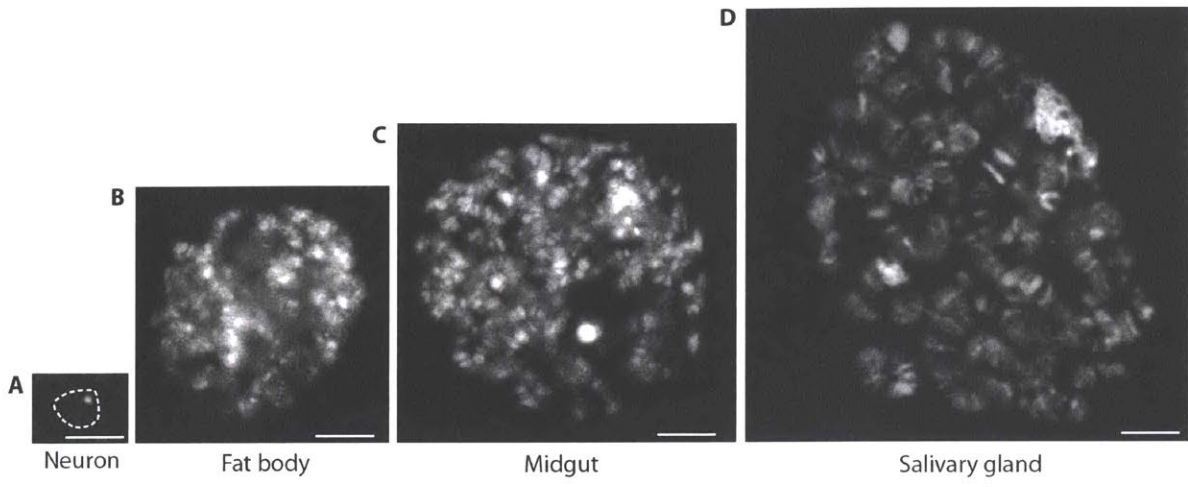
The correlation between increased DNA content and very large cell size suggests that there is a requirement for a minimal nuclear to cytoplasmic ratio and a limitation to how large cells can become by increasing mass through growth alone (Cavalier-Smith, 1985). One example cited as an argument against a need for increased DNA content with a large cell size are eggs, which can fill with yolk to attain an enormous size. In 1912 Conklin tested which components of cytoplasm could reflect nuclear size, evaluating the contribution of yolk by separating it from cytoplasm and measuring cell size during early cleavage in sea snail embryos. He concluded that the relationship between nuclear size and cell size was determined not by the total cytoplasm but by the active cytoplasm without yolk (Conklin, 1912).

Another example that argues against a minimal nuclear to cytoplasmic ratio is neurons:

Figure 1-2. Correlation of nuclear size with DNA content.

DAPI-stained nuclei isolated from various *Drosophila* tissues: (A) third instar larval brains, (B) fat body, (C) midgut, and (D) salivary glands are shown (all shown to the same scale with scale bars of 5 μ m). A single diploid neuronal nucleus is outlined in (A). The ploidy level quantified for the fat body nucleus shown is 74C, the midgut 177C, and the salivary gland nucleus is 1824C. Although the mean ploidy levels for fat body nuclei are 225C, 171C for midgut, and 1669C for salivary gland, there is a range of nuclear ploidy within each of these tissues. (The image in (A) is from Laura Frawley, (B,C) from Sharon Li, and (D) from Jessica Von Stetina, all at the Whitehead Institute). This figure and figure legend were originally published in Frawley and Orr-Weaver, 2015.

Figure 1-2



these cells can be extremely large as a result of their axons, which can be a meter or more in length. A barrier excludes cytoplasm from the axons, however, making it likely that axonal volume is not monitored as part of the cytoplasmic volume (Song et al., 2009; Yoshimura and Rasband, 2014). Purkinje cells are neurons that can be enormous due to large dendritic arbors, raising the question of their nuclear to cytoplasmic ratio. There are conflicting reports in the literature regarding whether or not these cells are polyploid, and reinvestigation of the ploidy of Purkinje cells with newer microscopy tools would be highly informative (Lapham, 1968; Manuelidis and Manuelidis, 1974; Mann et al., 1978; Brodsky et al., 1979; Weimann et al., 2003).

We still do not know which components contribute to the size relationship between the nucleus and the cell or why increased DNA content leads to an increase in cell size. Although it had been proposed that causality perhaps occurs in the reverse direction, with increased cytoplasmic volume leading to increased nuclear size, *Drosophila* and plant mutants in which DNA content is primarily affected clearly establish that cell volume follows nuclear size (Royzman et al., 1999; Walker et al., 2000; Sher et al., 2012). One possibility that will be valuable to investigate is whether the gene copy numbers of components of the ribosome (ribosomal proteins or rRNA) are limiting, making cell size above a threshold dependent on increased ploidy. Such a possibility could also explain why increased ploidy leads to increased cell size, if it results in increased numbers of ribosomes that lead to increased translation and cellular mass.

A potential complication of the use of ploidy as a means to increase cell size is that, for a sphere, surface area increases with the square of the radius whereas volume increases with the cube of the radius. Thus, with increasing DNA content the nuclear surface area will not keep up

with increasing nuclear volume: if the nuclei are flat, however, the two parameters will scale together. It is notable that in many polyploid cell types in both plants and animals the nuclei are flat rather than spherical and in addition contain many involutions in the nuclear envelope (Bourdon et al., 2012; Buntrock et al., 2012). We speculate that these may be mechanisms to increase the surface area of the nuclei: adequate surface area could be critical for sufficient numbers of nuclear pores to ensure adequate mRNA transport from the nucleus.

Specialized functions of polyploid cells

Growth by polyploidization rather than by an increase in cell number via proliferation provides advantages in some developmental contexts such as in organs in which one tissue layer provides a barrier. Specifically, it enables cells to maintain intercellular junctional integrity while increasing in size by orders of magnitude to accommodate an increasing mass of underlying tissue layers in development. Two polyploid cell types that provide barriers include *Drosophila* subperineurial glia (SPG) (Unhavaithaya and Orr-Weaver, 2012) and rodent trophoblast giant cells (TGCs) (Rossant and Cross, 2001; Cross, 2005; Watson and Cross, 2005; Zybina and Zybina, 2005).

SPG form the blood-brain barrier (BBB) through pleated septate junctions (Stork et al., 2008; Desalvo et al., 2011; Hatan et al., 2011). Our lab discovered that polyploidy is critical for the function of SPG and the integrity of BBB (Unhavaithaya and Orr-Weaver, 2012). After reducing SPG ploidy by expressing either *double parked (dup)* RNAi or *proliferating cell nuclear antigen (pcna)* RNAi, breaks in the septate junctions were observed. Furthermore, the BBB was no longer functional as TetraRhodamine dextran (10kDa) dye penetrated into the brain after it was injected into the larval abdominal cavity (Unhavaithaya and Orr-Weaver, 2012).

The increased cell size of TGCs is a result of increased ploidy and is thought to aid in

their ability to form a placental barrier between the maternal and embryonic tissues (Rossant and Cross, 2001; Cross, 2005; Watson and Cross, 2005). During early mammalian development, TGCs enter the endocycle and reach ploidy levels of 512C (Barlow and Sherman, 1974; Sher et al., 2013). It has been postulated that the strategy of increasing the size of these cells via the endocycle rather than increasing cell number by mitosis is to maintain a continuous placental barrier. Polyploidy may not be a requirement for TGC function, however, as reducing TGC ploidy four-fold by conditional inactivation of E2F7 and E2F8, two transcription factors required for the TGC endocycle, did not affect fetal viability (Chen et al., 2012).

Megakaryocytes need to be large to fulfill their function in platelet production, which occurs via platelet budding from the cytoplasm. Polyploidy is necessary to produce megakaryocytes with an adequate cytoplasmic volume to produce sufficient numbers of platelets (Nagata et al., 1997; Ravid et al., 2002).

Polyploidization as a response to injury

Polyploidization has been shown to occur in response to injury and stress in mammalian hepatocytes and cardiomyocytes as well as in *Drosophila* epidermal cells and follicle cells (FCs) (Meckert et al., 2005; Miyaoka et al., 2012; Losick et al., 2013; Pandit et al., 2013; Senyo et al., 2013; Tamori and Deng, 2013; Losick et al., 2016).

Rodent and human hepatocytes utilize both the endocycle and endomitosis to attain ploidy values of up to 8C during normal liver development (Vinogradov et al., 2001; Duncan, 2013; Gentric and Desdouets, 2014). The function of polyploidy in hepatocytes is unclear, but may be to increase metabolism, to confer resistance against DNA damage, to inactivate apoptosis, or to provide genetic variation (Duncan et al., 2012; Gentric et al., 2012; Hassel et al.,

2014; Orr-Weaver, 2015).

Interestingly, hepatocytes have the ability to undergo ploidy reversal, or to reenter mitosis after being in a polyploid state (Duncan, 2013). This phenomenon has also been coined the ‘ploidy conveyor model.’ Specifically, diploid cells can become polyploid by incomplete cytokinesis and polyploid cells can reenter mitosis to produce diploid cells (Pandit et al., 2012; Duncan, 2013). When polyploid cells proliferate, they form multipolar spindles generating hepatocytes with 2C or 4C, but also aneuploid cells (Duncan, 2013).

Ploidy reversal has been observed during liver regeneration. For example, following 70% hepatectomy, binucleate hepatocytes undergo reductional divisions, each producing two mononucleate hepatocytes (Miyaoaka et al., 2012). Miyaoaka and colleagues also studied the contribution of polyploid hepatocytes during regeneration. They found that hypertrophy and proliferation are about equally responsible for regeneration of the liver after 70% hepatectomy, but hypertrophy is entirely responsible for regeneration of the liver after 30% partial hepatectomy (Miyaoaka et al., 2012).

Despite studies showing E2F7 and E2F8 are needed during liver hypertrophy, conditional knockout of these transcription factors in rodents, do not have any observable defects in hepatocyte differentiation, zonation, metabolism, or liver regeneration (Pandit et al., 2012). Thus, polyploidization may not be required for normal hepatocyte function, although severe stress was not induced in this study, so it cannot be ruled out that polyploidization is a requirement under more severe stress conditions (Pandit et al., 2012).

Polyploid mammalian cardiomyocytes emerge during normal postnatal development. In fact, as many as 70% of human cardiomyocytes and at least 85% of rodent cardiomyocytes are polyploid (Soonpaa et al., 1996; Mollova et al., 2013). It has been speculated that polyploidy is

advantageous for cardiomyocytes because undergoing cytokinesis would require disassembly of sarcomeres, causing a temporary loss in contractile function (Anatskaya and Vinogradov, 2010; Pandit et al., 2013). Interestingly, evidence suggests that following human acute myocardial infarction, cardiomyocytes become polyploid via endomitosis as an adaptive response (Herget et al., 1997; Meckert et al., 2005; Senyo et al., 2013).

Finally, *Drosophila* epidermal cells and FCs are able to compensate for cell loss by polyploidization. In epidermal cells, wound-induced polyploidization (WIP) has been shown to compensate for cell loss (Losick et al., 2013; Losick et al., 2016). WIP is achieved by both cell fusion and by cell cycle alteration; cell fusion causes rapid repair, whereas the endocycle replaces lost cell mass. WIP is essential for wound repair because upon reduction of cell fusion or the endocycle, wound closure drastically slowed (Losick et al., 2013). Losick and colleagues hypothesized that WIP is advantageous post injury because larger cells can mechanically stabilize wounds better than their diploid counterparts (Losick et al., 2013). In the case of FCs, aberrant FCs are eliminated by a process called compensatory cellular hypertrophy in which the surrounding FCs undergo accelerated endocycles to compensate for the lost epithelial cells (Tamori and Deng, 2013).

Polyploidy as a strategy for increased gene expression or metabolism

Some polyploid cell types are highly metabolically active, such as *Drosophila* nurse cells, which synthesize and provide the oocyte with mRNAs, proteins, translational machinery and mitochondria (Spradling, 1993). Thus, another advantage of polyploidy could be that increased gene copy numbers facilitate high rates of biosynthesis and metabolism. This currently remains a hypothesis, however, until studies are carried out to examine whether gene expression levels are

increased in polyploid cells, i.e. whether the levels of transcript per gene per polyploid cell are higher than those in diploid counterparts. Recent techniques to rigorously quantify transcript levels per cell using normalization of RNA sequencing now permit the extent of the effect of polyploidy on gene expression to be analyzed in a large number of cell types. In addition to investigating gene expression, evaluation of the function of polyploidization will benefit from comparisons of translation and metabolic rates in polyploid versus diploid cells.

Until recently, it was understood that polyploidy is common in plants and invertebrates, but far more rare in mammals (Gandarillas et al., 2018). In addition to the mammalian polyploid cell types discussed previously, other tissues that utilize polyploidy include the endometrium (Das, 2009), epidermis (Zanet et al., 2010), retinal pigment epithelium (Starnes et al., 2016), and mammary glands (Banerjee et al., 1971; Rios et al., 2016). Recently, lactating mammary glands of humans, cow, seal, and wallaby have also been found to be polyploid, suggesting polyploidy may be an evolutionarily conserved mechanism for lactation (Rios et al., 2016).

Cell cycle regulation

Endocycling onset

Progression through the archetypal cell cycle is dependent on a family of serine/threonine protein kinases known as cyclin-dependent kinases (CDKs). Substrate phosphorylation by specific CDKs enables mitotic cells to progress through G1, S, G2, and M phases of the cell cycle. Entry into the endocycle requires all mitotic machinery to shut off. To achieve this, endocycling cells must suppress the mitotic machinery, specifically mitotic CDKs, both at the level of transcription of cyclin genes and by affecting Cyclin–CDK activity (MacAuley et al., 1998; Hattori et al., 2000; Sher et al., 2013).

Two mechanisms act on mitotic cyclin proteins: proteolytic targeting of cyclins by the E3 ubiquitin ligase anaphase-promoting complex/cyclosome (APC/C); and inhibition of the activity of Cyclin–CDK complexes by CDK inhibitors (CKIs). *Drosophila* cells mainly regulate mitotic Cyclin proteins via APC/C activation (Smith and Orr-Weaver, 1991; Sigrist and Lehner, 1997; Sun and Deng, 2007; Narbonne-Reveau et al., 2008), whereas plants and some mammalian cells rely heavily on CKI activation (Tanaka et al., 1998; Walker et al., 2000; Schnittger et al., 2002; Churchman et al., 2006; Haga et al., 2008; Ullah et al., 2008; Ullah et al., 2011). Much of our knowledge of polyploidy onset is derived from endocycling cells: the examples detailed below all occur in endocycling cells.

Multiple mechanisms can promote the transition into the endocycle in a tissue-specific manner. The molecular mechanism of the transition of *Drosophila* mitotic cells into the endocycle has been elucidated in the future larval tissues in the embryo as well as in adult follicle and midgut cells. The onset of the endocycle in future larval tissues of the *Drosophila* embryo is controlled by expression of the APC/C activator, Fizzy-related (*Fzr/Cdh1*). In *fzr* mutant embryos, epidermal cells undergo an additional round of division, and mitotic Cyclins accumulate in post-mitotic salivary gland cells, preventing them from transitioning into the endocycle (Sigrist and Lehner, 1997; Narbonne-Reveau et al., 2008).

In addition to suppression of mitotic cyclins, Skp1-Cullin-F-box (SCF)- mediated downregulation of Cyclin E protein levels is important for endocycle onset in follicle cells (Shcherbata et al., 2004). The role of the Notch signaling pathway in the transition into the endocycle for *Drosophila* adult follicle cells and midgut cells will be detailed in the section “Upstream signaling pathways controlling polyploidy.”

CKI activation inhibits CDKs and thus suppresses the mitotic machinery in TGCs. Experiments performed in cell culture demonstrate that, in the presence of fibroblast growth factor 4 (FGF4), the CKIs p21^{CIP1} and p57^{KIP2} are targeted for degradation after being phosphorylated by checkpoint kinase 1 (CHK1), causing trophoblast stem cells to remain in the mitotic cell cycle (Tanaka et al., 1998; Ullah et al., 2008; Ullah et al., 2011). Upon removal of FGF4, CHK1 is degraded, allowing p21^{CIP1} and p57^{KIP2} to accumulate and inhibit CDK1 activity, triggering endocycle entry and differentiation into TGCs (Ullah et al., 2008). Additionally, E2F transcriptional activator and repressor proteins are thought to be involved in the transition into the endocycle, as they affect the expression of mitotic regulators (Edgar et al., 2014).

Endocycling Arabidopsis cells rely on the activity of two plant-specific families of CKIs, SIAMESE (SIM) and SIAMESE-RELATED (Walker et al., 2000). SIM binds to the mitotic CDK CDKB1;1 and is also thought to inhibit activation of MYB3R1, a transcription factor that regulates the mitotic cyclin CYCLIN B1 (Schnittger et al., 2002; Churchman et al., 2006; Haga et al., 2008). Additional pathways contributing to the suppression of mitotic CDKs include the plant homolog of Fzr/Cdh1, *CCS52A*, E2F–RB complexes, and a second E3 ubiquitin ligase containing CULLIN 4 (De Veylder et al., 2002; Lammens et al., 2008; Larson-Rabin et al., 2008; Boudolf et al., 2009; Vanstraelen et al., 2009; Roodbarkerlari et al., 2010). A number of environmental and hormonal cues also affect the onset of the plant endocycle, as reviewed in Breuer et al. 2014.

Endocycle cycling

The details of maintenance of the endocycle are better understood than endocycle onset. Endocycles consist of repeated G and S phase oscillations. In both the canonical cell cycle and

the endocycle a period of low CDK activity during G phase is required for pre-replication complex (pre-RC) formation, a prerequisite for the initiation of DNA replication in S phase (Zielke et al., 2013). In the canonical cell cycle solely the period of telophase through early G1 has low Cyclin/CDK activity, permitting origins to be reset. In the endocycle, mitotic Cyclin proteins are absent, so only S-phase CDK complexes have to be downregulated. As SCF causes the degradation of Cyclin E, a period of low CDK activity is followed by a period of high CDK activity (resulting from transcriptional activation of *cyclin E*, see below), which promotes DNA synthesis while simultaneously inhibiting pre-RC formation and origin re-firing (Lilly and Spradling, 1996). An additional role for APC/C^{Fzr/Cdh1} in the endocycle is to target degradation of Geminin, a protein that inhibits replication licensing (Figure 1-3A) (Narbonne-Reveau et al., 2008).

The transcriptional activator E2F1 is a core oscillator essential for endocycle progression. Analyses using *Drosophila* salivary glands clearly demonstrate a biphasic oscillation in which E2F1 accumulates in late G phase and promotes the transcription of *cyclin E*, which leads to a complex of the Cyclin E protein with the S phase CDK2 that promotes DNA replication (Zielke et al., 2011). The S-phase-specific E3 ubiquitin ligase CRL4^{CDT2} targets E2F1 for proteolytic destruction, thereby lowering *cyclin E* transcription, and re-establishing a period of low CDK activity required for G phase pre-RC assembly (Figure 1-3B) (Zielke et al., 2011).

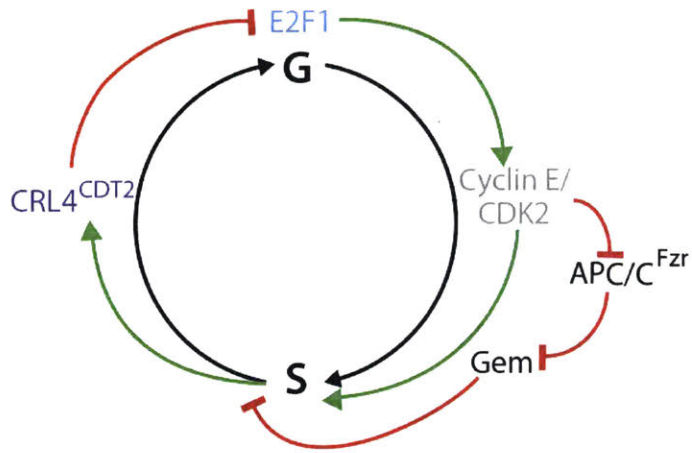
E2F also plays a critical role in the establishment of the biphasic oscillator in endocycling mouse TGCs. As in *Drosophila*, E2F transcriptional activators accumulate during late G phase, resulting in activity of the S-phase CDK complex Cyclin E–CDK2 during the G-to-S transition. High levels of Cyclin E–CDK2 promote DNA replication and inhibit APC/C^{Cdh1} activity, allowing the S-phase Cyclin A to accumulate. The Cyclin A–CDK2 complex creates a negative

Figure 1-3. Endocycle progression in Drosophila.

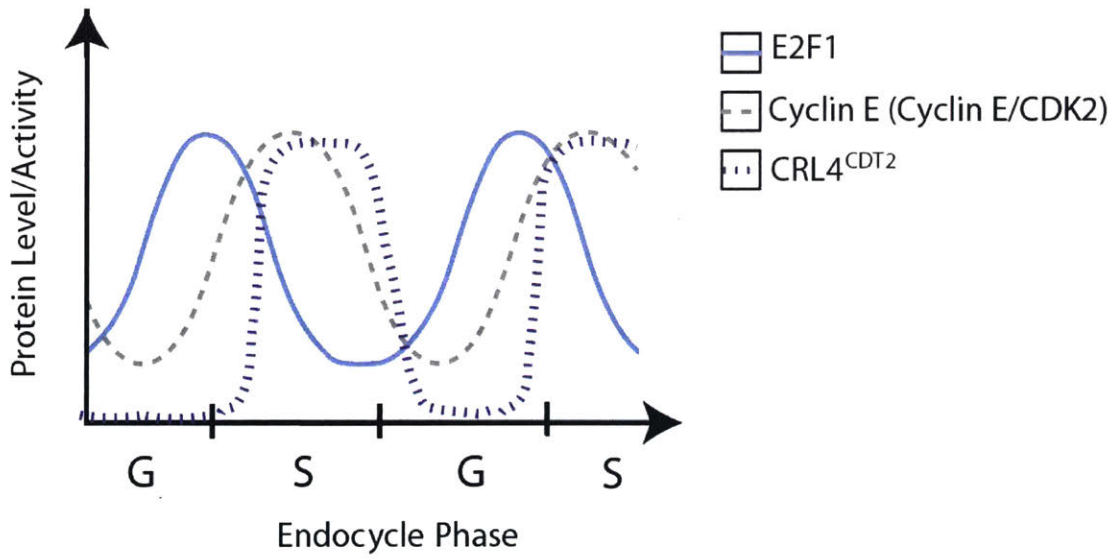
(A) Regulatory inputs to the endocycle. The E2F1 transcription factor promotes expression of *cyclin E*, leading to active Cyclin E–CDK2 kinase, which triggers the onset of S phase. Cyclin E–CDK2 inhibits APC/C^{Fzr/Cdh1} activity, thus allowing Geminin accumulation and preventing re-replication in a given S phase. Low Cyclin–CDK activity and G phase results as CRL4^{CDT2} targets E2F1 for degradation during S phase, leading to a decrease in Cyclin E. (B) Oscillation of regulators in the endocycle. Protein levels are indicated for E2F1 and Cyclin E and activity for CRL4^{CDT2}. Increased levels of E2F1 protein promote increases in Cyclin E and thus Cyclin E–CDK2 activity. Activation of CRL4^{CDT2} in S phase causes the destruction of E2F1. (Adapted from Edgar et al. 2014.) This figure and figure legend were originally published in Frawley and Orr-Weaver, 2015.

Figure 1-3

A



B



feedback loop by phosphorylating Cyclin E, thereby targeting it for degradation by the E3 ubiquitin ligase CRL1^{FBW7} (F-box and WD40 domain-containing protein 7) (Edgar et al., 2014).

CKIs additionally contribute to TGC endocycle progression, as Cyclin E–CDK2 activity is kept low during G phase by p57^{KIP2} (Hattori et al., 2000). There is some evidence in Arabidopsis that oscillations between high and low levels of CDKs contribute to endocycle progression. Both E2F and a second family of CKIs, KIP-related proteins (KRPs; related to mammalian p57 and p21), have been proposed to be involved in what is speculated to be a ‘quadruple negative feedback’ mechanism (Zhao et al., 2012). The hypothesized model includes inhibition of SCF^{FBL17} by RB-RELATED PROTEIN (RBR1), degradation of KRPs by SCF^{FBL17}, inhibition of the A-type CDK CDKA by KRPs, and inhibition of RBR1 via phosphorylation by CDKA (Zhao et al., 2012).

Endocycling versus endomitotic cells

In contrast to endocycling cells, which suppress mitotic players and oscillate only between S and G phases, endomitotic cells undergo aspects of mitosis and therefore must maintain the expression of some mitotic genes. Consequently, endomitotic cells need to cycle between G1, S, G2, and aspects of M phase (Figure 1-1C). Trakala and colleagues have provided insights into the nature of endomitotic progression in megakaryocytes (Trakala et al., 2015). The authors addressed which mitotic components are required for megakaryocyte polyploidization and function by ablating a number of mitotic factors, including: CDK1 and/or CDK2 to assess mitotic entry; Aurora B to assess mitotic progression; and the APC/C activator Cdc20 to assess mitotic exit. Interestingly, only ablation of APC/C^{Cdc20} caused mitotic arrest of megakaryocytes, whereas the absence of Aurora B, CDK1, and CDK2 did not significantly affect megakaryocyte

polyploidization or platelet levels. Upon CDK1 ablation, however, megakaryocytes switched to undergo polyploidy via the endocycle instead of endomitosis (Trakala et al., 2015). This switch in polyploidization mechanism is the first evidence that shows that the endocycle can substitute for endomitosis in megakaryocytes with no obvious detrimental effect on function.

Entry into a polyploid state requires the mitotic machinery to be shut off. Thus, once cells enter the endocycle, reentry into the mitotic cell cycle was thought to be impossible. However, hepatocytes (as discussed in the section “Polyploidization as a response to injury”) and *Drosophila* rectal papillae cells are capable of reentering the mitotic cell cycle after being in a polyploid state. Rectal papillae cells undergo two rounds of the endocycle during pupation to become octaploid followed by two mitotic divisions to increase cell number (Fox et al., 2010). These polyploid mitotic divisions are marked by a high level of segregation errors including: extended anaphase, chromosome bridges, and lagging chromosomes (Fox et al., 2010; Schoenfelder et al., 2014). Interestingly, these studies suggest that pre-mitotic endocycles promote a high level of aneuploidy tolerance (Schoenfelder et al., 2014).

Upstream signaling pathways controlling polyploidy

Notch pathway activation in *Drosophila* epithelial follicle cells surrounding the developing oocyte is triggered by the Notch ligand Delta expressed on the underlying germline nurse cells. This leads to inhibition of the Cdc25-type phosphatase String, which normally activates CDKs, and activation of the transcription factor Hindsight (Hnt) (Deng et al., 2001; Lopez-Schier and St Johnston, 2001). Hnt, in turn, prevents the transcriptional repressor Cut from suppressing $APC/C^{Fzr/Cdh1}$, which leads to the degradation of the mitotic Cyclins A, B, and

B3 (Sun and Deng, 2007). Notch signaling also promotes endocycle onset in enterocytes of the *Drosophila* gut, although the mechanism is not well understood (Wilson and Kotton, 2008).

In many polyploid cell types, Rho GTPase activity can be associated with cytokinesis failure as it is involved in regulation of the actin cytoskeleton and myosin II (Glotzer, 2001; Fededa and Gerlich, 2012). For example, in hepatocytes the RhoA pathway is never activated due to cytoskeletal disorganization (Margall-Ducos et al., 2007). Similarly, binucleate cardiomyocytes arise from the incorrect formation of the contractile ring (Engel et al., 2006). Lastly, in megakaryocytes, RhoA is inhibited by downregulation of a guanine exchange factor (Gao et al., 2012).

The Hippo and JNK pathways are involved in WIP (Losick et al., 2013; Losick et al., 2016). Specifically, upon injury, JNK signaling is induced in cells adjacent to the wound and leads to cells migrating to the wound (Losick et al., 2013; Losick et al., 2016). Additionally, post injury, the Hippo co-transcriptional activator Yorkie drives WIP to achieve reepitheliazation (Losick et al., 2016).

Differential DNA replication

An interesting feature of some endocycling cells is that DNA replication during S phase does not involve an integral doubling of the genome. This differential DNA replication can involve inhibition of replication of specific genomic regions causing reduced copy number, or underreplication (Figure 1-1D). The opposite has been observed in *Drosophila* follicle cells where overreplication of specific genomic intervals leads to amplification of gene copy number of those regions relative to overall cell ploidy (Spradling, 1981). The biological function of amplification in follicle cells is to generate enough eggshell protein in a short developmental

time window. These developmentally controlled amplicons have provided powerful models to decipher the regulation of metazoan replication origin activation and fork progression where the mechanism is repeated origin firing and bidirectional fork movement (Hua and Orr-Weaver, 2017).

The biological logic for underreplication is less clear. In *Drosophila*, the heterochromatin, which constitutes nearly 30% of the genome, is underreplicated in all polyploid or polytene tissues examined (Hammond and Laird, 1985a; Hammond and Laird, 1985b). It may be advantageous to these cells not to invest in duplicating genome regions that are gene poor. Euchromatic regions in *Drosophila* also can be underreplicated, to a lesser extent, with tissue specificity (Hua and Orr-Weaver, 2017). Underreplication of euchromatic regions is not causally linked to repression of gene expression, and it does not appear essential for viability or differentiation of these polytene cells (Belyakin et al., 2005; Nordman et al., 2011; Sher et al., 2012). Repression of replication at both the heterochromatic and euchromatic regions requires SUUR, a protein that localizes to and inhibits progression of replication forks (Belyakin et al., 2005; Nordman et al., 2011; Sher et al., 2012; Nordman et al., 2014). Interestingly, work on the *Drosophila* salivary glands has led to the proposal of underreplication as a mechanism for gene rearrangement, thereby creating genetic diversity (Yarosh and Spradling, 2014). Endocycling cells in plants appear to replicate their genomes fully, as do mammalian megakaryocytes (Caro et al., 2008; Breuer et al., 2010; Sher et al., 2013). In TGCs the heterochromatin is not underreplicated, but some euchromatic regions of the genome exhibit low, but reproducible, levels of underreplication, usually less than twofold (Sher et al., 2013; Hannibal et al., 2014). This indicates either that a subpopulation of the cells undergoes significant underreplication or that in rare S phases some intervals are prone to replication failure.

The *Drosophila* nervous system

Drosophila nervous system anatomy

The nervous system is composed of a complex network of neurons and glial cells. For decades, neurons were of most interest to scientists because they produce action potentials. In contrast, glial cells, named for the Greek word meaning glue, were thought to exclusively perform structural support functions. However, over the last two decades, our understanding of glial cells has evolved drastically. We now know that glial cells are not simply support cells, but are required for proper nervous system development, function, and maintenance (Stork et al., 2012). In mammals, glia account for only 90% of the nervous system where as the *Drosophila* nervous system is composed of only 10% glia (Allen and Barres, 2009; Stork et al., 2012). Therefore, *Drosophila* serves as an ideal model organism to study glia.

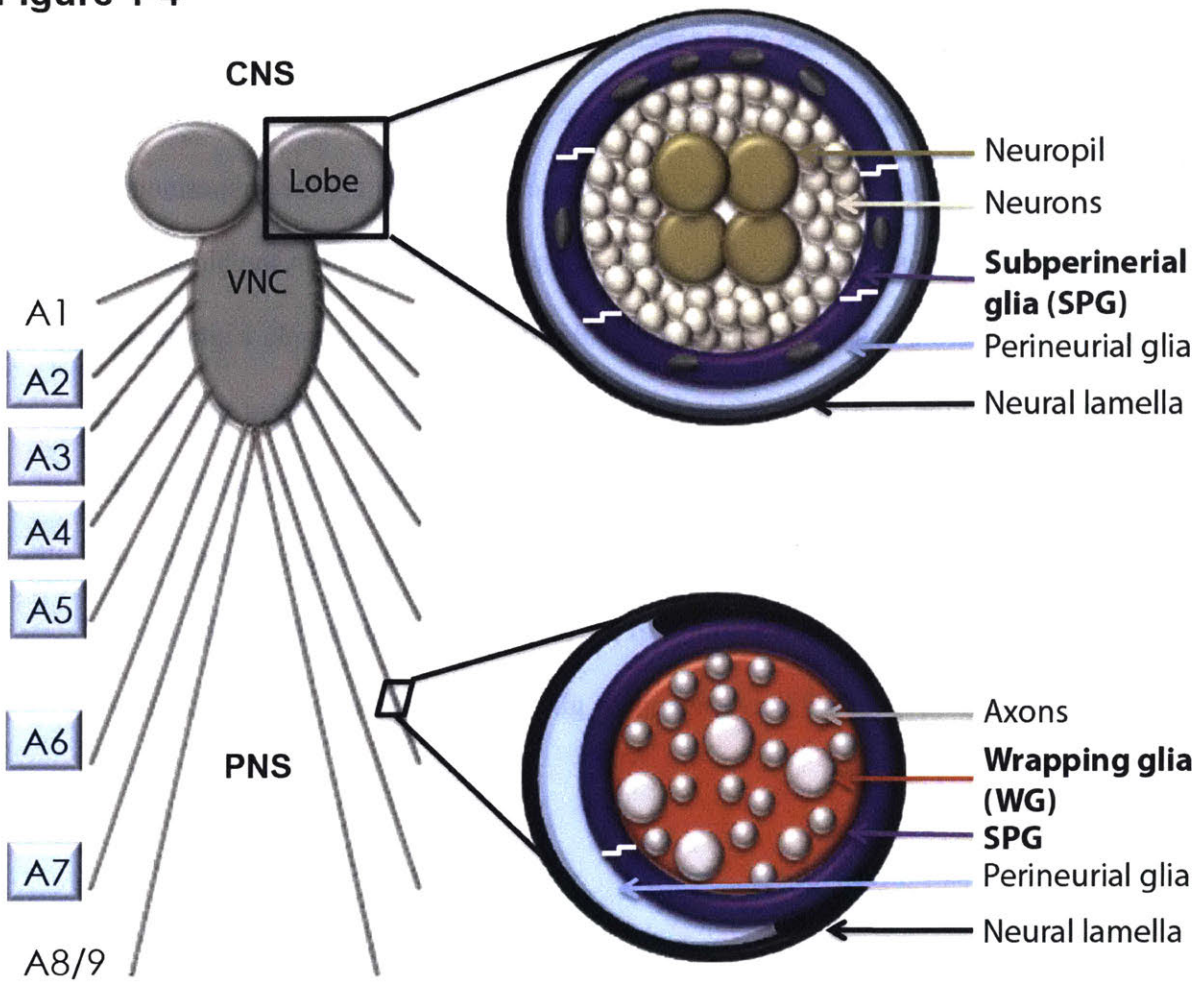
The *Drosophila* nervous system is composed of a central nervous system (CNS) and a peripheral nervous system (PNS). The CNS has two brain lobes and a ventral nerve cord (VNC), which is equivalent to the mammalian spinal cord, and the PNS is made up 16 peripheral nerves (Figure 1-4). Pioneer motor axons are guided to the edge of the VNC by peripheral glia and then project into the embryonic muscle field (Sepp et al., 2001). The peripheral glia then migrate along the newly formed peripheral nerves (Sepp et al., 2000). The peripheral glia also guide axons of sensory neurons that are born in the dorsolateral region of the embryonic muscle field to the VNC (Banerjee and Bhat, 2008).

The larval body plan is composed of three thoracic segments and eight abdominal segments. The eight peripheral nerves that originate from the VNC are named for the abdominal segment they innervate (the A2 nerve innervates abdominal segment A2, etc.). Additionally,

Figure 1-4. Drosophila nervous system.

Simplified schematic of the surface and ensheathing glia present in the Drosophila central and peripheral nervous systems (CNS/PNS). The surface of the CNS has an outer neural lamella (black). The first glial layer is the perineurial glia (blue). Subjacent are the subperineurial glia (SPG) (purple) that have septate junctions (white zigzags). The SPG form the blood-brain barrier that separates the neurons (silver) and neuropil (gold) from the hemolymph. Eight peripheral nerves protrude from the ventral nerve cord and are named for the abdominal segment they innervate. The peripheral nerves (A1-A8/9) are less complex than the CNS and have an outer neural lamella layer (black) and three glia layers: the perineurial (blue) and subperineurial glia (purple) and wrapping glia (red). In addition to the blood-nerve-barrier formed by the intracellular junction forming SPG cell, wrapping glia also help protect axons (gray) by ensheathing them.

Figure 1-4



nerve length is shortest at A1 and increases in length through A8/9 (Figure 1-4). Throughout larval development, the nerves increase in length tremendously. There is a 10-fold increase in length between the shortest and longest nerves within one developmental stage as well as a 50-fold increase in length of nerve A7 during larval development (von Hilchen et al., 2013). Nerves A2-A7 specifically have a fixed number of 12 peripheral glia that can be found in stereotypic locations (von Hilchen et al., 2008). Each nerve contains two regions, the nerve extension region (NER) and the muscle field area (MFA). Notably, when the length of nerve A2 is compared to the length of A7, the NER increases drastically in size while the MFA remains relatively constant (von Hilchen et al., 2013).

Glial subtypes and functions

In *Drosophila*, the transcription factor *glial cells missing* (*gcm*) is required for specification of almost all glial cell types (Jones et al., 1995). *gcm* is frequently referred to as a binary switch because *gcm* loss-of-function mutant embryos exhibit transformation of glia into neurons, whereas *gcm* gain-of-function mutant embryos exhibit differentiation of neurons into glia (Hosoya et al., 1995; Jones et al., 1995). Following *gcm* activation, its direct target *reversed polarity* (*repo*) is activated and serves as a pan-glial driver and nuclear marker (Stork et al., 2012). Interestingly, despite being a master regulator of glial cell fate in *Drosophila*, the mammalian *gcm* homologs Gcm1 and Gcm2 do not play a role in glial differentiation (Kim et al., 1998).

There are four categories of glia in *Drosophila*: cortex glia, neuropil glia, and surface glia in the CNS and the peripheral glia in the PNS. All of these glial classes can be found with similar characteristics throughout the late embryonic, larval, and adult nervous system (Stork et al.,

2012). Cortex glia are found in the cortex of the CNS and extensively wrap around neuronal cell boundaries (Pereanu et al., 2005). Their association with both the SPG and tracheal cells has led scientists to speculate that they may function to distribute gases and nutrients to the neurons they ensheath, and in this way, cortex glia are functionally analogous to mammalian astrocytes (Pereanu et al., 2005; Freeman and Doherty, 2006). Next, neuropil glia are composed of ensheathing and astrocyte glia and have similar functions as mammalian oligodendrocytes (Freeman and Doherty, 2006). *Drosophila* ensheathing glia surround the neuropil, effectively separating it from the cortex, whereas astrocytes infiltrate the complex network of dendrites, axons, and synapses within the neuropil (Freeman, 2015). The remaining two glial categories, surface glia and peripheral glia will be discussed in detail in the two sections below.

Over the last few decades, an array of glial drivers and markers has become available (Stork et al., 2012). Throughout our work, we visualized glial cells of interest using the GAL4 system. The GAL4 system allows for cell type and tissue specific expression. The system has two parts: the *gal4* gene encoding the yeast transcriptional activator and the upstream activation sequence (UAS), an enhancer to which GAL4 proteins specifically bind to and activate transcription. We used the G protein-coupled receptor Moody to mark SPG cells (Bainton et al., 2005; Schwabe et al., 2005) and the Na⁺,K⁺-ATPase β subunit Nervana2 (*Nrv2*) to mark WG cells (Sun et al., 1999). However, *Nrv2* is also expressed in cortex glia and SPG of the CNS so the field would benefit from a WG PNS only driver (Stork et al., 2012).

Surface glia and the blood-brain barrier

The surface glia are comprised of the perineurial glia (PG) and SPG. The PG is a discontinuous layer thought to secrete the extra-cellular matrix to provide an initial barrier that

excludes large particles from entering the neural microenvironment (Leiserson et al., 2000; Stork et al., 2008). SPG have a flattened morphology, are less than 1 μm in thickness and are enormous in size. The area of one SPG cell can be equivalent to 10,000 epithelial cells (Silies et al., 2007). One function of SPG cells is to form the BBB and blood-nerve barrier (BNB) (Bainton et al., 2005; Schwabe et al., 2005). Both the BBB and BNB are crucial to maintaining normal neuronal electrical conductance within the nervous system by isolating it from the potassium rich hemolymph. Structurally, the mammalian BBB is quite different from the *Drosophila* BBB. The mammalian BBB is composed of tight junction forming endothelial cells and basement membrane secreting pericytes (Armulik et al., 2010). Astrocyte endfeet then surround the pericytes and endothelial cells (Bernacki et al., 2008). Yet, despite the starkly different compositions, the *Drosophila* and mammalian BBB functions in a highly analogous manner.

Additionally, a series of recent papers show the SPG act as a niche for neuroblast reactivation, division and survival (Speder and Brand 2014; Bailey et al. 2015; Volkenhoff et al. 2015). Neuroblast reactivation during larval development is a consequence of calcium oscillations in the SPG that are coordinated by gap junctions (Speder and Brand, 2014). These calcium oscillations lead to the production and release of insulin-like peptides resulting in neuroblast reactivation (Chell and Brand, 2010; Sousa-Nunes et al., 2011). Incredibly, the SPG are also able to protect neuroblasts from hypoxia and oxidative stress by producing lipid droplets (Bailey et al., 2015). Polyunsaturated fatty acids inside of lipid droplets pose less of a threat to both the niche SPG and neuroblasts because they are less likely to undergo peroxidation than if they were on the cell membranes (Bailey et al., 2015). Finally, studies of metabolic coupling between surface glia and neurons revealed that glial glycolysis is crucial to neuronal survival (Volkenhoff et al., 2015).

As briefly discussed in “Specialized functions of polyploid cells”, our lab identified SPG as polyploid throughout the nervous system (Unhavaithaya and Orr-Weaver, 2012). In this study, Unhavaithaya found that increased SPG ploidy was accompanied by increased cell size. Additionally, he demonstrated that polyploid SPG are required for a functional BBB because when ploidy is reduced, there are visible breaks in septate junction markers, and the BBB is no longer functional (Unhavaithaya and Orr-Weaver, 2012). Unhavaithaya hypothesized that ploidy reduction was detrimental to BBB function due to the corresponding reduced SPG cell size. This hypothesis was tested by attempting to rescue the BBB defect by either increasing SPG cell size by overexpressing the oncogene *dMyc*, or by inhibiting neuronal growth by amino acid deprivation in a reduced SPG ploidy background. Strikingly, these reciprocal tests both rescued the BBB defect, suggesting increased SPG cell size is required to accommodate the growing neuronal mass.

This study also found that SPG ploidy is actively regulated by the underlying neuronal mass. Specifically, the *aurora-A* mutant that has increased brain volume (Wang et al., 2006) was used to increase the neuronal mass to determine if and how SPG cells respond. SPG responded by increasing in both SPG ploidy and cell size to accommodate the increased neuronal mass, retaining a functional BBB (Unhavaithaya and Orr-Weaver, 2012). Unhavaithaya’s finding that both endocycling and endomitotic SPG are present in the same brain lobe raises many questions about the properties of endomitotic SPG as well as developmental control of these variant cell cycles.

Wrapping glia of the PNS

The three glial layers present in the PNS are the PG, SPG, and WG. As in the CNS, the PG and SPG form a barrier excluding the hemolymph from inhibiting neural activity. In addition to being protected from the potassium rich hemolymph by the BNB, axons are further ensheathed by WG. Through lineage tracing, the Altenhein lab determined that there are three wrapping glia per nerve and that they do not divide during larval development (von Hilchen et al., 2013). These three nerves have been named WG1, WG5, and WG9 based on their location along the nerve. WG1 is present in the NER while WG5 and WG9 are located in the MFA.

During late embryonic stages, WG contact sensory and motor axon fascicles, but it is not until late second instar that the WG begin to ensheath axons individually (Stork et al., 2008; Matzat et al., 2015). Wrapping glia's ability to wrap axons occurs throughout development in a continuous and progressive manner (Figure 1-5) (Matzat et al., 2015). The Klämbt lab has coined the term "wrapping index" to describe the percentage of axons that are individually ensheathed by WG. They found that the distal NER of the peripheral nerves of a wild-type animal have an average wrapping index of 19%, meaning 19% of axons are individually wrapped. The extent of wrapping in other regions of the peripheral nerves has not been analyzed.

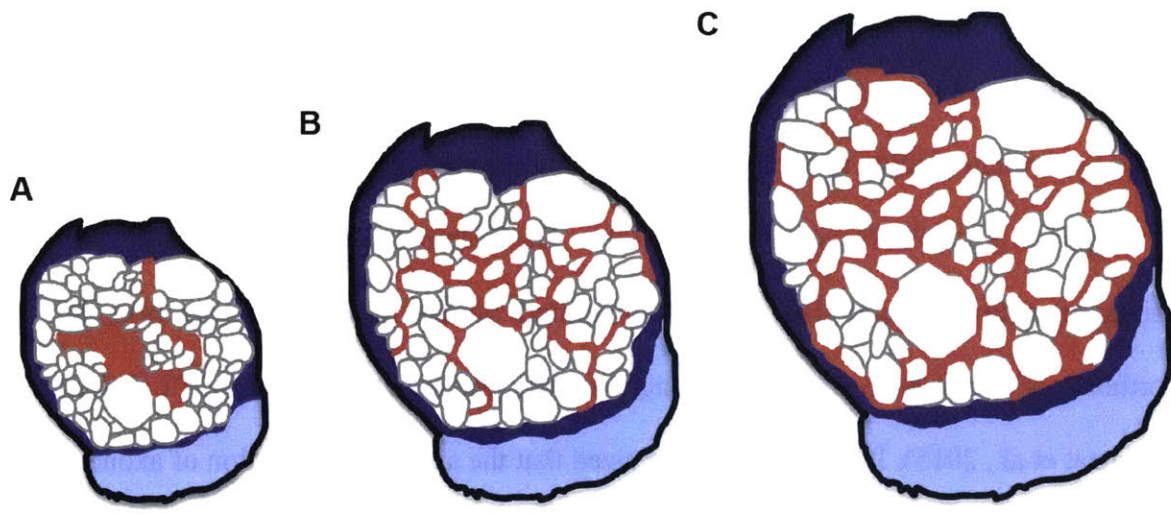
Drosophila do not myelinate neurons, and the majority of myelin ortholog genes are absent in the genome (Freeman and Doherty, 2006). However, the intricate ensheathment by the WG as well as the outer surface glia provide a sufficient amount of axonal insulation. Interestingly, the mutant *swiss cheese* leads to hyperwrapping of axons and leads to neurodegeneration (Dutta et al., 2016).

Wrapping glia resemble non-myelinating Schwann cells of the mammalian PNS. Non-myelinating Schwann cells, or Remak fibers, ensheath axons in small Remak bundles, but do not

Figure 1-5. Wrapping glia ensheathment of axons is a continuous and progressive process.

Neural lamella is shown in black, perineurial glia in blue, SPG in purple, WG in red, and axons in white with a gray outline. (A) In first larval instar, wrapping glia contact axons but do not yet individually ensheath axons. (B) By second larval instar, wrapping glia have extended their membranes and have begun to individually wrap axons. (C) By third instar approximately 19% of axons are individually ensheathed, while the remaining are wrapped in bundles. Note: these schematics are not to scale. Adapted from Stork 2008 and Maztat 2015.

Figure 1-5



form multiple layers around the axons as myelinating Schwann cells do. Receptor tyrosine kinase activity regulates axonal wrapping in Schwann cells. Specifically, axonally derived *neuregulin-1* (*nrg-1*) type III leads to differentiation of the Schwann cell lineage through binding to ErbB receptor tyrosine kinases (Michailov et al., 2004; Taveggia et al., 2005; Nave and Trapp, 2008). The Klämbt lab recently elucidated the signaling pathway required for WG differentiation. Similar to Schwann cells, *vein*, the ortholog of mammalian *nrg1*, is cell autonomously provided to activate EGFR signaling (Matzat et al., 2015). It has been hypothesized that the autocrine activation of axonal wrapping may be an evolutionary conserved mechanism because denervated Schwann cells initiate remyelination by expressing *Nrg1* (Stassart et al., 2012; Matzat et al., 2015).

Outlook

Recent research has focused on a longstanding issue in biology, producing a new appreciation of the strategy of implementing polyploidization. Systematic examination of the ploidy of differentiated tissues across the plant and animal kingdoms is likely to uncover additional examples and functions for which increased ploidy provides an advantage, as well as potential limitations. It will be particularly intriguing to reassess the ploidy of Purkinje cells as well as to examine ploidy levels in other mammalian nervous system cells types to see if ploidy utilization by the nervous system is universal across species.

In addition to these developmental insights, the field is now poised with powerful new tools to answer key mechanistic questions, such as why does increased ploidy cause an increase in cell size? Does polyploidy confer a metabolic advantage? Is there a

minimal karyoplasmic ratio and, if so, why? What are the properties of endomitotic SPG? How are transitions into the endocycle or endomitosis controlled in different developmental contexts? And what are the mechanisms and roles for differential DNA replication? It will be exciting to watch the answers to these questions emerge in different organisms.

Summary of thesis

This thesis investigates the regulation of variant cell cycles that contribute to SPG polyploidy throughout *Drosophila* larval development and identifies and characterizes a second polyploid nervous system cell type in the PNS. We first examine how the variant cell cycles the endocycle and endomitosis are differentially controlled in SPG cells, which use both variants to grow. We experimentally alter the ratio of endocycling to endomitotic SPG in the brain lobes by perturbing the Notch signaling pathway and the String Cdc25 phosphatase. Our findings provide evidence showing endomitotic SPG are capable of achieving higher ploidy and greater cell size compared to endocycling cells and are critical for BBB function.

Second, we explore how wrapping glia cells are able to ensheath axons given the extreme hypertrophy of the peripheral nerves throughout larval development. We uncover that WG ploidy correlates with nerve length and that ablating WG ploidy leads to defective axonal wrapping. We then investigate whether the three WG cells differentially contribute to overall ploidy and examine the extent of axonal wrapping throughout the peripheral nerves. Our findings identify wrapping glia as a second polyploid nervous system cell type and shed light on how wrapping glia are able to

ensheath axons.

REFERENCES

- Allen NJ, Barres BA. 2009. Glia — More Than Just Brain Glue. *Nat. Neurosci.* **457**: 675-677.
- Anatskaya OV, Vinogradov AE. 2010. Somatic Polyploidy Promotes Cell Function under Stress and Energy Depletion: Evidence from Tissue-Specific Mammal Transcriptome. *Funct Integr Genomics* **10**: 433-446.
- Armulik A, Genové G, Mäe M, Nisancioglu MH, Wallgard E, Niaudet C, He L, Norlin J, Lindblom P, Strittmatter K et al. 2010. Pericytes Regulate the Blood–Brain Barrier. *Nature* **468**: 557-561.
- Bailey AP, Koster G, Guillermier C, Hirst EM, MacRae JI, Lechene CP, Postle AD, Gould AP. 2015. Antioxidant Role for Lipid Droplets in a Stem Cell Niche of *Drosophila*. *Cell* **163**: 340-353.
- Bainton RJ, Tsai LT, Schwabe T, DeSalvo M, Gaul U, Heberlein U. 2005. *moody* Encodes Two GPCRs That Regulate Cocaine Behaviors and Blood-Brain Barrier Permeability in *Drosophila*. *Cell* **123**: 145-156.
- Banerjee MR, Wagner JE, Kinder DL. 1971. DNA Synthesis in the Absence of Cell Reproduction During Functional Differentiation of Mouse Mammary Gland. *Life Sci.* **10**: 867-877.
- Banerjee S, Bhat MA. 2008. Glial Ensheathment of Peripheral Axons in *Drosophila*. *J. Neurosci. Res.* **86**: 1189-1198.
- Barlow PW, Sherman MI. 1974. Cytological Studies on the Organization of DNA in Giant Trophoblast Nuclei of the Mouse and the Rat. *Chromosoma* **47**: 119-131.
- Belyakin SN, Christophides GK, Alekseyenko AA, Kriventseva EV, Belyaeva ES, Nanayev RA, Makunin IV, Consortium HFA, Kafatos FC, Zhimulev IF. 2005. Genomic Analysis of *Drosophila* Chromosome Underreplication Reveals a Link between Replication Control and Transcriptional Territories. *Proc. Natl. Acad. Sci. USA* **102**: 8269-8274.
- Bernacki J, Dobrowolska A, Nierwinska K, Malecki A. 2008. Physiology and Pharmacological Role of the Blood-Brain Barrier. *Pharmacol Rep* **60**: 600-622.
- Boudolf V, Lammens T, Boruc J, Van Leene J, Van Den Daele H, Maes S, Van Isterdael G, Russinova E, Kondorosi E, Witters E et al. 2009. CDKB1;1 Forms a Functional Complex with CYCA2;3 to Suppress Endocycle Onset. *Plant Physiol.* **150**: 1482-1493.
- Bourdon M, Pirrello J, Cheniclet C, Coriton O, Bourge M, Brown S, Moise A, Peypelut M, Rouyere V, Renaudin JP et al. 2012. Evidence for Karyoplasmic Homeostasis During Endoreduplication and a Ploidy-Dependent Increase in Gene Transcription During Tomato Fruit Growth. *Development* **139**: 3817-3826.
- Breuer C, Braidwood L, Sugimoto K. 2014. Endocycling in the Path of Plant Development. *Curr. Opin. Plant Biol.* **17**: 78-85.
- Breuer C, Ishida T, Sugimoto K. 2010. Developmental Control of Endocycles and Cell Growth in Plants. *Curr. Opin. Plant Biol.* **13**: 654-660.

- Brodsky VJ, Marshak TL, Mares V, Lodin Z, Fulop Z, Lebedev EA. 1979. Constancy and Variability in the Content of DNA in Cerebellar Purkinje Cell Nuclei. *Histochemistry* **59**: 233-248.
- Buntrock L, Marec F, Krueger S, Traut W. 2012. Organ Growth without Cell Division: Somatic Polyploidy in a Moth, *Ephestia kuehniella*. *Genome* **55**: 755-763.
- Caro E, Desvoyes B, Ramirez-Parra E, Sanchez MdP, Gutierrez C. 2008. Endoreduplication Control During Plant Development. *SEB Exp Biol Ser* **59**: 167-187.
- Cavalier-Smith, T. 1985. Cell volume and the evolution of eukaryotic genome size in *The Evolution of Genome Size* (ed. T. Cavalier-Smith), pp. 105-185. John Wiley and Sons.
- Chell JM, Brand AH. 2010. Nutrition-Responsive Glia Control Exit of Neural Stem Cells from Quiescence. *Cell* **143**: 1161-1173.
- Chen HZ, Ouseph MM, Li J, Pecot T, Chokshi V, Kent L, Bae S, Byrne M, Duran C, Comstock G et al. 2012. Canonical and Atypical E2Fs Regulate the Mammalian Endocycle. *Nat. Cell Biol.* **14**: 1192-1202.
- Chevalier C, Bourdon M, Pirrello J, Cheniclet C, Gévaudant F, Frangne N. 2013. Endoreduplication and Fruit Growth in Tomato: Evidence in Favour of the Karyoplasmic Ratio Theory. *J. Exp. Bot.* **65**: 2731-2746.
- Cho EH, Nijhout HF. 2013. Development of Polyploidy of Scale-Building Cells in the Wings of *Manduca sexta*. *Arthropod Struct. Dev.* **42**: 37-46.
- Churchman ML, Brown ML, Kato N, Kirik V, Hulskamp M, Inze D, De Veylder L, Walker JD, Zheng Z, Oppenheimer DG et al. 2006. Siamese, a Plant-Specific Cell Cycle Regulator, Controls Endoreplication Onset in *Arabidopsis thaliana*. *The Plant Cell Online* **18**: 3145-3157.
- Conklin EG. 1912. Cell Size and Nuclear Size. *J. Exp. Zool.* **12**: 1-98.
- Cross JC. 2005. How to Make a Placenta: Mechanisms of Trophoblast Cell Differentiation in Mice--a Review. *Placenta* **26 Suppl A**: S3-9.
- Das SK. 2009. Cell Cycle Regulatory Control for Uterine Stromal Cell Decidualization in Implantation. *Reproduction* **137**: 889-899.
- De Veylder L, Beeckman T, Beemster GTS, de Almeida Engler J, Ormenese S, Maes S, Naudts M, Van Der Schueren E, Jacquard A, Engler G et al. 2002. Control of Proliferation, Endoreduplication and Differentiation by the Arabidopsis E2Fa-DPa Transcription Factor. *EMBO J.* **21**: 1360-13
- Deng WM, Althausen C, Ruohola-Baker H. 2001. Notch-Delta Signaling Induces a Transition from Mitotic Cell Cycle to Endocycle in *Drosophila* Follicle Cells. *Development* **128**: 4737-4746.
- Desalvo MK, Mayer N, Mayer F, Bainton RJ. 2011. Physiologic and Anatomic Characterization of the Brain Surface Glia Barrier of *Drosophila*. *Glia* **59**: 1322-1340.
- Duncan AW. 2013. Aneuploidy, Polyploidy and Ploidy Reversal in the Liver. *Semin Cell Dev Biol.* **24**: 347-356.
- Duncan AW, Hanlon Newell AE, Bi W, Finegold MJ, Olson SB, Beaudet AL, Grompe M. 2012. Aneuploidy as a Mechanism for Stress-Induced Liver Adaptation. *J. Clin. Investig* **122**: 3307-3315.

- Dutta S, Rieche F, Eckl N, Duch C, Kretzschmar D. 2016. Glial Expression of Swiss Cheese (SWS), the *Drosophila* Orthologue of Neuropathy Target Esterase (NTE), Is Required for Neuronal Ensheathment and Function. *Dis. Models Mech* **9**: 283-294.
- Edgar BA, Orr-Weaver TL. 2001. Endoreplication Cell Cycles: More for Less. *Cell* **105**: 297-306.
- Edgar BA, Zielke N, Gutierrez C. 2014. Endocycles: A Recurrent Evolutionary Innovation for Post-Mitotic Cell Growth. *Nat. Rev. Mol. Cell Biol.* **15**: 197-210.
- Engel FB, Schebesta M, Keating MT. 2006. Anillin Localization Defect in Cardiomyocyte Binucleation. *J. Mol. Cell. Cardiol.* **41**: 601-612.
- Fededa JP, Gerlich DW. 2012. Molecular Control of Animal Cell Cytokinesis. *Nat. Cell Biol.* **14**: 440-447.
- Flemming AJ, Shen ZZ, Cunha A, Emmons SW, Leroi AM. 2000. Somatic Polyploidization and Cellular Proliferation Drive Body Size Evolution in Nematodes. *Proc. Natl. Acad. Sci. USA* **97**: 5285-5290.
- Fox DT, Duronio RJ. 2013. Endoreplication and Polyploidy: Insights into Development and Disease. *Development* **140**: 3-12.
- Fox DT, Gall JG, Spradling AC. 2010. Error-Prone Polyploid Mitosis During Normal *Drosophila* Development. *Genes Dev.* **24**: 2294-2302.
- Frawley LE, Orr-Weaver TL. 2015. Polyploidy. *Curr. Biol.* **25**: R353-358.
- Freeman MR. 2015. *Drosophila* central Nervous System Glia. *Cold Spring Harb Perspect Biol.* **7**: a020552.
- Freeman MR, Doherty J. 2006. Glial Cell Biology in *Drosophila* and Vertebrates. *Trends Neurosci* **29**: 82-90.
- Gandarillas A, Molinuevo R, Sanz-Gómez N. 2018. Mammalian Endoreplication Emerges to Reveal a Potential Developmental Timer. *Cell Death Differ.* **25**: 1-6.
- Gao Y, Smith E, Ker E, Campbell P, Cheng E-C, Zou S, Lin S, Wang L, Halene S, Krause DS. 2012. Role of RhoA-Specific Guanine Exchange Factors in Regulation of Endomitosis in Megakaryocytes. *Dev. Cell* **22**: 573-584.
- Gatti M, Baker BS. 1989. Genes Controlling Essential Cell-Cycle Functions in *Drosophila melanogaster*. *Genes Dev.* **3**: 438-453.
- Gentric G, Desdouets C. 2014. Polyploidization in Liver Tissue. *Am. J. Pathol* **184**: 322-331.
- Gentric G, Desdouets C, Celton-Morizur S. 2012. Hepatocytes Polyploidization and Cell Cycle Control in Liver Physiopathology. *Int J Hepatol.* **2012**: 282430.
- Glotzer M. 2001. Animal Cell Cytokinesis. *Annu. Rev. Cell Dev. Biol.* **27**: 351-386.
- Haga S, Ozaki M, Inoue H, Okamoto Y, Ogawa W, Takeda K, Akira S, Todo S. 2008. The Survival Pathways Phosphatidylinositol-3 Kinase (PI3-K)/Phosphoinositide-Dependent Protein Kinase 1 (Pdk1)/Akt Modulate Liver Regeneration through Hepatocyte Size Rather Than Proliferation. *Hepatology* **49**: 204-214.
- Hammond MP, Laird CD. 1985a. Chromosome Structure and DNA Replication in Nurse and Follicle Cells of *Drosophila melanogaster*. *Chromosoma* **91**: 267-278.
- Hammond MP, Laird CD. 1985b. Control of DNA Replication and Spatial Distribution of Defined DNA Sequences in Salivary Gland Cells of *Drosophila melanogaster*. *Chromosoma* **91**: 279-286.

- Hannibal RL, Chuong EB, Rivera-Mulia JC, Gilbert DM, Valouev A, Baker JC. 2014. Copy Number Variation Is a Fundamental Aspect of the Placental Genome. *PLoS Genet.* **10**: e1004290.
- Hassel C, Zhang B, Dixon M, Calvi BR. 2014. Induction of Endocycles Represses Apoptosis Independently of Differentiation and Predisposes Cells to Genome Instability. *Development* **141**: 112-123.
- Hatan M, Shinder V, Israeli D, Schnorrer F, Volk T. 2011. The Drosophila Blood Brain Barrier Is Maintained by GPCR-Dependent Dynamic Actin Structures. *J. Cell Biol.* **192**: 307-319.
- Hattori N, Davies TC, Anson-Cartwright L, Cross JC. 2000. Periodic Expression of the Cyclin-Dependent Kinase Inhibitor P57Kip2 in Trophoblast Giant Cells Defines a G2-Like Gap Phase of the Endocycle. *Mol. Biol. Cell* **11**: 1037-1045.
- Herget GW, Neuburger M, Plagwitz R, Adler CP. 1997. DNA Content, Ploidy Level and Number of Nuclei in the Human Heart after Myocardial Infarction. *Cardiovasc Res* **36**: 45-51.
- Hosoya T, Takizawa K, Nitta K, Hotta Y. 1995. Glial Cells Missing: A Binary Switch between Neuronal and Glial Determination in Drosophila. *Cell* **82**: 1025-1036.
- Hua BL, Orr-Weaver TL. 2017. DNA Replication Control During Drosophiladevelopment: Insights into the Onset of S Phase, Replication Initiation, and Fork Progression. *Genetics* **207**: 29-47.
- Huber MD, Gerace L. 2007. The Size-Wise Nucleus: Nuclear Volume Control in Eukaryotes. *J. Cell Biol.* **179**: 583-584.
- Jones BW, Fetter RD, Tear G, Goodman CS. 1995. Glial Cells Missing: A Genetic Switch That Controls Glial Versus Neuronal Fate. *Cell* **82**: 1013-1023.
- Kim J, Jones BW, Zock C, Chen Z, Wang H, Goodman CS, Anderson DJ. 1998. Isolation and Characterization of Mammalian Homologs of the Drosophila Gene Glial Cells Missing. *Proc. Natl. Acad. Sci. USA* **95**: 12364-12369.
- Lammens T, Boudolf V, Kheibarshekan L, Zalmas LP, Gaamouche T, Maes S, Vanstraelen M, Kondorosi E, La Thangue NB, Govaerts W et al. 2008. Atypical E2F Activity Restrains APC/CCCS52A2 Function Obligatory for Endocycle Onset. *Proc. Natl. Acad. Sci. USA* **105**: 14721-14726.
- Lapham LW. 1968. Tetraploid DNA Content of Purkinje Neurons of Human Cerebellar Cortex *Science* **159**: 310-312.
- Larson-Rabin Z, Li Z, Masson PH, Day CD. 2008. FZR2/CCS52A1 Expression Is a Determinant of Endoreduplication and Cell Expansion in Arabidopsis. *Plant Physiol.* **149**: 874-884.
- Lasek RJ, Dower WJ. 1971. *Aplysia californica*: Analysis of Nuclear DNA in Individual Nuclei of Giant Neurons *Science* **172**: 278-280.
- Leiserson WM, Harkins EW, Keshishian H. 2000. Fray, a Drosophila Serine/Threonine Kinase Homologous to Mammalian Pask, Is Required for Axonal Ensheathment. *Neuron* **28**: 1-14.
- Lilly MA, Spradling AC. 1996. The Drosophila Endocycle Is Controlled by Cyclin E and Lacks a Checkpoint Ensuring S-Phase Completion. *Genes Dev.* **10**: 2514-2526.
- Lopez-Schier H, St Johnston D. 2001. Delta Signaling from the Germ Line Controls the Proliferation and Differentiation of the Somatic Follicle Cells During Drosophila Oogenesis. *Genes Dev.* **15**: 1393-1405.

- Losick VP, Fox DT, Spradling AC. 2013. Polyploidization and Cell Fusion Contribute to Wound Healing in the Adult *Drosophila* Epithelium. *Curr. Biol.* **23**: 2224-2232.
- Losick VP, Jun AS, Spradling AC. 2016. Wound-Induced Polyploidization: Regulation by Hippo and Jnk Signaling and Conservation in Mammals. *PLoS One* **11**: e0151251.
- MacAuley A, Cross JC, Werb Z. 1998. Reprogramming the Cell Cycle for Endoreduplication in Rodent Trophoblast Cells. *Mol. Biol. Cell* **9**: 795-807.
- Mann DMA, Yates PO, Barton CM. 1978. The DNA Content of Purkinje Cells in Mammals. *J. Comp. Neur.* **180**: 345-348.
- Manuelidis L, Manuelidis EE. 1974. On the DNA Content of Cerebellar Purkinje Cells *in vivo* and *in vitro*. *Exp. Neurol.* **43**: 192-206.
- Margall-Ducos G, Celton-Morizur S, Couton D, Bregerie O, Desdouets C. 2007. Liver Tetraploidization Is Controlled by a New Process of Incomplete Cytokinesis. *J. Cell Sci.* **120**: 3633-3639.
- Matzat T, Sieglitz F, Kottmeier R, Babatz F, Engelen D, Klambt C. 2015. Axonal Wrapping in the *Drosophila* PNS Is Controlled by Glia-Derived Neuregulin Homolog Vein. *Development* **142**: 1336-1345.
- Meckert P, Rivello H, Vigliano C, Gonzalez P, Favaloro R, Laguens R. 2005. Endomitosis and Polyploidization of Myocardial Cells in the Periphery of Human Acute Myocardial Infarction. *Cardiovasc Res* **67**: 116-123.
- Mendell JE, Clemens KD, Choat JH, Angert ER. 2008. Extreme Polyploidy in a Large Bacterium. *Proc. Natl. Acad. Sci. USA* **105**: 6730-6734.
- Michailov GV, Sereda MW, Brinkmann BG, M FT, Haug B, Birchmeier C, Role L, Lai C, Schwab MH, Nave K-A. 2004. Axonal Neuregulin-1 Regulated Myelin Sheath Thickness. *Science* **304**: 700-703.
- Miyaoka Y, Ebato K, Kato H, Arakawa S, Shimizu S, Miyajima A. 2012. Hypertrophy and Unconventional Cell Division of Hepatocytes Underlie Liver Regeneration. *Curr. Biol.* **22**: 1166-1175.
- Mollova M, Bersell K, Walsh S, Savla J, Das LT, Park S-Y, Silberstein LE, dos Remedios CG, Graham D, Colan S et al. 2013. Cardiomyocyte Proliferation Contributes to Heart Growth in Young Humans. *Proc. Natl. Acad. Sci. USA* **110**: 1446-1451.
- Nagata Y, Muro Y, Todokoro K. 1997. Thrombopoietin-Induced Polyploidization of Bone Marrow Megakaryocytes Is Due to a Unique Regulatory Mechanism in Late Mitosis. *J. Cell Biol.* **139**: 449-457.
- Nagl W. 1978. Endopolyploidy and polytene in differentiation and evolution: Towards and understanding of quantitative variation of nuclear DNA in ontogeny and phylogeny. North-Holland Publishing Company, Amsterdam, Netherlands.
- Narbonne-Reveau K, Senger S, Pal M, Herr A, Richardson HE, Asano M, Deak P, Lilly MA. 2008. APC/CFzr/Cdh1 Promotes Cell Cycle Progression During the *Drosophila* Endocycle. *Development* **135**: 1451-1461.
- Nave K-A, Trapp BD. 2008. Axon-Glial Signaling and the Glial Support of Axon Function. *Annu. Rev. Neurosci.* **31**: 535-561.
- Neumann FR, Nurse P. 2007. Nuclear Size Control in Fission Yeast. *J. Cell Biol.* **179**: 593-600.

- Nordman J, Li S, Eng T, MacAlpine D, Orr-Weaver TL. 2011. Developmental Control of the DNA Replication and Transcription Programs. *Genome Res.* **21**: 175-181.
- Nordman JT, Kozhevnikova EN, Verrijzer CP, Pindyurin AV, Andreyeva EN, Shloma VV, Zhimulev IF, Orr-Weaver TL. 2014. DNA Copy-Number Control through Inhibition of Replication Fork Progression. *Cell Rep.* **9**: 841-849.
- Orr-Weaver TL. 2015. When Bigger Is Better: The Role of Polyploidy in Organogenesis. *Trends Genet.* **31**: 307-315.
- Pandit SK, Westendorp B, de Bruin A. 2013. Physiological Significance of Polyploidization in Mammalian Cells. *Trends Cell Biol* **23**: 556-566.
- Pandit SK, Westendorp B, Nantasanti S, van Liere E, Tooten PC, Cornelissen PW, Toussaint MJ, Lamers WH, de Bruin A. 2012. E2f8 Is Essential for Polyploidization in Mammalian Cells. *Nat. Cell Biol.* **14**: 1181-1191.
- Pereanu W, Shy D, Hartenstein V. 2005. Morphogenesis and Proliferation of the Larval Brain Glia in *Drosophila*. *Dev Biol* **283**: 191-203.
- Ravid K, Lu J, Zimmet JM, Jones MR. 2002. Roads to Polyploidy: The Megakaryocyte Example. *J. Cell Physiol.* **190**: 7-20.
- Rios AC, Fu NY, Jamieson PR, Pal B, Whitehead L, Nicholas KR, Lindeman GJ, Visvader JE. 2016. Essential Role for a Novel Population of Binucleated Mammary Epithelial Cells in Lactation. *Nat. Commun.* **7**: 1-12.
- Roeder AH, Chickarmane V, Cunha A, Obara B, Manjunath BS, Meyerowitz EM. 2010. Variability in the Control of Cell Division Underlies Sepal Epidermal Patterning in *Arabidopsis thaliana*. *PLoS Biol.* **8**: e1000367.
- Roeder AH, Cunha A, Ohno CK, Meyerowitz EM. 2012. Cell Cycle Regulates Cell Type in the *Arabidopsis* Sepal. *Development* **139**: 4416-4427.
- Roodbarkerlari F, Bramsiepe J, Weinl C, Marquardt S, Novak B, Jakoby MJ, Lechner E, Genschik P, Schnittger A. 2010. Cullin 4-Ring Finger-Ligase Plays a Key Role in the Control of Endoreplication Cycles in *Arabidopsis* Trichomes. *Proc. Natl. Acad. Sci. USA* **107**: 15275-15280.
- Rossant J, Cross JC. 2001. Placental Development: Lessons from Mouse Mutants. *Nat. Rev. Genetics* **2**: 538-548.
- Royzman I, Austin RJ, Bosco G, Bell SP, Orr-Weaver TL. 1999. ORC Localization in *Drosophila* Follicle Cells and the Effects of Mutations in *de2f* and *ddp*. *Genes Dev.* **13**: 827-840.
- Schnittger A, Schobinger U, Stierhof Y-D, Hulskamp M. 2002. Ectopic B-Type Cyclin Expression Induces Mitotic Cycles in Endoreduplicating *Arabidopsis* Trichomes. *Curr. Biol.* **12**: 415-420.
- Schoenfelder KP, Montague RA, Paramore SV, Lennox AL, Mahowald AP, Fox DT. 2014. Indispensable Pre-Mitotic Endocycles Promote Aneuploidy in the *Drosophila* Rectum. *Development* **141**: 3551-3560.
- Schwabe T, Bainton RJ, Fetter RD, Heberlein U, Gaul U. 2005. GPCR Signaling Is Required for Blood-Brain Barrier Formation in *Drosophila*. *Cell* **123**: 133-144.
- Senyo SE, Steinhauser ML, Pizzimenti CL, Yang VK, Cai L, Wang M, Wu TD, Guerquin-Kern JL, Lechene CP, Lee RT. 2013. Mammalian Heart Renewal by Pre-Existing Cardiomyocytes. *Nature* **493**: 433-436.
- Sepp KJ, Schulte J, Auld VJ. 2000. Developmental Dynamics of Peripheral Glia in *Drosophila melanogaster*. *Glia* **30**: 122-133.

- Sepp KJ, Schulte J, Auld VJ. 2001. Peripheral Glia Direct Axon Guidance across the CNS/PNS Transition Zone. *Dev Biol* **238**: 47-63.
- Shcherbata HR, Althausen C, Findley SD, Ruohola-Baker H. 2004. The Mitotic-to-Endocycle Switch in *Drosophila* Follicle Cells Is Executed by Notch-Dependent Regulation of G1/S, G2/M and M/G1 Cell-Cycle Transitions. *Development* **131**: 3169-3181.
- Sher N, Bell GW, Li S, Nordman J, Eng T, Eaton ML, MacAlpine DM, Orr-Weaver TL. 2012. Developmental Control of Gene Copy Number by Repression of Replication Initiation and Fork Progression. *Genome Res.* **22**: 64-75.
- Sher N, Von Stetina JR, Bell G, Matsuura S, Ravid K, Orr-Weaver TL. 2013. Fundamental Differences in Endoreplication in Mammals and *Drosophila* Revealed by Analysis of Endocycling and Endomitotic Cells. *Proc. Natl. Acad. Sci. USA* **110**: 9368-9373.
- Sigrist SJ, Lehner CF. 1997. *Drosophila* Fizzy-Related Down-Regulates Mitotic Cyclins and Is Required for Cell Proliferation Arrest and Entry into Endocycles. *Cell* **90**: 671-681.
- Silies M, Yuva Y, Engelen D, Aho A, Stork T, Klambt C. 2007. Glial Cell Migration in the Eye Disc. *J. Neurosci.* **27**: 13130-13139.
- Smith AV, Orr-Weaver TL. 1991. The Regulation of the Cell Cycle During *Drosophila* Embryogenesis: The Transition to Polyteny. *Development* **112**: 997-1008.
- Song AH, Wang D, Chen G, Li Y, Luo J, Duan S, Poo MM. 2009. A Selective Filter for Cytoplasmic Transport at the Axon Initial Segment. *Cell* **136**: 1148-1160.
- Soonpaa MH, Kim KK, Pajak L, Franklin M, Field LJ. 1996. Cardiomyocyte DNA Synthesis and Binucleation During Murine Development. *Am. J. Physiol.* **271**: H2183-2189.
- Sousa-Nunes R, Yee LL, Gould AP. 2011. Fat Cells Reactivate Quiescent Neuroblasts Via Tor and Glial Insulin Relays in *Drosophila*. *Nature* **471**: 508-512.
- Speder P, Brand AH. 2014. Gap Junction Proteins in the Blood-Brain Barrier Control Nutrient-Dependent Reactivation of *Drosophila* Neural Stem Cells. *Dev. Cell* **30**: 309-321.
- Spradling AC. 1981. The Organization and Amplification of Two Chromosomal Domains Containing *Drosophila* Chorion Genes. *Cell* **27**: 193-201.
- Spradling AC. 1993. Developmental genetics of oogenesis in *The Development of Drosophila melanogaster* (eds. M. Bate and A. Martinez Arias), pp. 1-70. Cold Spring Harbor, NY: Cold Spring Harbor Laboratory Press.
- Starnes AC, Huisinigh C, McGwin G, Sloan KR, Ablonczy Z, Smith RT, Curcio CA, Ach T. 2016. Multi-Nucleate Retinal Pigment Epithelium Cells of the Human Macula Exhibit a Characteristic and Highly Specific Distribution. *Vis Neurosci.* **33**: 583-514.
- Stassart RM, Fledrich R, Velanac V, Brinkmann BG, Schwab MH, Meijer D, Sereda MW, Nave K-A. 2012. A Role for Schwann Cell-Derived Neuregulin-1 in Remyelination. *Nat. Neurosci.* **16**: 48-54.
- Stork T, Bernardos R, Freeman MR. 2012. Analysis of Glial Cell Development and Function in *Drosophila*. *Cold Spring Harbor Protocols* **2012**: 1-17.
- Stork T, Engelen D, Krudewig A, Silies M, Bainton RJ, Klambt C. 2008. Organization and Function of the Blood-Brain Barrier in *Drosophila*. *J. Neurosci.* **28**: 587-597.

- Sun B, Xu P, Salvaterra PM. 1999. Dynamic Visualization of Nervous System in Live *Drosophila*. *Proc. Natl. Acad. Sci. USA* **96**: 110438-110443.
- Sun J, Deng W-M. 2007. Hindsight Mediates the Role of Notch in Suppressing Hedgehog Signaling and Cell Proliferation. *Dev. Cell* **12**: 431-442.
- Tamori Y, Deng W-M. 2013. Tissue Repair through Cell Competition and Compensatory Cellular Hypertrophy in Postmitotic Epithelia. *Dev. Cell* **25**: 350-363.
- Tanaka S, Kunath T, Hadjantonakis A-K, Nagy A, Rossant J. 1998. Promotion of Trophoblast Stem Cell Proliferation by Fgf4. *Science* **282**: 2072-2075.
- Taveggia C, Zanazzi G, Petrylak A, Yano H, Rosenbluth J, Einheber S, Xu X, Esper RM, Loeb JA, Shrager P et al. 2005. Neuregulin-1 Type III Determines the Ensheathment Fate of Axons. *Neuron* **47**: 681-694.
- Trakala M, Rodríguez-Acebes S, Maroto M, Symonds CE, Santamaría D, Ortega S, Barbacid M, Méndez J, Malumbres M. 2015. Functional Reprogramming of Polyploidization in Megakaryocytes. *Dev. Cell* **32**: 155-167.
- Ullah Z, de Renty C, DePamphilis ML. 2011. Checkpoint Kinase 1 Prevents Cell Cycle Exit Linked to Terminal Cell Differentiation. *Mol. Cell. Biol.* **31**: 4129-4143.
- Ullah Z, Kohn MJ, Yagi R, Vassilev LT, DePamphilis ML. 2008. Differentiation of Trophoblast Stem Cells into Giant Cells Is Triggered by P57/Kip2 Inhibition of Cdk1 Activity. *Genes Dev.* **22**: 3024-3036.
- Unhavaithaya Y, Orr-Weaver TL. 2012. Polyploidization of Glia in Neural Development Links Tissue Growth to Blood-Brain Barrier Integrity. *Genes Dev.* **26**: 31-36.
- Vanstraelen M, Baloban M, Da Ines O, Cultrone A, Lammens T, Boudolf V, Brown SC, De Veylder L, Mergaert P, Kondorosi E. 2009. APC/CCCS52A Complexes Control Meristem Maintenance in the Arabidopsis Root. *Proc. Natl. Acad. Sci. USA* **106**: 11806-11811.
- Vinogradov AE, Anatskaya OV, Kudryavtsev BN. 2001. Relationship of Hepatocyte Ploidy Levels with Body Size and Growth Rate in Mammals. *Genome / National Research Council Canada = Genome / Conseil national de recherches Canada* **44**: 350-360.
- Volkenhoff A, Weiler A, Letzel M, Stehling M, Klambt C, Schirmeier S. 2015. Glial Glycolysis Is Essential for Neuronal Survival in *Drosophila*. *Cell Metab.* **22**: 437-447.
- von Hilchen CM, Beckervordersandforth RM, Rickert C, Technau GM, Altenhein B. 2008. Identity, Origin, and Migration of Peripheral Glial Cells in the *Drosophila* Embryo. *Mech. Dev.* **125**: 337-352.
- von Hilchen CM, Bustos AE, Giangrande A, Technau GM, Altenhein B. 2013. Predetermined Embryonic Glial Cells Form the Distinct Glial Sheaths of the *Drosophila* Peripheral Nervous System. *Development* **140**: 3657-3668.
- Walker JD, Oppenheimer DG, Concienne J, Larkin JC. 2000. Siamese, a Gene Controlling the Endoreduplication Cell Cycle in *Arabidopsis thaliana* Trichomes. *Development* **127**: 3931-3940.
- Wang H, Somers GW, Bashirullah A, Heberlein U, Yu F, Chia W. 2006. Aurora-a Acts as a Tumor Suppressor and Regulates Self-Renewal of *Drosophila* Neuroblasts. *Genes Dev.* **20**: 3453-3463.
- Watson ED, Cross JC. 2005. Development of Structures and Transport Functions in the Mouse Placenta. *Physiology* **20**: 180-193.

- Weimann JM, Johansson CB, Trejo A, Blau HM. 2003. Stable Reprogrammed Heterokaryons Form Spontaneously in Purkinje Neurons after Bone Marrow Transplant. *Nat. Cell Biol.* **5**: 959-966.
- Wilson AA, Kotton DN. 2008. Another Notch in Stem Cell Biology: *Drosophila* Intestinal Stem Cells and the Specification of Cell Fates. *Bioessays* **30**: 107-109.
- Yarosh W, Spradling AC. 2014. Incomplete Replication Generates Somatic DNA Alterations within *Drosophila* polytene Salivary Gland Cells. *Genes Dev.* **28**: 1840-1855.
- Yoshimura T, Rasband MN. 2014. Axon Initial Segments: Diverse and Dynamic Neuronal Compartments. *Curr. Opin. Neurobiol.* **27**: 96-102.
- Zanet J, Freije A, Ruiz M, Coulon V, Sanz JR, Chiesa J, Gandarillas A. 2010. A Mitosis Block Links Active Cell Cycle with Human Epidermal Differentiation and Results in Endoreplication. *PLoS One* **5**: e15701.
- Zhao XaA, Harashima H, Dissmeyer N, Pusch S, Weimer AK, Bramsiepe J, Bouyer D, Rademacher S, Nowack MK, Novak B et al. 2012. A General G1/S-Phase Cell-Cycle Control Module in the Flowering Plant *Arabidopsis thaliana*. *PLoS Genet.* **8**: e1002847.
- Zhimulev IF. 1974. Comparative Study of the Function of Polytene Chromosomes in Laboratory Stocks of *Drosophila melanogaster* and the L(3)TI Mutant (Lethal Tumorous Larvae) *Chromosoma* **46**: 59-76.
- Zielke N, Edgar BA, DePamphilis ML. 2013. Endoreplication. in *Cold Spring Harb Perspect Biol.* **5**: a012948-a012948.
- Zielke N, Kim KJ, Tran V, Shibutani ST, Bravo MJ, Nagarajan S, van Straaten M, Woods B, von Dassow G, Rottig C et al. 2011. Control of *Drosophila* Endocycles by E2F and CRL4(CDT2). *Nature* **480**: 123-127.
- Zybina T, Zybina E. 2005. Cell Reproduction and Genome Multiplication in the Proliferative and Invasive Trophoblast Cell Populations of Mammalian Placenta. *Cell Biol. Int.* **29**: 1071-1083.

Chapter Two:

Variant Cell Cycles Regulated by Notch Signaling Control Cell Size and Ensure a Functional Blood-Brain Barrier

Jessica R. Von Stetina^{1,2}, Laura E. Frawley^{1,2,3}, Yingdee Unhavaithaya⁴,
and Terry L. Orr-Weaver^{2,3}

Whitehead Institute² and Dept. of Biology, Massachusetts Institute of Technology³,
Cambridge, MA 02142; Decision Resources Group⁴, Burlington, MA 01803

This chapter was published: Von Stetina J.R., Frawley L.E., Unhavaithaya Y., Orr-Weaver T.L. 2018. Variant Cell Cycles Regulated by Notch Signaling Control Cell Size and Ensure a Functional Blood-Brain Barrier. *Development* **145**: dev157115-157126.

¹ These authors contributed equally to this work. Experiments and analyses in Figures 2-1 D,E third instar only, 2-3 C-E, 2-6 A-G, 2-8, 2-9 A-D, 2-11 G-L, 2-12 M, 2-13 A,C,E and Table 2-4 were performed by L.E.F. Experiments and analyses in Figures 2-2, 2-3A,B, 2-11A-F, 2-12 A-L and Tables 2-2 and 2-3, were performed by L.E.F. and J.V.S.

ABSTRACT

Regulation of cell size is crucial in development. In plants and animals two cell cycle variants are employed to generate large cells by increased ploidy: the endocycle and endomitosis. The rationale behind the choice of which of these cycles is implemented is unknown. We show that in the *Drosophila* nervous system the subperineurial glia (SPG) are unique in using both the endocycle and endomitosis to grow. In the brain, the majority of SPG initially endocycle, then switch to endomitosis during larval development. The Notch signaling pathway and the String Cdc25 phosphatase are crucial for the endocycle versus endomitosis choice, providing the means experimentally to change cells from one to the other. This revealed fundamental insights into the control of cell size and the properties of endomitotic cells. Endomitotic cells attain a higher ploidy and larger size than endocycling cells, and endomitotic SPG are necessary for the blood-brain barrier. Decreased Notch signaling promotes endomitosis even in the ventral nerve cord SPG that normally are mononucleate, but not in the endocycling salivary gland cells, revealing tissue-specific cell cycle responses.

INTRODUCTION

Regulation of cell size and thus tissue and organ size is crucial for proper body formation and function in development. In many developmental contexts the production of very large cells is achieved through polyploidy, an increase in DNA content (Orr-Weaver 2015). Polyploidy permits cells to attain sizes much larger than can result from growth alone. In plants and animals, polyploidy generally results from one of two cell cycle variant classes, the endocycle or endomitosis (Frawley and Orr-Weaver 2015). In the endocycle, DNA replication alternates with a gap phase in the absence of mitosis, yielding cells with a single, polyploid nucleus. Initially most commonly referred to as endoreduplication, the term endocycle has been used widely in the field for the past few decades to emphasize the cyclic nature of DNA replication and the crucial role of conserved cell cycle regulators (Fox and Duronio 2013; Edgar et al. 2014). Endomitosis classically was defined as mitosis occurring within an intact nuclear envelope. This occurs in a restricted number of cell types, typically found in insects (Nagl 1978). We and others have extended this term to include all cell cycle variants in which some aspects of mitosis such as anaphase A or even nuclear division occur in the absence of cytokinesis (Fox and Duronio 2013; Frawley and Orr-Weaver 2015). Thus whereas the endocycle produces mononucleate polyploid cells, endomitosis can produce mononucleate or multinucleate polyploid cells, depending on the specific form of endomitosis. Although increased ploidy leads to increased cell size, it is unclear what distinctions or advantages single versus multiple nuclei could impart.

In mammals both the endocycle and endomitosis are used; for example the placental trophoblast giant cells (TGCs) endocycle, whereas the blood megakaryocytes

(MgKs) endomitose. In TGCs, the increase in cell size driven by polyploidy is hypothesized to facilitate their function of providing a barrier between the maternal and embryonic tissues (Rossant and Cross 2001; Cross 2005; Watson and Cross 2005). Polyploidy leads to an increase in MgK cytoplasmic volume that permits adequate platelet production (Ravid et al. 2002). In *Drosophila*, many differentiated cell types become polyploid via the endocycle. Moreover, replicated sister chromatids are held in register to produce polytene chromosomes with stereotypic banding patterns. Increases in ploidy facilitate robust gene expression, as in the *Drosophila* germline nurse cells that synthesize and deposit maternal stores into the developing oocyte (Spradling 1993). Regulation of cell size by ploidy also dictates the size of anatomical structures produced by polyploid cells such as the bristles on the adult body (Salle et al. 2012).

Recently our understanding of this repertoire was expanded by our identification of a role for polyploidy in the *Drosophila* nervous system. The subperineurial glia (SPG) cells in the *Drosophila* larval brain, a subset of surface glia, do not increase in number during development, but rather increase their size by polyploidization (Unhavaithaya and Orr-Weaver 2012). The SPG are present throughout the nervous system: in the brain lobes, the ventral nerve cord (VNC), and the peripheral nerves (Limmer et al. 2014). SPG are fascinating cells that function both as the blood-brain barrier (BBB) and as a niche and energy metabolism center to control reactivation and division of the underlying neuroblasts (Bainton et al. 2005; Schwabe et al. 2005; Speder and Brand 2014; Bailey et al. 2015; Volkenhoff et al. 2015). Increased SPG cell size due to changes in ploidy is necessary to coordinate growth with increasing underlying neuronal mass in order to maintain the integrity of the BBB without disruption of the SPG envelope by cell division

and cytokinesis (Unhavaithaya and Orr-Weaver 2012). Interestingly, either decreases or increases in SPG ploidy lead to defects in the BBB (Li et al. 2017).

All of the previously characterized *Drosophila* tissues employ the endocycle to increase their ploidy and are mononucleate, with the exception of the binucleate cells of the male accessory gland (Edgar and Orr-Weaver 2001; Taniguchi et al. 2012). The SPG are unique because in the brain two types of SPG cells are observed: mononucleate and multinucleate (Unhavaithaya and Orr-Weaver 2012). Functional roles for these two SPG types are unknown, as is the cell cycle mechanism, developmental timing and regulation of their formation. The SPG provide the opportunity to investigate whether a specific cell type can undergo both the endocycle and endomitosis, to monitor the impact of these two variant cell cycles on increased cell size through cell ploidy, and to explore how signaling pathways affect the choice between the two.

RESULTS

Developmental cell cycle control in the SPG

The presence of both mono and multinucleate cells in the SPG of the third instar larval brain led us to hypothesize that two different types of variant cell cycles lead to increases in SPG ploidy (Unhavaithaya and Orr-Weaver 2012). Mononucleate SPG could result from an endocycle with solely gap and S phases, whereas multinucleate SPG could be the consequence of a form of endomitosis in which nuclear division occurs in the absence of cytokinesis. This is in contrast to the mononucleate SPG in the VNC and peripheral nervous system (PNS). Here we tested the hypothesis that the SPG in the brain lobe undergo two types of variant cell cycles.

We first investigated when these two types of SPG cells appear in development. It was previously shown that SPG cell number does not increase during the three larval instar phases but that SPG ploidy increases (Unhavaithaya and Orr-Weaver 2012), but now we examined the temporal transition and ploidy of the mononucleate versus multinucleate cells. We dissected brains from first- and second instar larvae in which SPG nuclei were labeled by *UAS-GFP^{nls}* driven by *moody-GAL4*. Mononucleate versus multinucleate SPG were distinguished by labeling the cell boundaries with Neurexin IV (NRXIV)-GFP, a component of septate junctions (Banerjee et al. 2010). In contrast to third instar larvae, in which about 70% of brain SPG are multinucleate, nearly all of the first instar larvae were mononucleate. We identified only 4% in first instar brains that had multiple nuclei, and these had only two nuclei (Fig. 2-1A-D). The number of multinucleate SPG increased to 68% in second instar, with nearly all having two nuclei and few having four nuclei. By third instar 18% had two, 35% had four, and 14% had eight nuclei (Fig. 2-2D). We examined the position of multinucleate versus mononucleate SPG in the brain lobes by scoring their presence in the half of each lobe of the third instar brain adjacent to the VNC versus distal. We observed that 97% of brain lobes had mononucleate SPG located adjacent to the VNC, whereas only 3% of the lobes had mononucleate SPG located distally (Fig. 2-3A,B); 97% of scored mononucleate SPG cells themselves were found to be proximal to the VNC (Fig. 2-3B).

We next analyzed whether the mononucleate SPG present in first instar larvae were endocycling, as it was possible they were arrested in the mitotic cell cycle or in a G0 state. We measured the ploidy of the nuclei at two points in the first instar stage, and in the second- and third instar stages. In early first instar larvae the SPG range between

Figure 2-1. Appearance of multinucleate SPG occurs between the first- and second-instar larval stages. In this and all subsequent figures of larval brain micrographs, the SPG nuclei are labeled with *UAS-GFP^{mls}* driven by *moody-GAL4* and shown in white or green. See Table 2-1 for complete genotypes for all figures. (A) Whole brain from first instar larva with brain lobes predominantly containing mononucleate SPG. (A') Enlargement of the right brain lobe in A. (B) Whole brain from second instar larva in which the majority of SPG are multinucleate. (B') Enlargement of the right brain lobe in B. (C) Whole brain from wandering third instar larva. Both mononucleate and multinucleate SPG can be seen in the brain lobes. (C') Enlargement of the right side brain lobe in C. In A', B' and C' and subsequent figures SPG outlines marked by NRXIV-GFP are highlighted in white. Scale bars for A, B, C, 100 μ m. (D) Scatter plot showing the percentage of multinucleate SPG from *GAL4* driver alone brains. First instar, n=130 SPG, 25 brains, two biological replicates; second instar, n=75 SPG, 16 brains, one biological replicate; third instar, n=375 SPG, 29 brains, two biological replicates). Of the 67% multinucleate SPG in second instar larvae, 86% were binucleate and 14% were tetranucleate. Kruskal-Wallis with Dunn's multiple comparisons test, **** $P < 0.0001$. (E) Scatter plot showing DNA ploidy C values per SPG cell during larval development. Early first instars, 24-28 hrs after egg deposition (AED), n=60 SPG, 19 brains; mid first instars, 36-40 hrs AED, n=102 SPG, 19 brains; second instars, 60-64 hrs AED, n=32 SPG, 17 brains; third instars, wandering larvae, n= 128 SPG, 58 brains. Data from first- and second- instars, one biological replicate; third instars, seven biological replicates. Mann-Whitney, two-tailed test, **** $P < 0.0001$. The y-axis contains a break and two different scales to better show the lower ploidy C values in early

versus mid-first instars. Scatter plots, mean \pm 95% confidence interval (c.i.). (F)

Proposed model for developmental cell cycle control in the SPG. Nearly all SPG transition from mitosis to the endocycle during embryogenesis. By the second instar larval stage, approximately 30% of SPG remain in the endocycle, whereas approximately 70% switch to endomitosis. The endocycle leads to polyploid cells with a single nucleus whereas endomitosis leads to multinucleate cells.

Figure 2-1

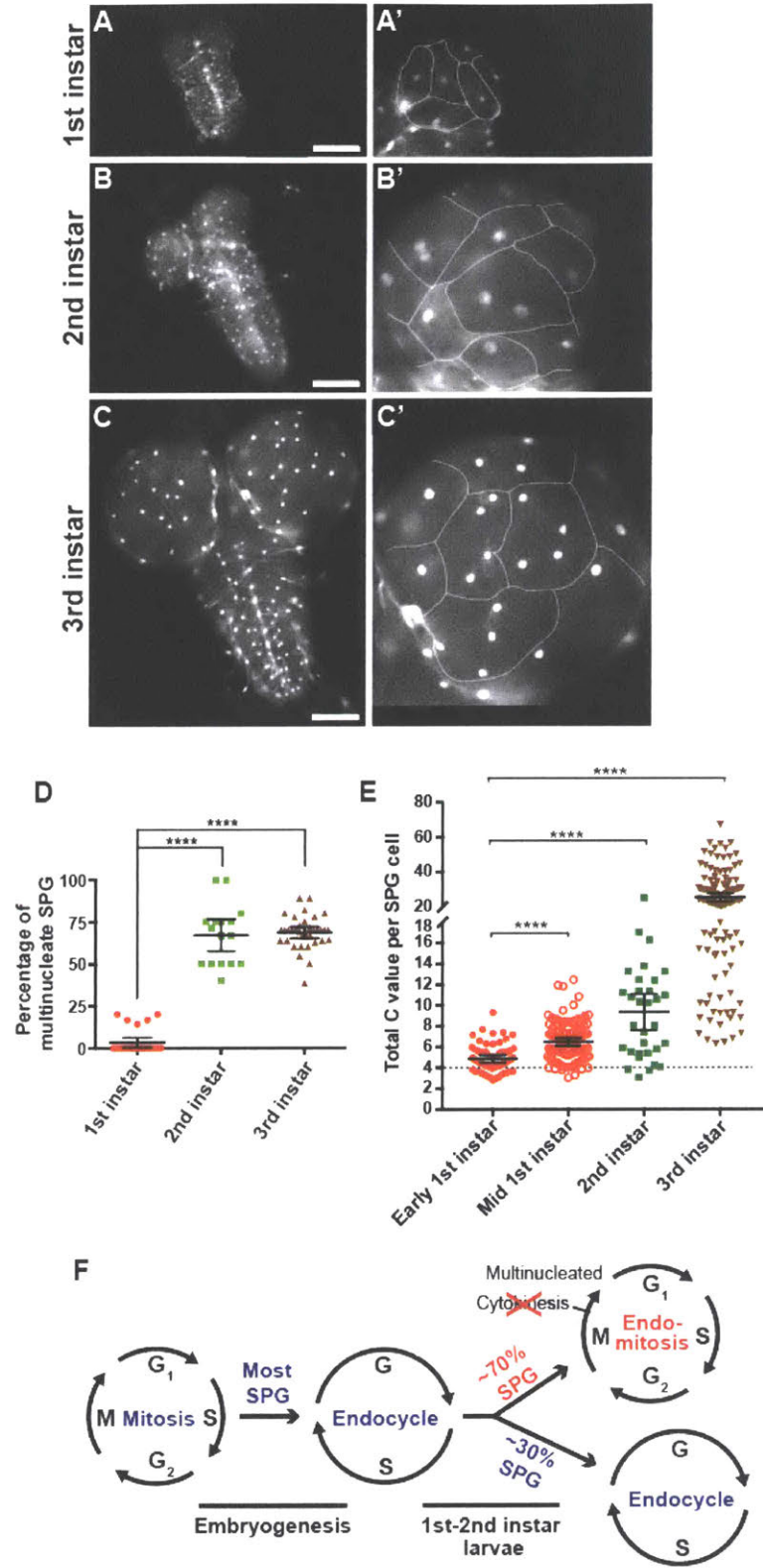


Table 2-1. Abbreviation and full genotypes used throughout the manuscript

Abbreviation	Full genotype
<i>GAL4</i> control (brain)	+; <i>moody-GAL4</i> , <i>UAS-GFP^{nls}/+</i> ; <i>NRXIV::GFP/+</i>
<i>Dcr2</i> OE (brain)	<i>UAS-Dicer2/+</i> ; <i>moody-GAL4</i> , <i>UAS-GFP^{nls}/+</i> ; <i>NRXIV::GFP/+</i>
<i>Su(H)</i> RNAi (brain)	<i>UAS-Suppressor of Hairless</i> RNAi/+; <i>moody-GAL4</i> , <i>UAS-GFP^{nls}/+</i> ; <i>NRXIV::GFP/+</i>
<i>N</i> RNAi (brain)	+; <i>moody-GAL4</i> , <i>UAS-GFP^{nls}/UAS-Notch</i> RNAi; <i>NRXIV::GFP/+</i>
<i>Dcr2</i> OE; <i>DI</i> RNAi (brain)	<i>UAS-Dicer2/+</i> ; <i>moody-GAL4</i> , <i>UAS-GFP^{nls}/UAS-Delta</i> RNAi; <i>NRXIV::GFP/+</i>
<i>Dcr2</i> OE; <i>stg</i> RNAi (brain)	<i>UAS-Dicer2/+</i> ; <i>moody-GAL4</i> , <i>UAS-GFP^{nls}/+</i> ; <i>NRXIV::GFP/UAS-string</i> RNAi
<i>stg</i> OE (brain)	+; <i>moody-GAL4</i> , <i>UAS-GFP^{nls}/+</i> ; <i>NRXIV::GFP/UAS-string</i>
<i>cycB</i> RNAi (brain)	+; <i>moody-GAL4</i> , <i>UAS-GFP^{nls}/+</i> ; <i>NRXIV::GFP/UAS-cyclinB</i> RNAi
<i>fkh-GAL4</i> control (SG)	+; +; <i>forkhead-GAL4/+</i>
<i>Su(H)</i> RNAi (SG)	<i>UAS-Suppressor of Hairless</i> RNAi/+; +; <i>forkhead-GAL4/+</i>
<i>Myc</i> rescue (SG)	<i>UAS-Suppressor of Hairless</i> RNAi/+; <i>UAS-Myc/+</i> ; <i>forkhead-GAL4/+</i>

Figure 2-2. Inhibition of *Notch* signaling leads to a shift from the endocycle to endomitosis and increased mitoses in endomitotic SPG. (A) *GAL4* control brain lobe. (B) *Su(H)* RNAi brain lobe. Scale bars, 50 μ m. (C) Scatter plot showing the percentage of mononucleate SPG. *Dcr2* OE is the control for *Dcr2* OE; *DI* RNAi. *GAL4* control, n=375 SPG, 29 brains; *Su(H)* RNAi, n=312 SPG, 22 brains; *N* RNAi, n=313 SPG, 23 brains; *Dcr2* OE, n=389 SPG, 19 brains; *Dcr2* OE; *DI* RNAi, n=670 SPG, 47 brains. *Dcr2* OE data, one biological replicate, all other data, two biological replicates. Kruskal-Wallis with Dunn's multiple comparisons test, *** $P=0.0007$; **** $P<0.0001$, mean \pm 95% c.i.. (The *Dcr2* OE data are the same as in Fig. 2-7D and the *GAL4* control data are the same as in Fig. 2-1D (third instar) and 2-7D). (D-E) Histograms showing the number of nuclei per SPG cell, displayed as percentages of the total SPG cells. (D) *GAL4* control, n=207 SPG, 38 brains; *Su(H)* RNAi, n=206 SPG, 25 brains; *N* RNAi, n=208 SPG, 17 brains, three biological replicates. Mann-Whitney, two-tailed test, * $P=0.037$; **** $P=0.0003$. (E) *Dcr2* OE, n=320 SPG, 19 brains; *Dcr2* OE; *DI* RNAi, n=466 SPG, 27 brains, one biological replicate. Mann-Whitney, two-tailed test, not significant (n.s). $P=0.14$.

Figure 2-2

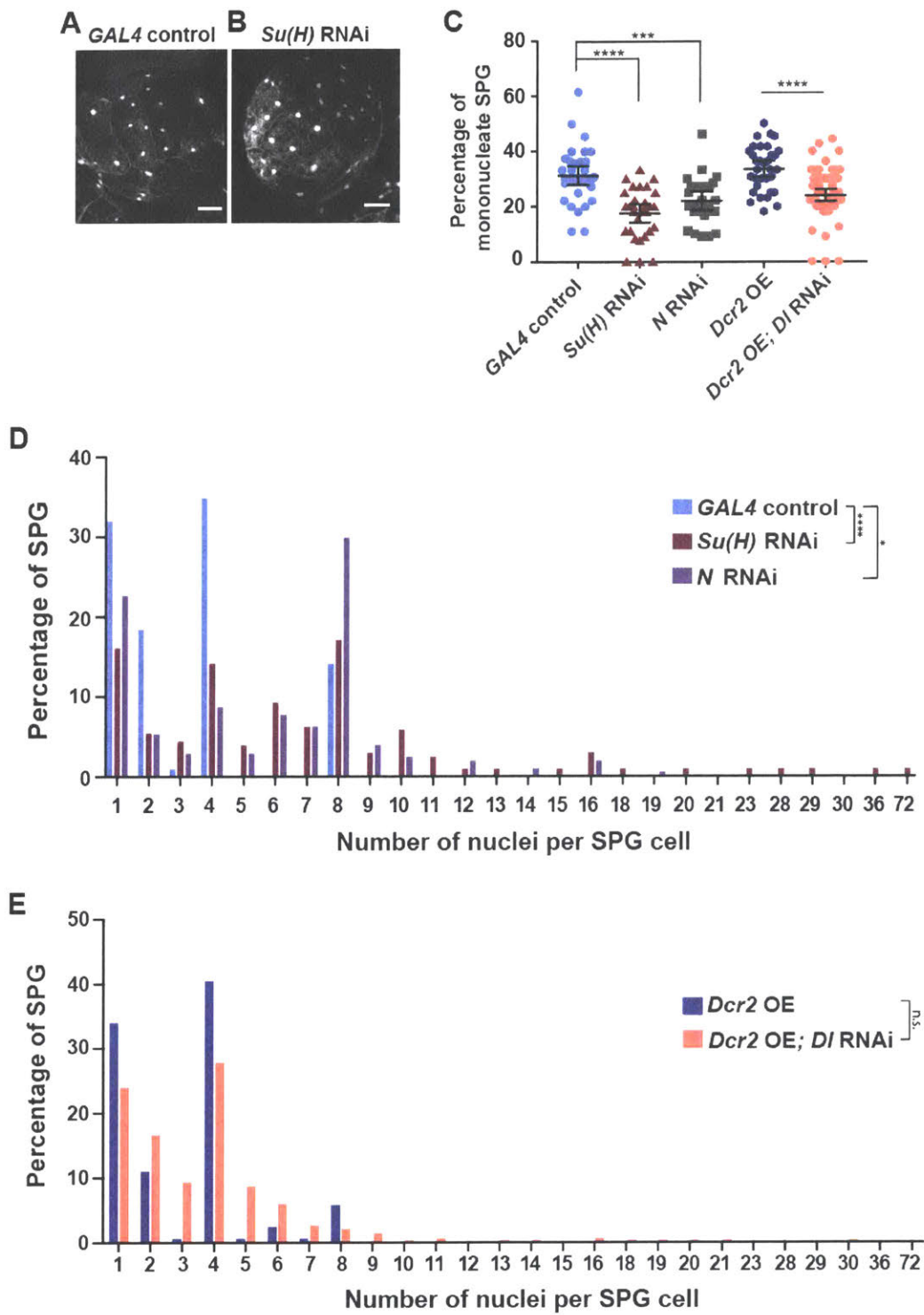
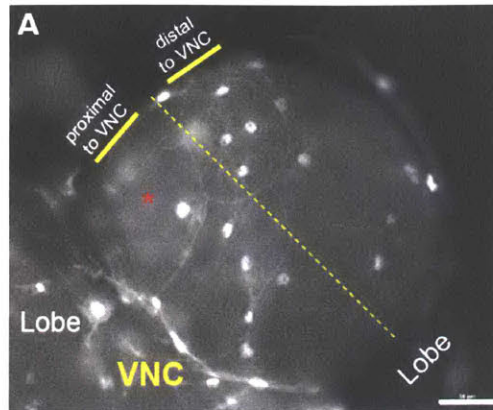


Figure 2-3. Analysis of the position of mononucleate SPG relative to the VNC. (A)

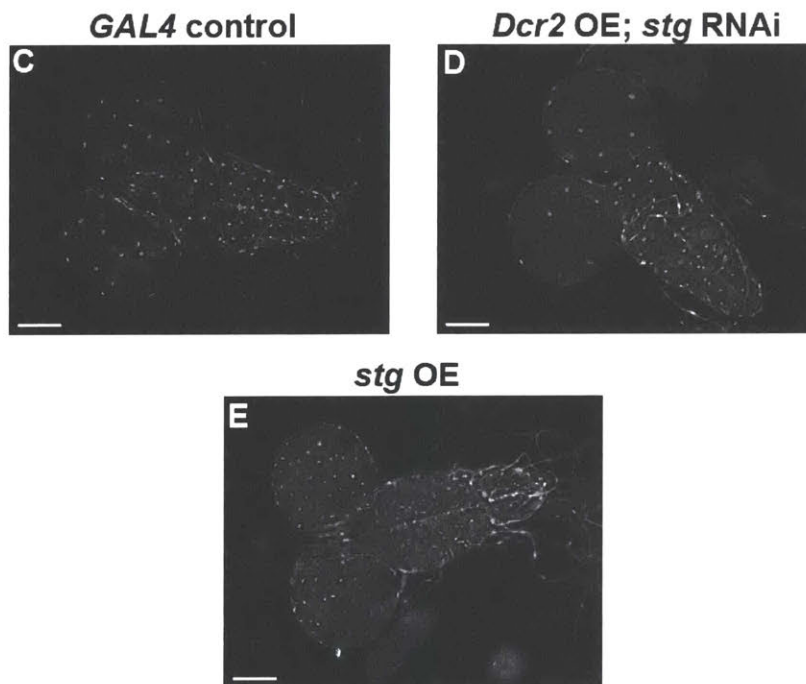
Brain lobes from wandering third instar larvae were analyzed for the number of mononucleate SPG cells adjacent to or distal to the VNC. This was done by drawing a line on the middle of each brain hemisphere image and scoring the number of SPG on the side adjacent to the VNC versus distal. Images were acquired from either dorsal or ventral sides of the lobes, depending on where mononucleate SPG cells were found. In 97% percent of all the lobes examined (B), mononucleate cells were found proximal to the VNC rather than distal (n=33 lobes, two biological replicates) (Chi-squared test, $P=4.1 \times 10^{-8}$). Red asterisk marks the mononucleate SPG found in the half lobe shown. Scale bar, 50 μ m. (C-E) Whole brains from *GAL4* control (C), *Dcr2* OE; *stg* RNAi (D), and *stg* overexpression (OE). Scale bars, 100 μ m.

Figure 2-3



B Quantification of Proximity of Mononucleate SPG to VNC

Samples scored	Percentage of lobes with mononucleate SPG proximal to VNC	Percentage of mononucleate SPG proximal to VNC
28 brains	97% (33/34 lobes)	97% (62/64 SPG cells)



2.8C and 9.3C, with a mean of 4.9C (Fig. 2-1E). The cells with a ploidy higher than 4C are most likely endocycling. This is supported by the finding that the ploidy of the cells increases to a range of 3C to 12.4C with a mean of 6.5C by mid-first instar as well as the fact that we observed EdU incorporation in ~12% of these SPG (Fig. 2-1E, Fig. 2-4A-A"). Finally, we tested whether the cells were in a mitotic state by staining with antibodies to the mitotic cell cycle markers Cyclin B and phospho-histone H3. The level of Cyclin B staining was uniformly low across the SPG cell layer in the first instar brain lobe (Fig. 2-5). Furthermore, none of the SPG examined showed detectable phospho-H3 staining (Fig. 2-4B-B"). We conclude from the increased ploidy, detectable DNA replication, and absence of mitotic markers that at least 93% of the SPG in the larval brain are in the endocycle by the mid-first instar stage. These cells most likely continue endocycling during larval development, as the percent of mononucleate SPG stays constant after the second instar yet the ploidy of these cells increases from first- to third instar larval stage (Fig. 2-1 D,E, Fig. 2-6A).

Several lines of evidence indicate that the multinucleate cells appearing between the first and second instar result from endomitosis. First, the number of SPG cells does not change during development, and thus cell fusion does not occur (Unhavaithaya and Orr-Weaver 2012). Second, the ploidy and number of nuclei in the multinucleate SPG increase during development (Fig. 2-1E, 2-2D). Third, we previously observed that SPG with multiple nuclei label with anti-phospho-H3 during larval stages (Unhavaithaya and Orr-Weaver 2012). Fourth, and most importantly, the mitosis-activating Cdc25 phosphatase String (Stg) is required for multinucleate SPG.

Figure 2-4. DNA replication but no mitotic markers are detected in first instar SPG prior to the switch to endomitosis. (A-A'') Brain lobe from mid-to-late first instar larvae (~30-40 hrs AED) stained with anti-GFP (A; marks both nuclei and cell boundaries) and labeled with EdU (A') to mark SPG in S phase. Nuclei also were identified by DAPI staining (not shown). (A'') GFP (green) and EdU (red) merged channels. We detected EdU incorporation in 12% of the SPG (n=39 brains, 459 SPG, one biological replicate). Yellow arrows point to two SPG nuclei positive for EdU (circled). The white arrows show EdU-labeled nuclei in other tissue layers in the brain. (B-B'') Brain lobe from mid-first instar larvae (~36 hrs AED) stained with anti-GFP (B) and phosphorylated-histone H3 (PHH3) (B'). (B'') GFP (green) and PHH3 (magenta) merged channels. No PHH3 positive SPG were detected at this developmental time point (n=19 brains, 257 SPG, one biological replicate). Yellow arrows and circles point to PHH3 positive SPG nuclei in the lobe. White arrows show mitotic cells in other tissue layers in the brain. Scale bars in all panels, 25 μ m.

Figure 2-4

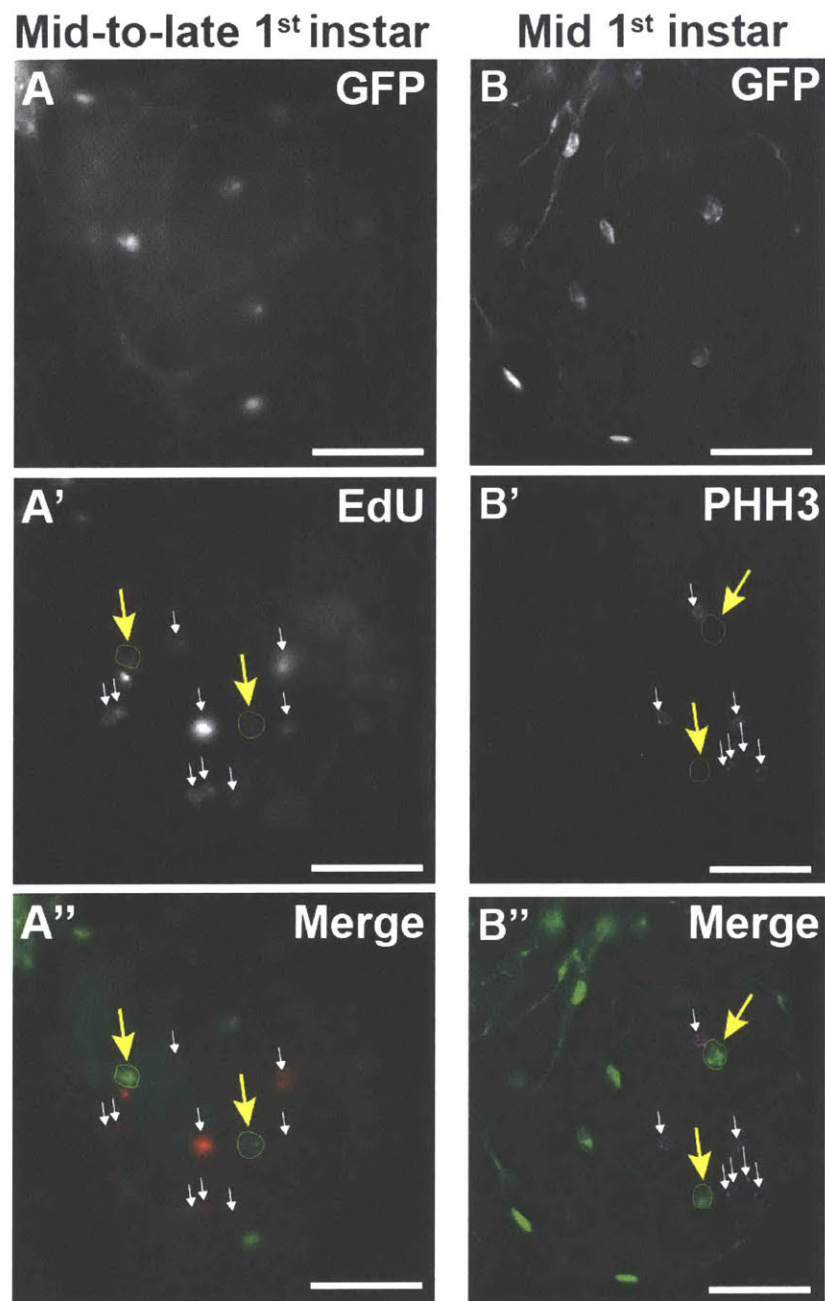


Figure 2-5. Cyclin B protein levels are upregulated in SPG in brain lobes at the second instar larval stage. (A-F) Single confocal scans of larval brain lobes or salivary glands stained with DAPI (first column, blue in merge), anti-GFP (second column; marks both SPG or salivary gland nuclei and SPG cell boundaries, green in merge) and anti-Cyclin B (CycB) (third column, red in merge). (A, C) First instar larval brain lobe from *GAL4* control showing basal CycB protein levels in SPG and in polyploid salivary gland cells from same developmental stage. (D) Larval brain lobe from *GAL4* control second instar larva showing increased CycB signal in SPG at the developmental window when the transition to multiple nuclei occurs. (F) CycB levels in second instar larval salivary gland. (B, E) Larval brain lobe from first instar *cycB* RNAi larvae showing basal CycB levels at the first instar stage but significantly decreased levels of CycB at the second instar larval stage. Dotted lines in third columns of panels A-C and F outline brain lobes and salivary glands. Scale bars, 10 μ m. (G) Orthogonal views of first and second instar larval brains showing CycB protein levels in the SPG layer (bottom panels). Top panels show the merge with nuclear localized GFP (green), anti-CycB (red) and DAPI (blue). (H) Graph of corrected total anti-CycB fluorescence from single scanned images for each indicated genotype and sample. First instar *GAL4* control larval brain lobes (n=15 brains), salivary glands (n=5), VNCs (n=18), *cycB* RNAi larval brain lobes (n=13 brains); second instar *GAL4* control larval brain lobes (n=12 brains), salivary glands (n=5), VNCs (n=19), *cycB* RNAi larval brain lobes (n=17 brains). Data from one biological replicate. Mann-Whitney, two-tailed test, *** $P=0.0003$; **** $P<0.0001$. Although the *cycB* RNAi establishes the specificity of the CycB antibody staining, it did not eliminate protein and did not affect endomitosis. (I-J) Fluorescence *in situ* hybridization (FISH) analysis to

determine the efficiency of RNAi knockdown in SPG. (I) Orthogonal views of third instar (~120 hrs AED) brain lobe FISH samples showing *N*, *Su(H)* or *stg* transcripts (bottom panels) in the SPG layer. Top panels show the merge with nuclear localized GFP (green), FISH signal (red) and DAPI (blue). (J) Graph of corrected total *in situ* fluorescence from single scanned images for each individual genotype and sample from third instar larva. *GAL4* control (*N* probe: n=20 half lobes, 20 brains; *Su(H)* probe: n=33 half lobes, 19 brains; *stg* probe: n=18 half lobes, 17 brains); *N* RNAi (*N* probe: n= 22 half lobes, 22 brains); *Su(H)* RNAi (*Su(H)* probe: n= 43 half lobes, 29 brains; *stg* probe: n=18 half lobes, 16 brains); *stg* OE (*stg* probe: n= 32 half lobes, 14 brains); *Dcr2* OE (*stg* probe: n= 32 half lobes, 21 brains); *Dcr2* OE; *stg* RNAi (*stg* probe: n=25 half lobes, 19 brains). Y axis, *in situ* fluorescence arbitrary units. Data from one biological replicate. Mann-Whitney, two-tailed test, * $P=0.0333$; ** $P<0.0030$; **** $P<0.0001$; n.s.=not significant. In both G and I, asterisks mark GFP-labeled nuclei from mononucleate SPG (*) or from multinucleate SPG (**). Complete genotypes are in Table 2-1.

Figure 2-5

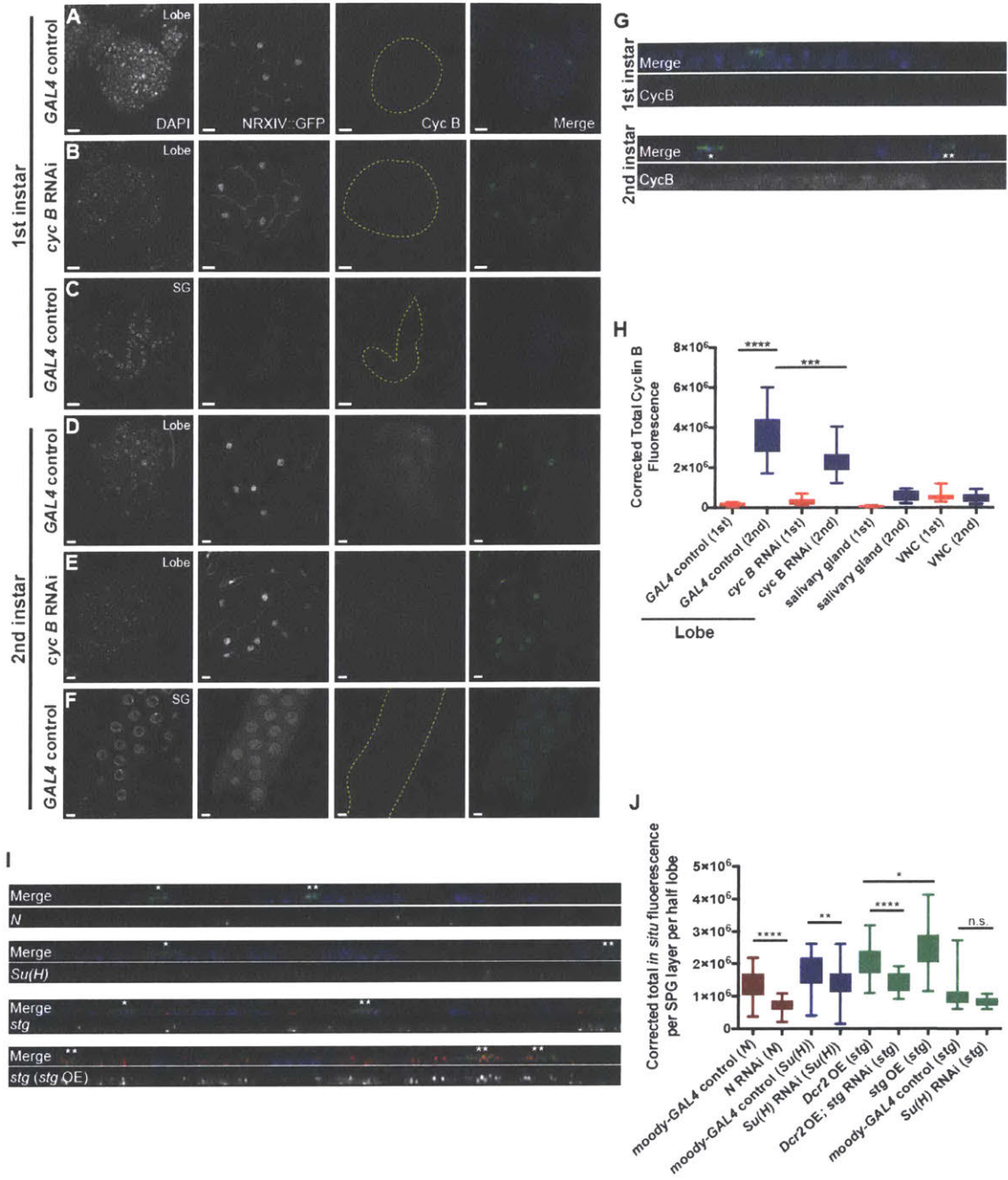
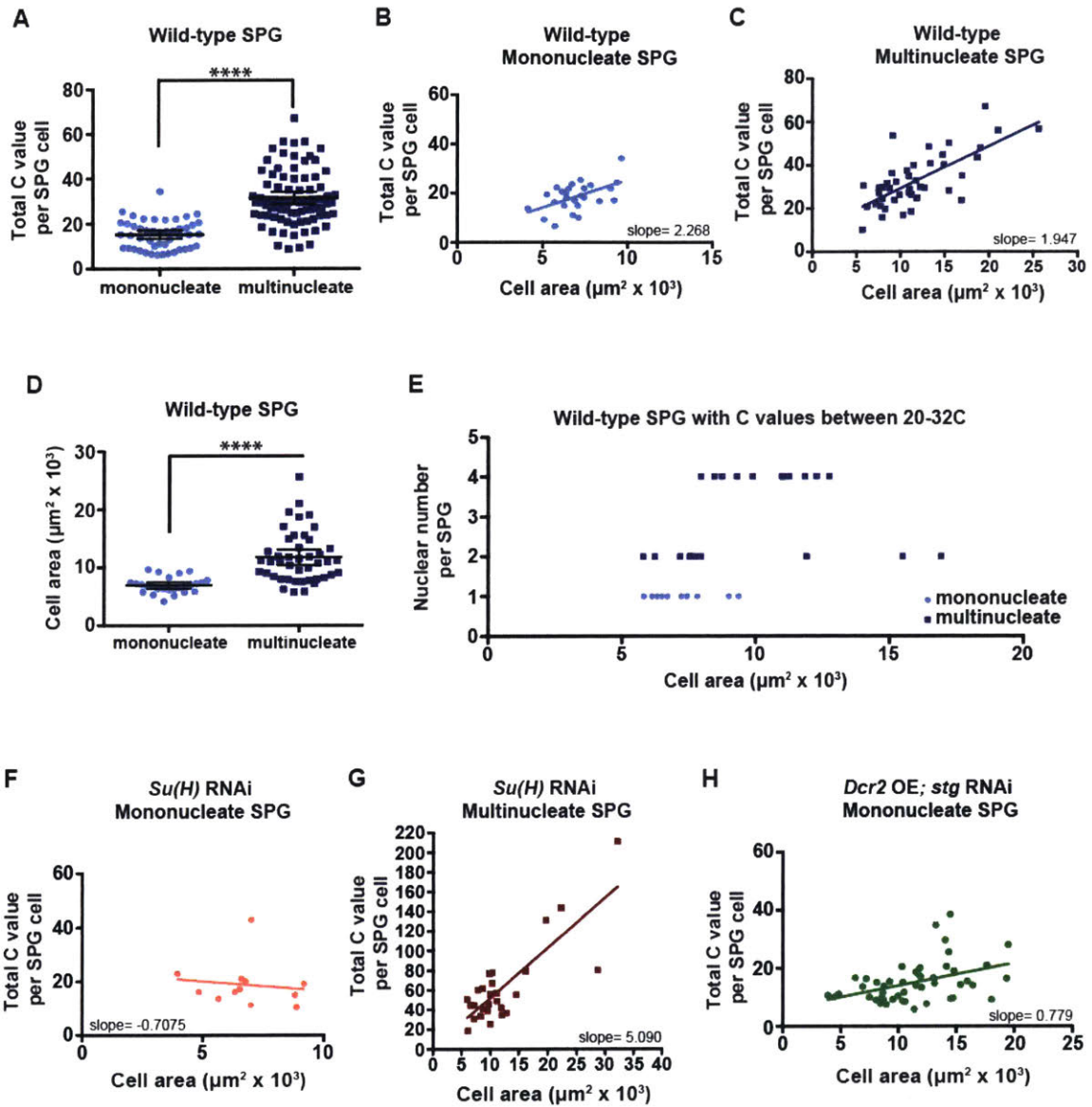


Figure 2-6. Endomitotic cells are larger than endocycling cells. (A) Scatter plot showing DNA ploidy C values of individual mono and multinucleate SPG in the brain lobe. Mononucleate, n=47 SPG, 41 brains; multinucleate, n=81 SPG, 58 brains, seven biological replicates. Data are the same as Fig 2-1E (third instar). Mann-Whitney, two-tailed test, **** $P < 0.0001$. (B-C) Plots showing DNA ploidy C values of mono or multinucleate SPG as a function of cell area ($\mu\text{m}^2 \times 10^3$) with linear regression. (B) Mononucleate, n= 26 SPG, 24 brains, three biological replicates. Spearman correlation coefficient $r=0.47$, $P=0.015$; slope= 2.268 C value/ $\mu\text{m}^2 \times 10^3$, $P=0.0053$. (C) Multinucleate, n=44 SPG, 33 brains, three biological replicates. Spearman correlation coefficient $r=0.60$, $P < 0.0001$; slope= 1.947 C value/ $\mu\text{m}^2 \times 10^3$, $P < 0.0001$. (D) Scatter plot showing cell area ($\mu\text{m}^2 \times 10^3$) of individual mono or multinucleate SPG in the brain lobe (mononucleate, n=26 SPG, 24 brains; multinucleate, n=44 SPG, 33 brains), three biological replicates each. Mann-Whitney, two-tailed test, **** $P < 0.0001$. (E) Cell area ($\mu\text{m}^2 \times 10^3$) in relation to SPG nuclear number. Only cells having a ploidy between 20-32C are plotted (n=31 SPG; 23 brains, three biological replicates). Spearman correlation coefficient $r=0.60$, $P=0.0004$. The ploidy values and size for each cell are given in Table 2-4. (F-G) Plots showing DNA ploidy C values of mono or multinucleate SPG as a function of cell area ($\mu\text{m}^2 \times 10^3$) with linear regression. (F) *Su(H)* RNAi mononucleate, n= 12 SPG, 12 brains, three biological replicates. Spearman correlation coefficient $r=-0.18$, $P=0.57$; slope= -0.7075 C value/ $\mu\text{m}^2 \times 10^3$, $P= 0.68$. (G) *Su(H)* RNAi multinucleate, n= 28 SPG, 15 brains, three biological replicates. Spearman correlation coefficient $r=0.54$, $P=0.003$; slope= 5.090 C value/ $\mu\text{m}^2 \times 10^3$, $P < 0.0001$. (H) *Dcr2* OE; *stg* RNAi mononucleate, n= 48 SPG, 15 brains, one biological replicate. Spearman

correlation coefficient $r=0.42$, $P<0.003$; slope= $0.779 \text{ C value}/\mu\text{m}^2 \times 10^3$, $P<0.003$.

Scatter plots (A,D) mean \pm 95% c.i.. All samples were collected from wandering third instar larvae.

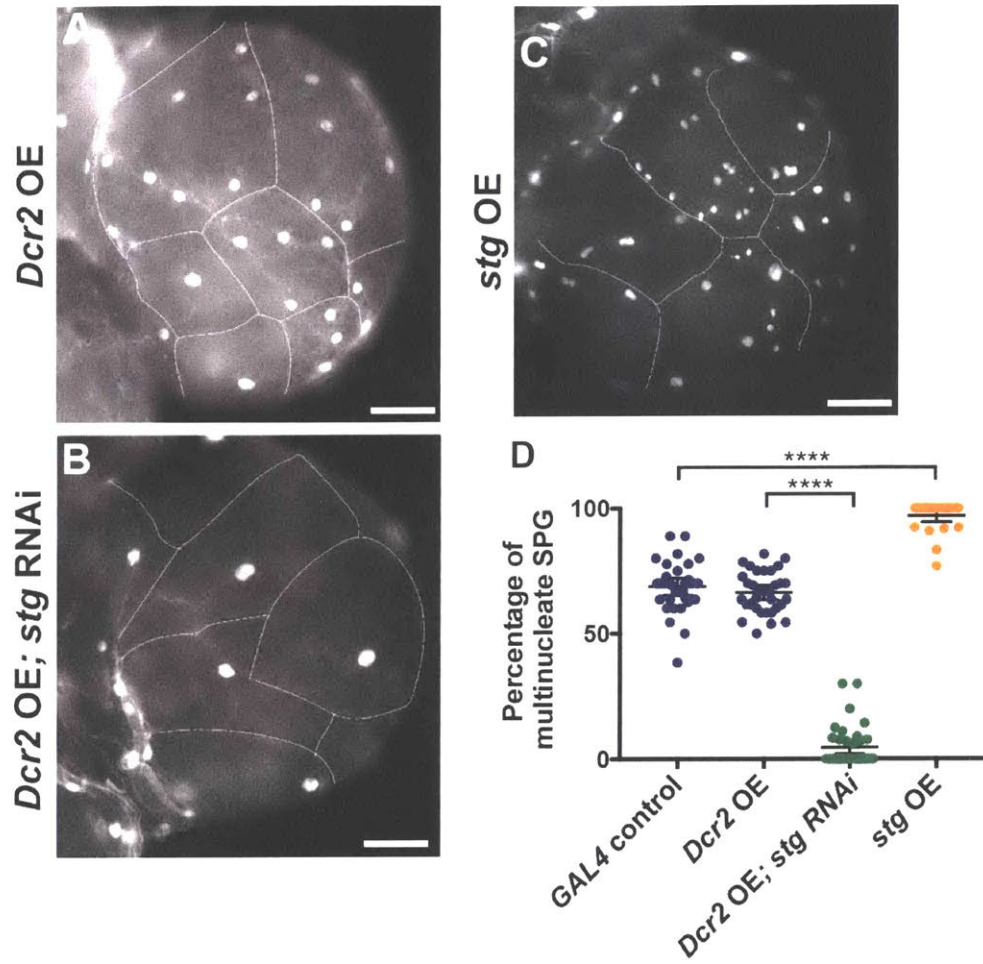
Figure 2-6



Stg is a crucial activator of mitosis in *Drosophila*, and we find that its levels control the number of SPG with multiple nuclei. It has been shown previously that mitotic Cyclin/CDK kinase is off and dispensable for the endocycle (Edgar et al. 2014). The Cdc25 phosphatase Stg is essential for active Cyclin B/CDK1 and mitosis in *Drosophila* but is repressed in the endocycle (Edgar and O'Farrell 1990; Deng et al. 2001). Therefore we evaluated the role of Stg and presumably active mitotic Cyclin/CDK in the appearance of multinucleate SPG by reducing its levels by RNAi specifically in the SPG with the *moody-GAL4* driver (Fig. 2-5J). Reduction of *stg* function dramatically inhibited the appearance of multinucleate SPG (Fig. 2-7A,B), causing 95% of third instar brain SPG to be mononucleate (Fig. 2-3C,D, Fig. 2-7D). In contrast, overexpressing Stg specifically in the SPG increased the percentage of multinucleate SPG to 97% in the third instar brain (Fig. 2-3C,E, Fig. 2-5I,J, Fig. 2-7C,D), although it did not increase the percentage of multinucleate SPG in the first instar brain (5% compared to 4% for the control). We also observed a significant increase in the percentage of mononucleate SPG in third instar brains (40% (n=499 SPG, 23 brains) compared to 31% (n=373 SPG, 20 brains) in the control, $P=0.02$) when *stg* RNAi was induced with the *Glilotactin-GAL4* driver (Schulte et al. 2003). Overexpression of *stg* with *Glilotactin-GAL4* also significantly increased the percentage of multinucleate SPG in third instar brains (99% (n=532 SPG, 23 brains) compared to 69% (n=373 SPG, 20 brains) in the control, $P<0.0001$). The effect of changes in Stg expression on the percentage of mononucleate versus multinucleate SPG is consistent with our observation that Cyclin B protein is not detectable in first instar SPG, but the protein is present in second instar SPG in the brain lobes (Fig. 2-5). Taken together, these results indicate that mitosis and nuclear division

Figure 2-7. Levels of the cell cycle phosphatase Stg affect endomitosis in SPG. (A) Control brain lobe showing both endocycling (mononucleate) and endomitotic (multinucleate) SPG. (B) *Dcr2* OE; *stg* RNAi brain lobe with only mononucleate SPG. (C) *stg* overexpression (OE) brain lobe with mostly endomitotic SPG. All brain lobes are from wandering third instar larvae. Scale bars, 100 μ m. (D) Scatter plot showing the percentage of multinucleate SPG. *GAL4* control, n=375 SPG, 29 brains, two biological replicates; *Dcr2* OE, n=389 SPG, 19 brains, one biological replicate; *Dcr2* OE; *stg* RNAi, n=421 SPG, 19 brains, two biological replicates; *stg* OE, n=286 SPG, 13 brains, one biological replicate. Mann-Whitney, two-tailed test, **** P <0.0001, mean \pm 95% c.i.. Data from *GAL4* control from Fig. 2-1D (third instar).

Figure 2-7



occur in the SPG in the absence of cell division, a form of endomitosis that initiates between the first- and second instar stages in 70% of the SPG (Fig. 2-1F). This proportion remains constant through the third instar, although the SPG ploidy continues to increase (Fig. 2-1D,E, Fig. 2-6A).

Collectively, the results on the mononucleate and multinucleate SPG are most simply explained by the SPG cells in the brain lobes becoming polyploid by two different cell cycle variants, the endocycle and endomitosis. Direct imaging of mitotic divisions in the brain SPG is not technically possible because it would not only require *ex vivo* culturing of the first instar larval brain for at least 24 hours and up to three days but also producing hormonal shifts to mimic the larval molts; such culturing conditions have not been developed. Moreover, there are only about 10 multinucleate SPG cells per brain lobe, and each of these undergoes only one nuclear division at some point within a 24-hour window.

Because at least 93% of brain SPG are endocycling in mid-first instar brain lobes and 70% initiate endomitosis between first- and second instar stages, we conclude that SPG cells can undergo two cell cycle transitions, from mitotic divisions to the endocycle late in embryogenesis or early first instar and then from the endocycle to endomitosis at the end of first instar. Although we failed to detect phospho-H3 in mononucleate SPG we cannot exclude the possibility that these cells have some mitotic characteristics at some point during larval development, but the level of mitotic activity is insufficient for nuclear divisions.

Notch signaling inhibits endomitosis

Given the dynamic cell cycle transitions occurring in the brain SPG, we investigated potential developmental regulators. Notch (N) signaling has been demonstrated to link cell cycle alteration to developmental events. It has been shown to trigger endocycle onset in *Drosophila* adult follicle and midgut cells (Deng et al. 2001; Lopez-Schier and St Johnston 2001; Micchelli and Perrimon 2006; Ohlstein and Spradling 2006), but in contrast is necessary for the mitotic divisions that follow the two endocycles in the rectal papillae (Schoenfelder et al. 2014).

We reduced the levels of Su(H), the transcription factor that is the major N signaling downstream effector (Bray 2006), by RNAi in SPG cells, using the same experimental strategy described above for *stg*. We also reduced the N receptor by RNAi in the SPG under *moody-GAL4* control. We observed differences in the ratio of mononucleate to multinucleate SPG in *Su(H)* RNAi third instar brains when compared to control brains (Fig. 2-2A,B). Quantification revealed a significantly decreased number of mononucleate cells relative to multinucleate cells in *Su(H)* RNAi and *N* RNAi (Fig. 2-2C). A mean of 31% of control SPG were mononucleate, but only 18% of *Su(H)* RNAi SPG and 22% of *N* RNAi cells were mononucleate. Driving *Su(H)* RNAi with *Glilotactin-GAL4* also significantly reduced the percent of mononucleate SPG in the third instar brains (24% (n=413 SPG, 24 brains) compared to 31% (n=373 SPG, 20 brains) in the control, $P=0.0004$). Therefore, similar to its role in blocking cell proliferation and promoting the endocycle in the adult follicle cells and midgut, our results indicate that N signaling acts to maintain the endocycle and inhibit endomitosis in the SPG. *Su(H)*

RNAi did not significantly change the level of *stg* mRNA in the SPG (Fig. 2-5J), so the effect of N signaling on endomitosis in the SPG may not be via inhibition of *stg*.

The finding that N activity retains cells in the endocycle raised the question of the source of the ligand. To test whether signaling between SPG, such as lateral inhibition, might affect the endocycle versus endomitosis decision, we reduced Delta (DI) levels in the SPG with RNAi driven by *moody-GAL4*. This also resulted in a significantly lower percentage of SPG undergoing endocycles (Fig. 2-2C). Thus lateral inhibition between SPG in the brain lobe mediated by DI-N interactions may retain some SPG in the endocycle. However, *moody-GAL4* driven *DI* RNAi occurred in all SPG, including those in the VNC that are solely mononucleate. Therefore, given that the endocycling brain SPG lie in the half of the brain lobe closest to the VNC, it is possible that DI on the SPG in the VNC that are in direct contact with the brain lobe SPG may cause them to remain in the endocycle.

Ablation of the Notch signaling pathway perturbs mitotic divisions during endomitosis

The SPG provided the opportunity to define the characteristics of endomitosis. Normally an integral number of mitotic divisions occur, such that nearly all the cells contain two, four, or eight nuclei (Fig. 2-2D). In addition to increasing the percentage of SPG cells undergoing endomitosis, the number of nuclear divisions was increased when Su(H), N, and DI were perturbed. Up to 72 nuclei were observed in third instar brain SPG from *Su(H)* RNAi animals (Fig. 2-2D). RNAi against *N* also increased nuclear divisions, shown by the percentage of SPG with eight nuclei being more than doubled compared to the driver-alone control (Fig. 2-2D). Moreover, cells with odd numbers of nuclei were present with all three methods of reducing N signaling (Fig. 2-2D,E). To

date, no roles for Su(H) in cell cycle regulation independent of N have been described. Thus, the greater effect of *Su(H)* RNAi on nuclear number over *N* RNAi could be due to differential knockdown levels or to differences in the threshold levels required for activation of the signaling pathway between Su(H) and N.

The increased nuclear number observed when N signaling was reduced was associated with a significant decrease in the ploidy of individual nuclei (Fig. 2-8A,B). Notably, nuclei with less than a 2C genomic content were present when N signaling was perturbed (Fig. 2-8B). Whereas only 1.4% of nuclei quantified in control endomitotic SPG cells had a C value of less than or equal to a diploid 2C, this percentage increased to 18% in *Su(H)* RNAi endomitotic SPG (Fig. 2-8B). The nuclei with less than a diploid DNA content could result from errors in mitotic chromosome segregation, as we observe anaphase bridges, or perhaps from mitosis occurring in the absence of completed DNA replication. Problems separating polytene chromosomes in mitosis also could account for cells with less than 2C content.

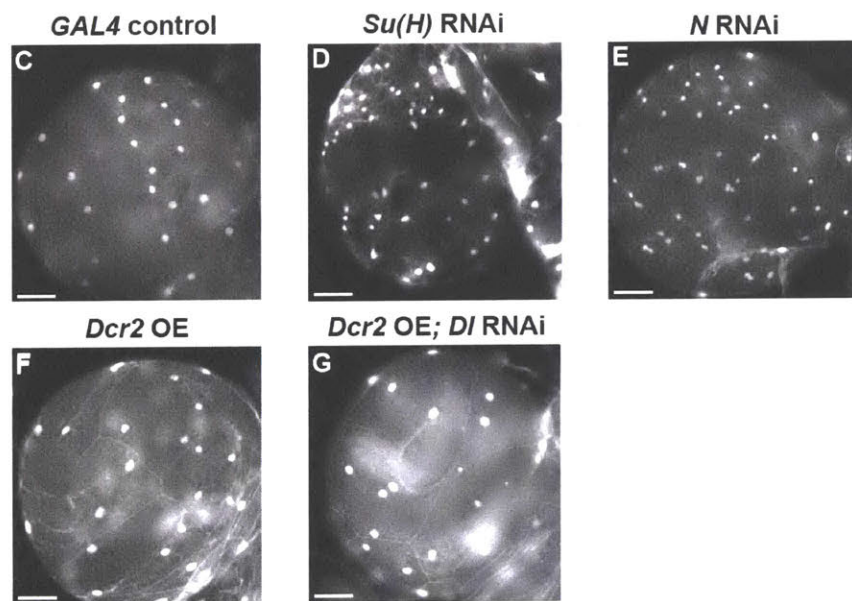
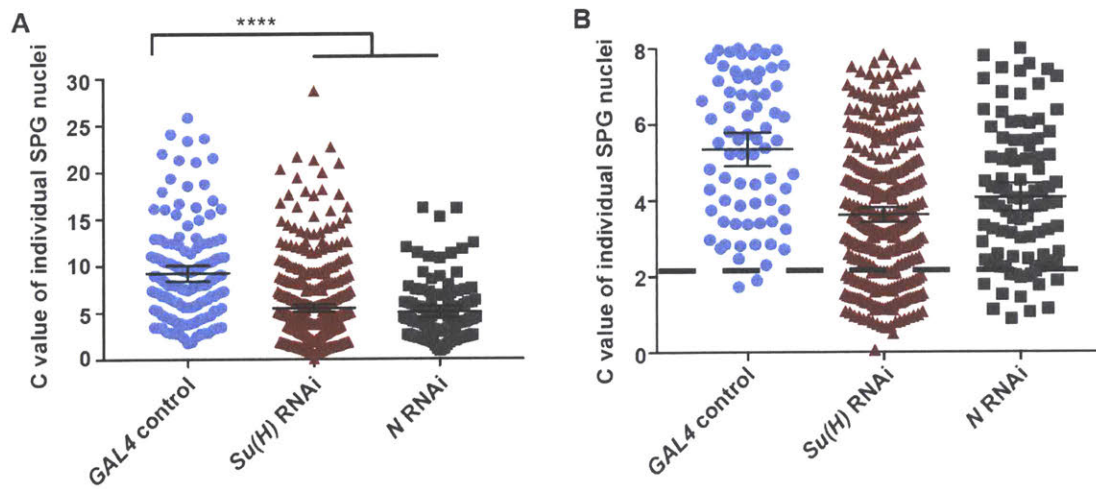
SPG in the VNC but not salivary gland cells are capable of endomitosis

Drosophila polyploid rectal papillar cells are able to return to mitotic divisions after endocycling (Fox et al. 2010), the only tissue to date observed to switch out of the endocycle during *Drosophila* development. Given the striking promotion of endomitosis by the reduction of Su(H) function in polyploid SPG cells, we investigated whether other larval endocycling tissues retain the ability to enter mitosis.

The SPG in the VNC endocycle: they increase ploidy throughout larval development, incorporate EdU, and yet remain mononucleate and lack phospho-H3 staining (Unhavaithaya and Orr-Weaver 2012). We investigated whether perturbing N

Figure 2-8. Decreased Notch signaling results in a larger population of SPG cells having a C value equal to or less than diploid 2C. (A) Scatter plot showing the DNA ploidy C values of individual nuclei from multinucleate (endomitotic) SPG in brain lobes of wandering third instar larvae. *GAL4* control, n=147 nuclei, 44 SPG, 33 brains; *Su(H)* RNAi, n=436 nuclei, 44 SPG, 25 brains; *N* RNAi, n=110 nuclei, 17 SPG, 17 brains. Data from three biological replicates. Kruskal-Wallis with Dunn's multiple comparisons test, **** $P < 0.0001$, mean \pm 95% c.i.. (B) Scatter plot showing the DNA ploidy C values of individual endomitotic nuclei in the brain lobe with equal to or less than 8C values. The data are a subset of the data from panel A with the axes expanded so that nuclei with less than 2C ploidy can be easily visualized. The percentage of nuclei with less than 2C were calculated from the data in panel A, not the subset of data in panel B. Dotted line indicates the diploid 2C value. (C-G) Brain lobes from wandering third instar larvae in which Notch signaling was perturbed. *GAL4* control (C), *Su(H)* RNAi (D), *N* RNAi (E), *Dcr2* OE (F), and *Dcr2* OE; *Dl* RNAi (G). Scale bars, 100 μ m. See Table 2-1 for complete genotypes.

Figure 2-8



signaling or overexpressing the Stg Cdc25 phosphatase could cause SPG in the VNC to undergo endomitosis by scoring the number of larvae whose VNC contained at least one multinucleate cell (Fig. 2-9A-D, Table 2-2). RNAi against *Su(H)* or *N* led to SPG in the VNC with multiple nuclei, as did overexpression of the *stg* gene. These multinucleate cells were readily detectable by third instar, but also had begun to appear by the first instar for *N* RNAi and *stg* overexpression (Table 2-2). Multinucleate cells in the first instar VNC, however, were rare, with animals having only one or two such cells. Thus we scored by animal rather than SPG cell number, and we think that the differences in percentage of multinucleation after *N* knockdown between first and third instar are unlikely to be biologically significant. We conclude that although SPG in the VNC normally do not undergo endomitosis they retain the capability of doing so if mitotic Cyclin/CDK is activated.

By contrast, the endocycling cells of the salivary gland did not undergo endomitosis when *N* signaling was reduced, and *Su(H)* appears to play a distinct role in this tissue. We used the *forkhead-GAL4* (*fkh-GAL4*) driver (Henderson and Andrew 2000) to express *Su(H)* RNAi specifically in salivary glands beginning from when they first enter the endocycle during embryogenesis. Salivary glands were dissected from wandering third instar larvae, fixed, and stained with DAPI to visualize DNA. In contrast to SPG, we did not observe any salivary gland cells with more than one nucleus (Fig. 2-9E,F) and also did not detect staining with the mitotic marker phospho-H3 (data not shown). The failure of *Su(H)* RNAi to drive endocycling cells in the salivary gland into endomitosis is correlated with low levels of Cyclin B protein, although the SPG in the VNC also have low levels (Fig. 2-5C,F,H).

Figure 2-9. Endocycling SPG of the VNC are susceptible to enter endomitosis, but salivary gland endocycling cells are not. (A-D) VNCs from *GAL4* control (A), *Su(H)* RNAi (B), *Dcr2* OE; *stg* RNAi (C), and *stg* overexpression (OE) (D) wandering third instar larvae. Yellow arrow in (B) points to a binucleate SPG. Scale bars, 25 μ m. See also Table 2-2. (E,F) Close up images of salivary glands from *fkh-GAL4* alone control (E) and *Su(H)* RNAi (F) stained with DAPI, NRXIV antibody, and DAPI and NRXIV merged. NRXIV staining shows the cell boundaries, revealing all the salivary gland cells in *Su(H)* RNAi larvae to be mononucleate. Scale bars, 50 μ m. (G-I) DAPI-stained salivary glands from wandering third instar larvae. Control *fkh-GAL4* alone (G), *Su(H)* RNAi (H) or *Su(H)* RNAi; *UAS-Myc* rescued (I) salivary glands. fb, fat body. Scale bars, 100 μ m. (K) Scatter plot showing DNA ploidy values from wandering third instar salivary gland nuclei. Control *OrR* n=58 nuclei, 9 salivary glands; *fkh-GAL4* alone control n=53 nuclei, 10 salivary glands; *Su(H)* RNAi n=50 nuclei, 8 salivary glands; *dmyc* rescue n=41 nuclei, 8 salivary glands, one biological replicate. Mann-Whitney two-tailed with Bonferroni adjustment, two-tailed test, * $P=0.033$; ** $P=0.0053$; **** $P=8.2\times 10^{-26}$; ***** $P=6.9\times 10^{-31}$, mean \pm 95% c.i.. (K-P) Alkaline phosphatase *in situ* hybridization revealed a reduction in transcript levels of *Myc* (L) and *eIF4E* (O) in *Su(H)* RNAi salivary glands (M,P). Probes homologous to the sense strands were used as a control (K,N); anti-sense probes (M, P, N, Q). sg, salivary gland; fb, fat body. Scale bars, 100 μ m. (Q) Corrected total alkaline phosphatase signals (arbitrary units) for *Myc* (*fkh-GAL4* alone control, n=19 salivary glands (SGs); *Su(H)* RNAi, n=25 SGs) and *eIF4E* (*fkh-GAL4* alone control, n=11 SGs; *Su(H)* RNAi, n=11 SGs) transcripts from single scanned images for each

indicated genotype, two biological replicates. Mann-Whitney, two-tailed test,

** $P=0.0024$; **** $P<0.0001$.

Figure 2-9

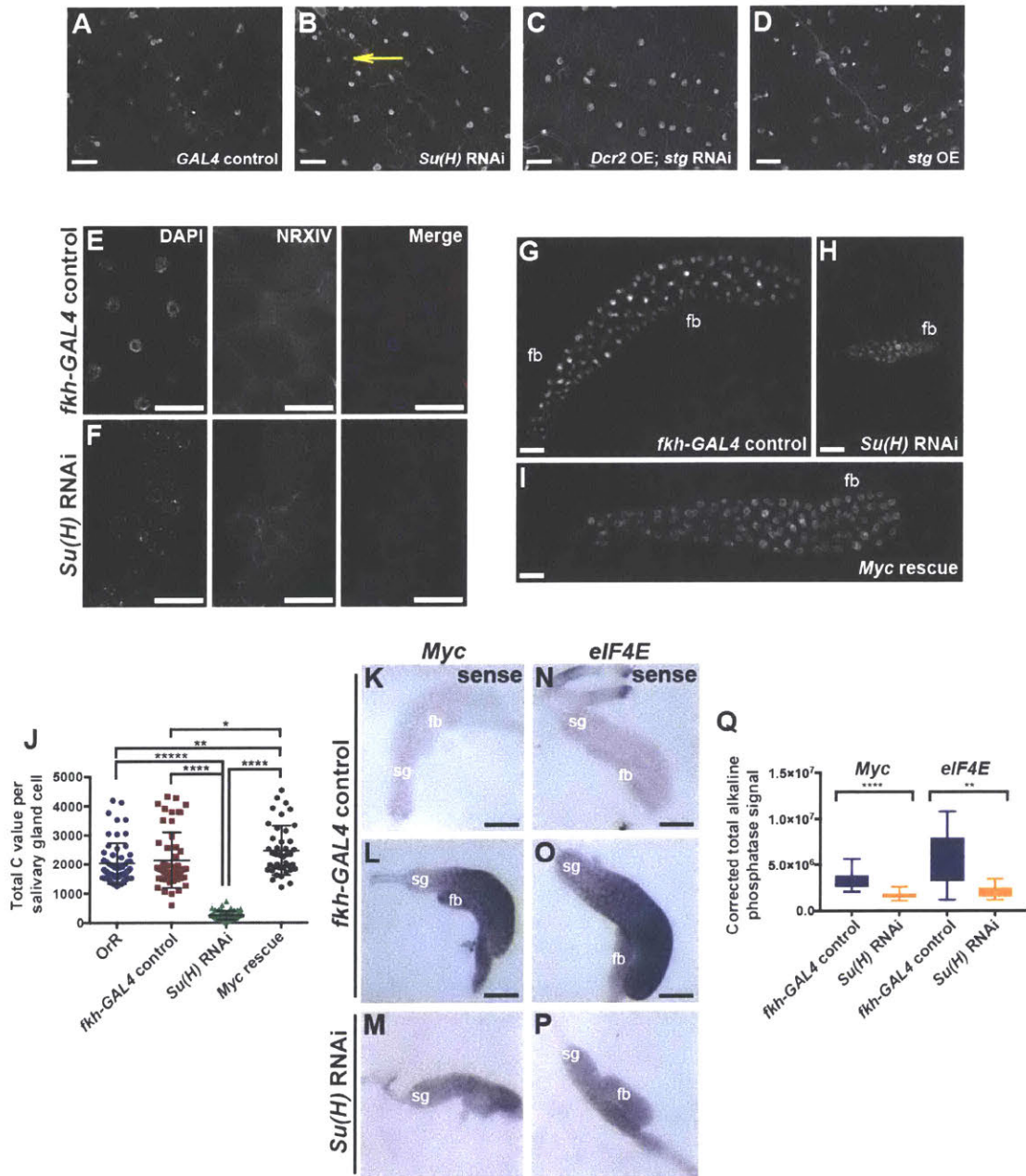


Table 2-2. Percentage of animals of the indicated genotype with at least one multinucleate (endomitotic) SPG present in the VNC at first and third instar

Genotype	% first instar (n)	% third instar (n)
<i>GAL4</i> control	3 (33)	0 (30)
<i>Su(H)</i> RNAi	0 (18)	42 (31)
<i>N</i> RNAi	29 (17)	7 (30)
<i>stg</i> OE	6 (17)	100 (32)
<i>Dcr2</i> OE	0 (18)	6 (30)
<i>Dcr2</i> OE; <i>stg</i> RNAi	0 (12)	0 (31)

Data from first instars, one biological replicate. Data from third instars: *GAL4* control, *N* RNAi and *stg* OE, two biological replicates; *Su(H)* RNAi, three biological replicates; *Dcr2* OE, one biological replicate; and *Dcr2* OE; *stg* RNAi, five biological replicates.

Reduction of N signaling did not result in endomitosis in the salivary gland, in contrast to the SPG, yet *Su(H)* RNAi expression in this tissue did affect ploidy and growth (Fig. 2-9G-J). Whereas the mean ploidies for wild-type OrR and *fkh-GAL4* control salivary glands were 2031C and 2148C, respectively, *Su(H)* RNAi salivary glands had a mean ploidy of 256C (Fig. 2-9J). EdU incorporation measurements showed that this correlated with a reduction of the number of cells in S phase (Fig. 2-10A-F,J). Analysis of polytene chromosome spreads from salivary glands also revealed strong defects in chromosome structure accompanying *Su(H)* RNAi (Fig. 2-10K-Q).

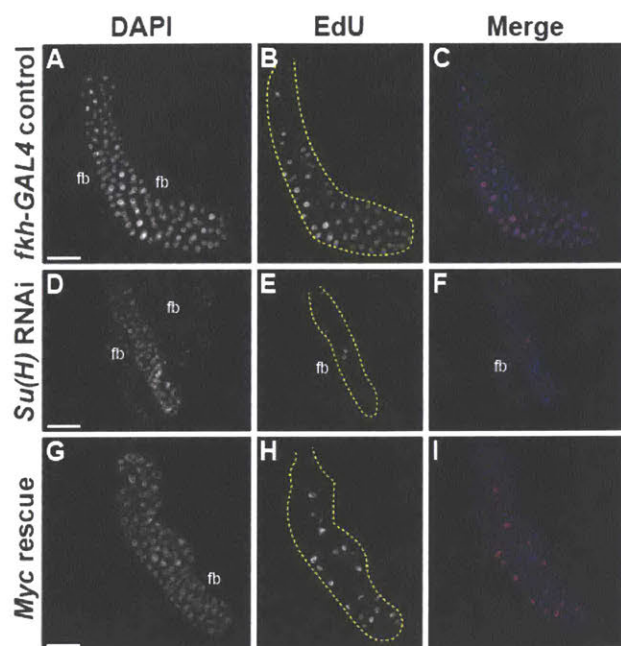
A connection between N signaling through Su(H) and Myc-mediated cell growth was found in *Drosophila* neural stem cells (NSCs) (Song and Lu 2011). It was shown that Su(H) directly activates *dMyc* transcription, which in turn increases the mRNA expression of the translation initiation factor *eIF4E* to promote cell growth and subsequent maintenance of NSC fate. Given these findings, we asked whether a similar N-mediated regulation of growth happens in the salivary glands. We analyzed *dMyc* and *eIF4E* mRNA levels in salivary glands from 96-120 hrs AED larvae by alkaline phosphatase *in situ* hybridization. We found that relative to *fkh-GAL4* controls, *Su(H)* RNAi salivary glands had decreased levels of *dMyc* and *eIF4E* mRNAs (Fig. 2-9K-Q).

These findings suggested that *dMyc* is a key downstream effector of Su(H) signaling in regulating growth in salivary glands, prompting us to test whether its overexpression might be able to rescue the *Su(H)* RNAi phenotypes. Indeed, the cell size, ploidy, and EdU incorporation defects resulting from *Su(H)* RNAi were fully rescued by *dMyc* overexpression (Fig. 2-9G-J; Fig. 2-10G-J). Our results argue that in

Figure 2-10. *Su(H)* RNAi salivary glands have S-phase and chromosomal defects.

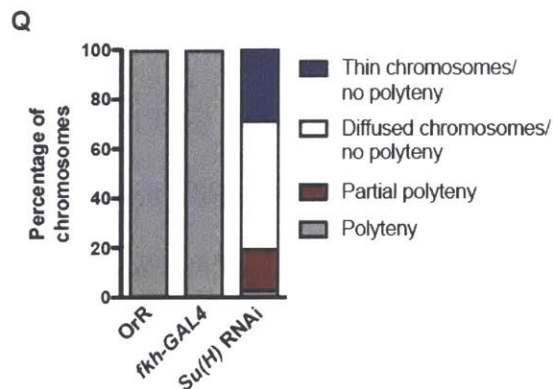
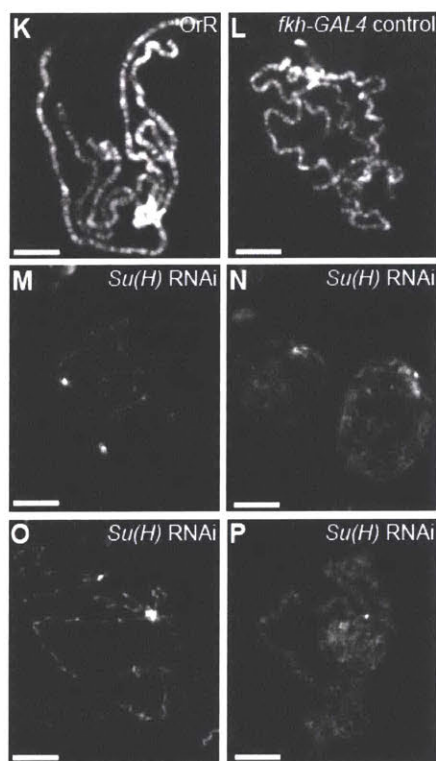
(A-J) *Su(H)* RNAi salivary glands have a reduction of nuclei in S-phase. *fkh-GAL4* alone control (A-C), *Su(H)* RNAi (D-F) or *Su(H)* RNAi; *UAS-Myc* rescued (G-I) salivary glands from 96-120 hours AED third instar larvae were labeled with EdU (Alexa-594, red) to monitor nuclei in S phase and with DAPI to stain DNA (blue). Panels A, D, G DAPI; panels B, E, H EdU; panels C, F, I DAPI and EdU merged. Yellow dotted lines outline the salivary glands in panels B, E and H. fb, fat body. Scale bars, 100 μ m. (J) Quantification of EdU incorporation in salivary glands for control, *Su(H)* RNAi and *Myc* rescue from one biological replicate. (K-Q) *Su(H)* RNAi chromosomes have morphological defects. Images of salivary gland chromosome squashes from wandering third instar larvae stained with DAPI (shown in white). *OrR* (K) and *fkh-GAL4* alone (L) control chromosome spreads illustrating normal thickness and the banding pattern representative of polyteny. (M-P) *Su(H)* RNAi chromosome spreads showing different defects including thinning (M) or diffusion (N) of the chromosomes, or partial polyteny (O). A small percentage of the *Su(H)* RNAi chromosomes appear relatively normal (P). Scale bars, 20 μ m. (Q) Quantification of polytene chromosome morphology. (*OrR* control, n=600 chromosomes; *fkh-GAL4* alone control, n=600 chromosomes; *Su(H)* RNAi, n=629 chromosomes, one biological replicate). See Table 2-1 for complete genotypes.

Figure 2-10



J Quantification of EdU incorporation in SG

Genotype	Average percentage of EdU positive nuclei	
<i>fkh-GAL4</i> control	33%	(n=3,329 nuclei; 24 SGs)
<i>Su(H)</i> RNAi	7.8%	(n=3,036 nuclei; 26 SGs)
<i>Myc</i> rescue	19%	(n=740 nuclei; 6 SGs)



contrast to the SPG where Su(H) and N signaling regulate the choice between the endocycle and endomitosis, in the salivary gland Su(H) solely controls the endocycle, regulating growth and ploidy via dMyc.

The presence of both endocycling and endomitotic SPG is required for the blood-brain barrier

The developmentally triggered onset of endomitosis in the SPG and failure of salivary gland cells to undergo endomitosis when Su(H) was reduced raised the issue of the function and requirement for endomitotic SPG. The key role of SPG is to form the BBB through septate junctions (Stork et al. 2008), and we have shown that ploidy is crucial to increase SPG cell size as the nervous system develops while preserving intact septate junctions (Unhavaithaya and Orr-Weaver 2012). The effect of perturbation of N signaling or changes in the levels of Stg permitted us to evaluate the role of endomitosis in the BBB, as decreased N signaling increased the percentage of endomitotic SPG, reduction of Stg converted the brain to nearly entirely endocycling SPG, and overexpression of Stg caused nearly all SPG in the brain to endomitose.

We measured functionality of the BBB by injecting rhodamine-conjugated dextran into the third instar larval body cavity of control, RNAi, and overexpression animals and then scoring the percentage of brains into which the dye penetrated. Although dye penetrated the BBB in only 2% of *moody-GAL4* injected larvae, dye penetration was detected in 69% of *Su(H)* RNAi, 29% of *N* RNAi, and 50% of *stg* overexpression brain lobes (Fig. 2-11, Table 2-3, Fig. 2-12). RNAi against *stg* also affected the BBB as the dye penetrated 52% of brain lobes (Fig. 2-11, Fig. 2-12). The

Figure 2-11. The blood-brain barrier becomes defective when the percentage of endomitotic SPG is altered. Dye penetration assays were performed in brains of wandering third instar larvae. (A-F) No dye signal was detected inside the lobes of driver-alone control brains (A-C). By contrast, the injected dye penetrated the *Su(H)* RNAi brains (D-F). The dashed lines in the rhodamine dextran panels mark the edges of the brain lobes. Scale bars, 100 μ m. See also Table 2-3. (G-L) Analysis of the septate junction markers NRXIV and DLG in the brain lobes of wandering third instar larvae. (G-I) No visible septate junction breaks were detected in *GAL4* control brains. (J-L) Visible NRXIV and DLG breaks were detected in *Dcr2* OE; *stg* RNAi brains. (J'-L') Enlargement of septate junction breaks in panels K-M. White arrows point to breaks. For n and *P* values see Fig. 2-12M. Scale bars, 25 μ m.

Figure 2-11

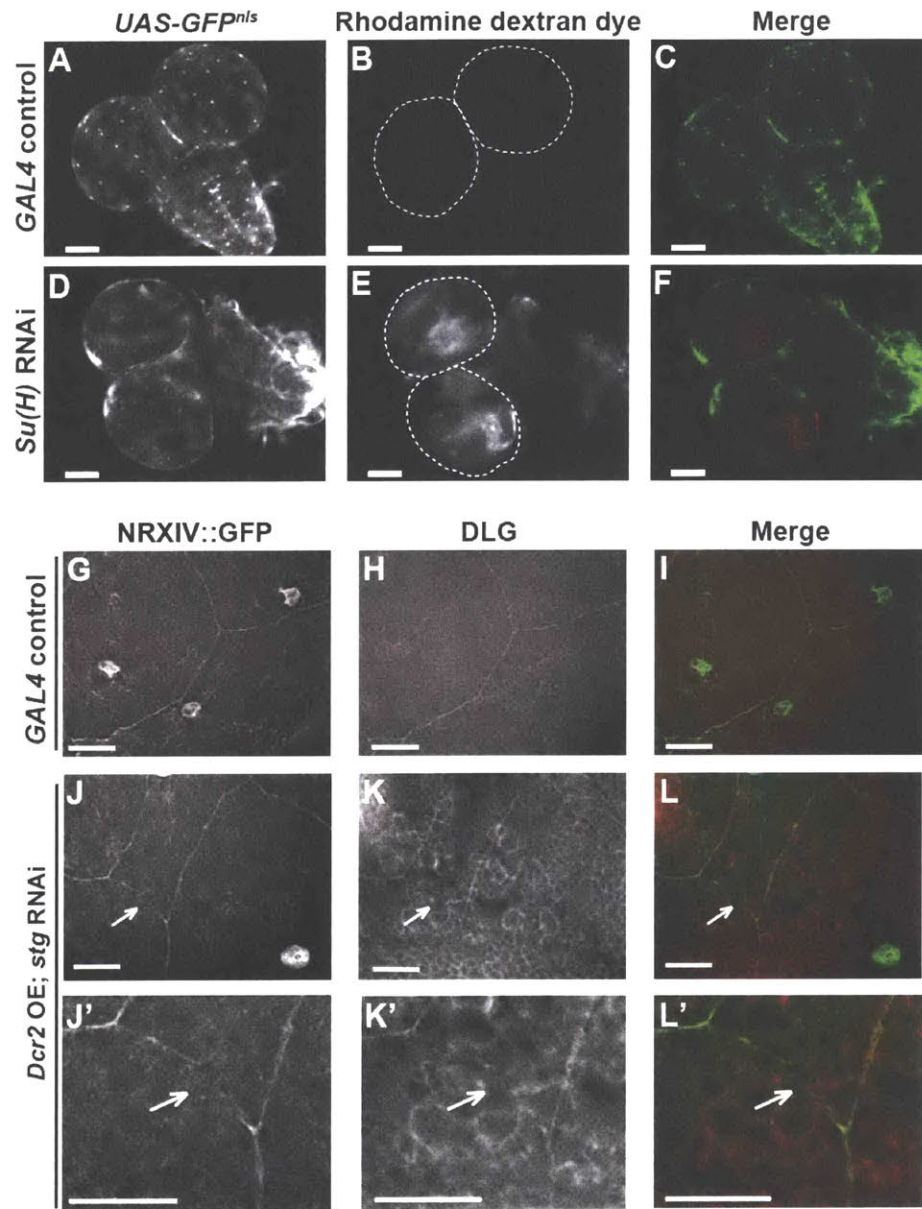


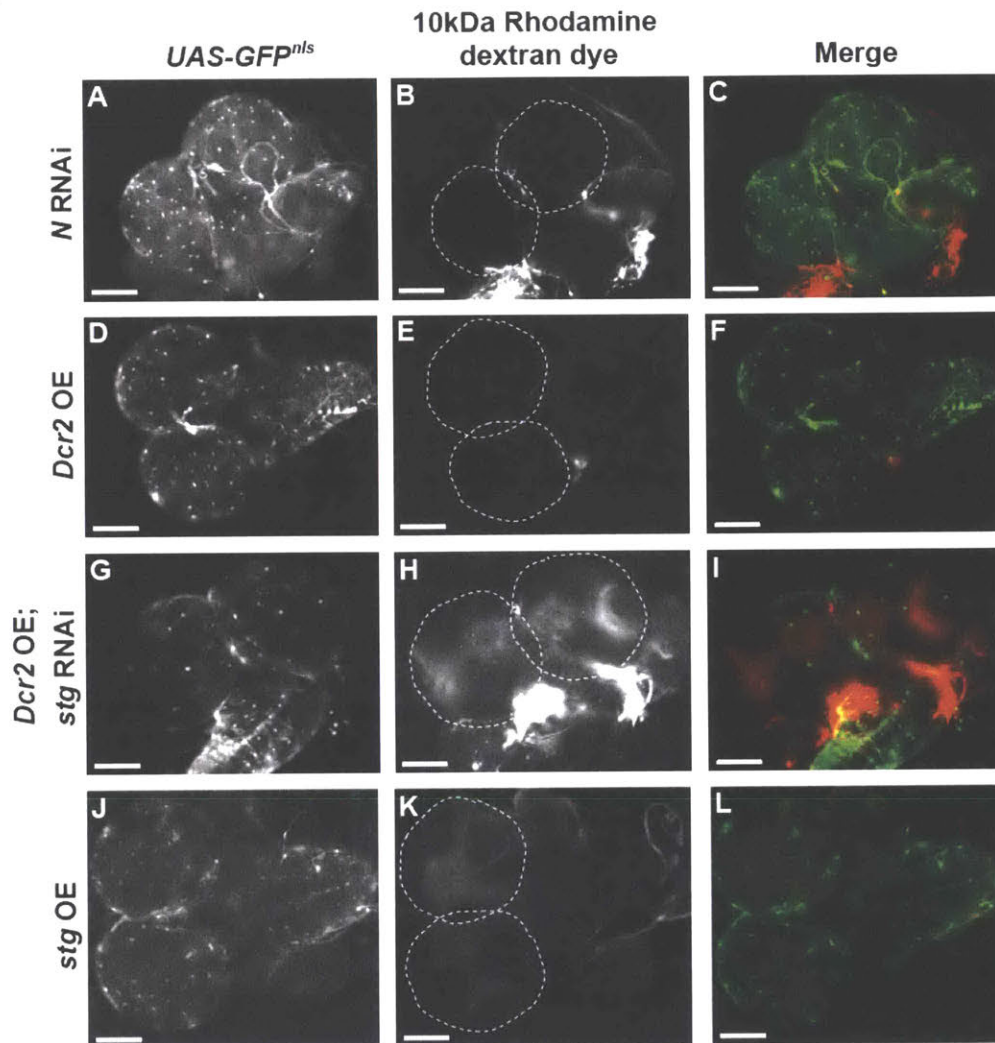
Table 2-3. The percentage of brains of animals of the indicated genotype showing dye penetration

Genotype	% (n)
<i>GAL4</i> control	2 (46)
<i>Su(H)</i> RNAi	69 (58)
<i>N</i> RNAi	29 (35)
<i>stg</i> OE	50 (26)
<i>Dcr2</i> OE	20 (49)
<i>Dcr2</i> OE; <i>stg</i> RNAi	52 (42)

Dye penetration was significantly increased in *Su(H)* RNAi ($P=4.4 \times 10^{-12}$), *N* RNAi ($P=1.7 \times 10^{-5}$), *stg* OE ($P=6.0 \times 10^{-7}$) and *Dcr2* OE; *stg* RNAi ($P=0.002$) brains relative to corresponding controls, Chi-square test. *GAL4* control and *stg* OE data, two biological replicates. *Su(H)* RNAi, *N* RNAi, *Dcr2* OE, and *Dcr2* OE; *stg* RNAi data, three biological replicates.

Figure 2-12. Dye penetration of the BBB and visible breaks in the septate junctions are observed when the percentage of endomitotic SPG is altered. Dye penetration assays were performed in brains of wandering third instar larvae in which different transgenes were driven in the SPG by *moody-GAL4*. (A-C) In 71% of animals no dye signal was detected inside the lobes expressing *N* RNAi. (D-F) In 80% of animals no dye signal was detected inside the *Dcr2* OE lobes. (G-I) In 52% of larvae dye penetrated the lobes expressing *Dcr2* OE; *stg* RNAi. (J-L) In 50% of animals dye penetrated the lobes with *stg* overexpression (OE). The dashed lines in the rhodamine dextran panels mark the edges of the brain lobes. For N and P values see Table 2-3. Scale bars, 100 μ m. (M) Quantification of visible breaks in the septate junction markers NRXIV and DLG for the genotypes listed from brain lobes of wandering third instar larvae. Relative to *GAL4* control, the visible breaks in DLG, NRXIV, and both DLG and NRXIV were significantly increased for *Su(H)* RNAi (Chi-squared test, $P=0.0017$, $P=0.0033$, and $P=0.0033$, respectively). No significant difference was found for *stg* OE brains (Chi-squared test, $P=0.080$, $P=0.081$, $P=0.16$). Relative to *Dcr2* OE, the visible breaks in NRXIV and both DLG and NRXIV were significantly increased for *Dcr2* OE; *stg* RNAi (Chi-squared test, $P=0.038$ and $P=0.038$, respectively; DLG, $P=0.052$). *GAL4* control and *Su(H)* RNAi data from four biological replicates; *stg* OE and *Dcr2* OE data from three biological replicates; *Dcr2* OE; *stg* RNAi from five biological replicates. Complete genotypes are in Table 2-1.

Figure 2-12



M Quantification of Visible Breaks in Septate Junction Markers

Genotype	NRXIV breaks	DLG breaks	Both NRXIV and DLG breaks	N
<i>GAL4</i> control	0%	7%	0%	30
<i>Su(H)</i> RNAi	19%	35%	19%	31
<i>stg</i> OE	10%	23%	6%	31
<i>Dcr2</i> OE	0%	10%	0%	29
<i>Dcr2</i> OE; <i>stg</i> RNAi	14%	31%	14%	29

RNAi depletion experiments for *stg* were done in the presence of *Dicer2* to enhance knockdown. Induction of *dicer2* alone affects the BBB, as 20% of brains in *UAS-dicer2; moody-GAL4* showed dye penetration (Table 2-3). Nevertheless, depletion of *stg* showed a percentage of brains with dye penetration significantly higher than this control (Table 2-3).

Blocking polyploidization of SPG by inhibiting DNA replication led to reduced cell size, BBB defects and ruptured intercellular septate junctions (Unhavaithaya and Orr-Weaver 2012). The results above showed that either increasing or decreasing the proportion of endomitotic SPG caused BBB defects. To determine whether this could be due to alterations of the SPG cell envelope, we visualized septate junctions by staining with an antibody to the Discs large 1 (DLG) protein as well as with the NRXIV-GFP fusion (Fig. 2-11G-L). RNAi against *Su(H)* and *stg*, and overexpression of *stg* all resulted in breaks in septate junction tracks visible with both protein markers, in contrast to driver alone controls (Fig. 2-11G-L, Fig. 2-12M). Breaks in the septate junctions were significantly increased in *Su(H)* and *Dcr2* overexpression; *stg* RNAi brains. Although breaks were elevated following *Stg* overexpression, the significance was borderline. These results are consistent with the BBB defects resulting from breakage of the septate junctions.

The relationship between ploidy, nuclear number and cell size in the endocycle versus endomitosis

Given that the presence of endomitotic SPG is crucial for the BBB, we compared how endomitosis and the endocycle affect cell size, total cell ploidy, and shape. The SPG tissue layer has to maintain a seal around the proliferating neuronal mass of the brain

during larval development; consequently, SPG cell size is critical. One possibility was that endocycling versus endomitotic SPG had a different shape and that the right combination of these shapes enabled them to cover and seal each brain lobe. We noted however that there is not a difference in cell shape arising from the two cell cycles (data not shown).

We examined whether the total cell ploidy differed between endocycling and endomitotic SPG. As noted above, endomitotic SPG have up to eight nuclei, with four being the most frequent. We quantified DAPI fluorescence intensity in all of the nuclei in each SPG cell labeled with GFP^{nls}, marking the cell boundaries with NRXIV-GFP. There was a significant difference: endocycling cells had a mean ploidy of 15C, whereas endomitotic cells had a mean ploidy of 31C (Fig. 2-6A).

We next examined how SPG cell size correlated with ploidy in the two variant cell cycles. The SPG are flat cells of depth less than 1mm, and thus their area reflects cell size (Stork et al. 2008; Limmer et al. 2014). As expected, cell size scales with total cellular DNA content in both cell cycle types (Fig. 2-6B,C). The mean area of the population of endomitotic SPG was larger than the endocycling SPG (Fig. 2-6D), consistent with their increased ploidy levels.

In addition to increased ploidy causing increased cell size, we wondered whether increased nuclear number might also contribute to the increased size of endomitotic SPG. We compared cell size to nuclear number for endocycling and endomitotic SPG with different ploidies (Fig. 2-13A) as well as within a ploidy range of 20-32C (Fig. 2-6E). Nuclear number indeed augments cell size, as cells with four nuclei were larger than cells

Figure 2-13. Relationship between nuclear number, ploidy and cell area. All brains were collected from wandering third instar larvae. (A) Increased nuclear number in SPG correlates with increased cell area. Cell area ($\mu\text{m}^2 \times 10^3$) in relation to SPG nuclear number (n=70 SPG; 36 brains, three biological replicates). Spearman correlation coefficient $r=0.60$, $P<0.0001$. (B) Scatter plot showing the DNA ploidy C values of individual endocycling and endomitotic SPG cells in *Dcr2* OE versus *Dcr2* OE; *stg* RNAi brain lobes. Mann-Whitney, two-tailed test, **** $P < 0.0001$; n.s.=not significant. *Dcr2* OE: n=16 endocycling SPG, 18 endomitotic SPG, 15 brains, one biological replicate. *Dcr2* OE; *stg* RNAi: n=48 endocycling SPG, 15 brains, one biological replicate. (C) Scatter plot showing the DNA ploidy C values of individual endocycling and endomitotic SPG cells in *GAL4* control versus *Su(H)* RNAi brain lobes. The control data are from Figure 2-6. *Su(H)* RNAi: n=33 endocycling SPG, 24 brains; n=44 endomitotic SPG, 33 brains, six biological replicates. Mann-Whitney, two-tailed test, **** $P<0.0001$; n.s.=not significant. (D) Scatter plot showing cell areas ($\mu\text{m}^2 \times 10^3$) of individual endocycling and endomitotic SPG in *Dcr2* OE versus *Dcr2* OE; *stg* RNAi brain lobes. Mann-Whitney, two-tailed test, **** $P < 0.0001$; n.s.=not significant. *Dcr2* OE: n=16 endocycling SPG, 18 endomitotic SPG, 15 brains, one biological replicate. *Dcr2* OE; *stg* RNAi: n=48 endocycling SPG, 15 brains, one biological replicate. (E) Scatter plot showing cell area ($\mu\text{m}^2 \times 10^3$) of individual *GAL4* control and *Su(H)* RNAi endocycling and endomitotic SPG cells in the brain lobe. Data from *GAL4* controls are the same presented in Figure 2-6D. *Su(H)* RNAi: n=12 endocycling SPG, 12 brains, n=28 endomitotic SPG, 15 brains, three biological replicates. Mann-Whitney, two-tailed

test, *** $P=0.0002$; **** $P<0.0001$; n.s.=not significant. Scatter plots, mean \pm 95% c.i..

See Table 2-1 for complete genotypes.

Figure 2-13

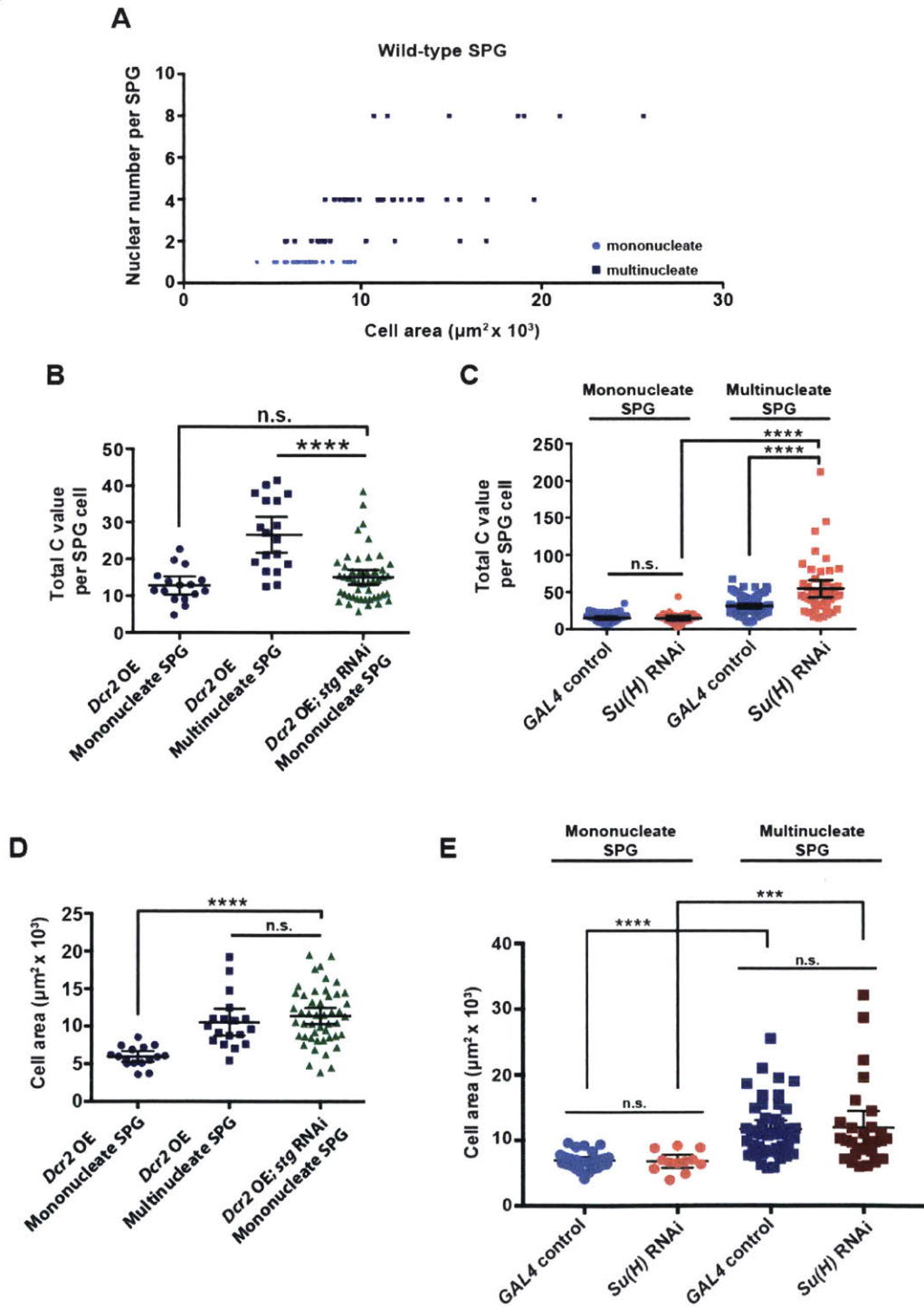


Table 2-4. SPG nuclear number, cell area and ploidy (20C-32C range)

	Nuclei number	Cell area (μm^2)	Ploidy (C value)
SPG 1	1	7800	23
SPG 2	1	6700	24
SPG 3	1	7200	25
SPG 4	1	5800	22
SPG 5	1	9000	22
SPG 6	1	9400	24
SPG 7	1	6100	21
SPG 8	1	7400	22
SPG 9	1	6300	20
SPG 10	1	6500	22
SPG 11	2	15000	28
SPG 12	2	7700	21
SPG 13	2	5800	31
SPG 14	2	8000	24
SPG 15	2	6200	21
SPG 16	2	17000	24
SPG 17	2	7200	22
SPG 18	2	7600	29
SPG 19	2	7500	27
SPG 20	2	12000	25
SPG 21	4	13000	29
SPG 22	4	8800	29
SPG 23	4	11000	26
SPG 24	4	8500	31
SPG 25	4	8000	30
SPG 26	4	12000	25
SPG 27	4	9900	26
SPG 28	4	11000	27
SPG 29	4	9300	24
SPG 30	4	11000	29
SPG 31	4	12000	30

of the same ploidy with one or two nuclei (Table 2-4). We conclude that both ploidy and nuclear number contribute to SPG cell size, and that endomitosis likely is a mechanism to increase cell size in the brain lobes to maintain the BBB. This is consistent with the smaller SPG cell size in the VNC and absence of endomitosis in these cells.

We examined cell size in the *stg* and *Su(H)* RNAi lines to test whether the higher ploidy associated with endomitotic cells compared with endocycling cells persisted with these perturbations, and to investigate whether cell sizes also were altered. As expected, in *stg* RNAi; *Dcr2* overexpression SPG, which were nearly all endocycling, the ploidy was equivalent to wild-type endocycling SPG, but reduced compared to wild-type endomitotic SPG (Fig. 2-13B). The *Su(H)* RNAi SPG that were multinucleate and had higher nuclear numbers than wild-type multinucleate SPG correspondingly had higher ploidy levels (Fig. 2-13C). Unexpectedly, in both of these RNAi conditions the normal positive link between ploidy and cell size became uncoupled, at least by the third instar stage when cell size was measured (Fig. 2-6F-H, Fig. 2-13D,E). When either *Su(H)* or *Stg* were reduced, mononucleate cells of the same ploidy exhibited a larger range of sizes (Fig. 2-6F,H), and cells of the same size exhibited a larger range of ploidy (especially the multinucleate *Su(H)* RNAi cells, Fig. 2-6G). Thus the defects in the BBB may not be due solely to an alteration of SPG cell size.

DISCUSSION

Drosophila SPG cells illustrate the developmental strategy of employing variant cell cycles for organogenesis. Here we find that SPG in the brain lobe can undergo two cell cycle changes during development, initiating the endocycle but reinstating nuclear division to increase nuclear number during endomitosis. The promotion of mitosis requires the *Stg Cdc25*

phosphatase and is limited by N signaling. Importantly, the presence of endomitotic SPG is essential for the BBB. These results support the conclusion that endomitosis and increased nuclear number are a mechanism for further increases in cell size beyond those attained by the endocycle.

The role and regulation of endomitosis in the SPG

Despite the prevalence of polyploidy throughout the plant and animal kingdoms and the consistent correlation between ploidy and cell size, it remains a mystery why size scales with ploidy. We found that endomitotic cells are larger than endocycling cells, but this is due only in part to their higher ploidy. Interestingly, increased nuclear number also contributes to increased cell size. The SPG are flat cells, and the localization of the nuclei throughout the cell in endomitotic SPG could facilitate better distribution of gene products than in the endocycling cells in which large regions of the cytoplasm are distant from the nucleus. The properties of SPG in a brain tumor mutant are consistent with the use of endomitosis and increased nuclear number augmenting cell size. We previously found that in a tumor mutant with unregulated neuroblast cell divisions, the SPG respond by increasing their ploidy, thereby preserving the BBB (Unhavaithaya and Orr-Weaver 2012). We note that this is associated with an increased nuclear number in the endomitotic SPG cells, likely permitting a further size increase in the SPG in response to the increased underlying neuronal mass.

Two unexpected findings that remain to be understood mechanistically are: (1) endomitotic cells of a given ploidy can exhibit a range of cell size; and (2) perturbation of N signaling or cell cycle regulation can uncouple the relationship between size and ploidy. It may be that gene expression is not uniform across the multiple nuclei of an endomitotic cell, resulting in variance of growth and cell size with respect to nuclear number. Signals from surrounding

cell layers may differentially control the growth of wild-type endomitotic SPG and could promote the growth of *stg* RNAi endocycling SPG such that by the third instar stage they are able to attain the size normally associated with the endomitotic cells of increased ploidy.

The active developmental control of the onset of endomitosis in the SPG between first- and second-larval instar will make it important in the future to identify the developmental cues promoting the onset of endomitosis and distinguishing which SPG cells remain in the endocycle. Given the requirement for both N and DI in the SPG for endocycling cells, it is possible that lateral inhibition causes some cells to endocycle and others to endomitose. This explanation, however, is not easily reconcilable with the spatial distribution of the two classes of SPG in the brain. Another possibility is that the DI ligand is present in SPG in the VNC, causing them and the brain SPG closest to the VNC to remain in the endocycle.

In addition to defining developmental signals, questions remain about cell cycle control. The mechanism through which N signaling ensures both the regulation of nuclear division at a cellular level and the accuracy of mitosis remain to be defined. It is unclear whether N signaling can directly repress *stg* in the SPG. Reduction of Su(H) did not alter levels of *stg* mRNA, but Stg activity may be controlled post-translationally, because the Cdc25 phosphatase is known to be controlled by phosphorylation (Myer et al. 2005). Such regulation could explain why Cyclin B and Stg levels appear the same in endocycling and endomitotic SPG, despite the genetic experiments showing that perturbation of *stg* levels impacts the percentage of SPG in endomitosis.

Ensuring a functional BBB

We found that the BBB is defective in the absence of endomitotic SPG following *stg* RNAi. A key question is whether the BBB defect is primarily a consequence of cell cycle changes. In *Drosophila* the *stg* gene has not been observed to have functions or effects outside of cell cycle regulation, thus the simplest explanation is that endomitosis itself is required for SPG function in the BBB. As discussed above, we hypothesize that endomitosis and the presence of multiple nuclei affect gene expression. The SPG subjected to *stg* RNAi have reduced ploidy compared to endomitotic SPG, and this also could impact gene expression. Because the *stg* RNAi cells can grow to nearly endomitotic size, the BBB defects may not be due primarily to cell size. The results here agree with previous work demonstrating that a functional BBB is dependent on proper SPG ploidy: either increases or decreases in ploidy lead to BBB defects (Unhavaithaya and Orr-Weaver 2012; Li et al. 2017). In these latter studies ploidy was decreased by inhibiting DNA replication or increased in response to increased levels of Yorkie and Cyclin E and thus, as in the case of changing *Stg* levels, cell cycle changes led to BBB defects. It will be interesting to determine why SPG function is so sensitive to correct ploidy.

Given the many roles N signaling can play in development, N may regulate SPG in multiple ways. Thus when N signaling is reduced not only the ratios between the cell cycle variants but also differentiation of the SPG may be affected, leading to BBB defects. The defective BBB is unlikely to result from reduced expression of septate junction components, however, given that Su(H) has not been observed to bind to the regulatory regions of any of the genes encoding septate junction proteins (Contrino et al. 2012; Housden et al. 2013; Terriente-Felix et al. 2013; Slattery et al. 2014; Skalska et al. 2015).

Developmental control of the cell cycle

We note several other cases in which cell cycle changes affecting cell differentiation and function have been investigated. A recent study in megakaryocytes shows that these cells remain functional to make platelets when switched from endomitosis to the endocycle (Trakala et al. 2015), in contrast to our results with *stg* RNAi demonstrating that endomitotic SPG are essential. In *C. elegans*, a group of intestinal cells undergo one round of endomitosis under CDC-25 control to become binucleate at the end of the first-larval stage. CDC-25 is then targeted for destruction, and the cells subsequently endoreduplicate (Lee et al. 2016). In mammalian hepatocytes the E2F7 and 8 transcription factors are required for polyploidization, but when they are knocked out hepatocyte differentiation and liver regeneration do not appear to be affected (Pandit et al. 2012). Thus in this case, polyploidy may not play a crucial role.

The work presented here highlights distinct cell cycle capabilities in development and differentiation. In contrast to the brain SPG, SPG in the VNC do not normally undergo endomitosis yet are susceptible to change from the endocycle to endomitosis. Loss of Su(H) in the salivary gland, however, did not cause a return to mitosis. dMyc is not the essential downstream target of Su(H) in the SPG, as overexpression of dMyc does not rescue the endomitosis defects (data not shown). By contrast, *Su(H)* RNAi revealed a crucial role for Su(H) in promoting increased ploidy in the endocycle and thus growth in the salivary gland by regulation of dMyc levels. These results illustrate the developmental plasticity of the cell cycle. Although the endocycle increases cell size, endomitosis results in larger, higher ploidy cells that are required in the brain lobe SPG. Thus endomitosis appears to be a cell cycle variant that can be employed to meet extreme demands for cell growth and gene expression during development and organogenesis.

MATERIALS AND METHODS

Fly strains

Drosophila strains used in this study were: Oregon R; *pUdsGFP-Su(H)* RNAi (gift from Anette Preiss, University of Hohenheim); *fkf-GAL4 (III)* (provided by Deborah Andrew, Johns Hopkins University); *UAS-Myc (II)* (BDSC #9674); *moody-GAL4(II)* (provided by Christian Klämbt, University of Münster), and *NrxIV::GFP* (Banerjee et al. 2010); *UAS-N* RNAi (II) (VDRC #1112); *UAS-CycB* RNAi (BDSC #34544); *UAS-Dl* RNAi (MR182, II; gift from Matthew Rand, University of Rochester Medical Center); *UAS-Dcr2 (X)*(VDRC#60010); *UAS-stg* RNAi (III) (VDRC#17760; gift from Don Fox, Duke University School of Medicine); *UAS-stg* (BDSC #4778).

Antibodies

Primary antibodies used were mouse anti-CycB [Developmental Studies Hybridoma Bank (DSHB), F2F4, 1:15] and anti-DLG (DSHB 4F3, 1:15), rabbit anti-NRXIV (Manzoor Bhat, University of Texas Health Science Center; 1:1,000), anti-phospho-Histone H3 (Ser10) (EMD Millipore #06-570, 1:400), rat anti-ELAV (DSHB 7E8A10, 1:15) and guinea pig anti-GFP (gift from Mary-Lou Pardue, MIT; 1:400). The GFP-Booster nanobody (Chromotek #gba488) was used at 1:400. Secondary antibodies used were Alexa Fluor 568 goat anti-mouse or anti-rabbit (1:1,000) (Life Technologies), Alexa Fluor 647 goat anti-rabbit (1:1,000) (Life Technologies), and RRX and Cy5 conjugated to donkey/goat anti-rabbit or anti-rat (1:250) (Jackson ImmunoResearch).

Dissection, fixation and antibody staining of larval tissues

Larval brains and salivary glands were dissected in either unsupplemented Grace's medium or PBS, fixed in 4% formaldehyde/PBS for 30 minutes, washed in PBST (0.3% TritonX-100) and blocked for 1 hour at room temperature with blocking solution (PBST, 2.5% goat and 2.5% donkey serum).

Mono versus multinucleate SPG ratios

To determine SPG nuclear number we outlined the cell boundaries of wandering third instar larval brains by using either a NRXIV antibody or the NRXIV::GFP fusion protein. Mononucleate versus multinucleate SPG were scored after 3D reconstruction was performed using the Zeiss 710 Confocal microscope using an LD LCI Plan-Apochromat 25X/0.8Imm Korr DIC M27 objective and analyzed using ZEN Software (Zeiss) for eight *GAL4* control, *Su(H)* RNAi and *N* RNAi brain lobes. For the remaining *GAL4* control, *Su(H)* RNAi and *N* RNAi brain lobes and all *Dcr2* overexpression; *DI* RNAi brains whole lobes were imaged from the Nikon eclipse inverted microscope. For first- and second- instar larvae, images of half lobes from the Nikon eclipse inverted microscope were used. To quantify the percentage of mononucleate versus multinucleate SPG, Z-stacks and/or single frames of both the dorsal- and/or ventral-most surfaces of the brain were analyzed. To score all SPG we demanded that the full outline of the SPG cell to be visible in the NRXIV-GFP channel either in single scanned images or in multiple focal planes from Z- stacks. Thus, any out of focus nuclei that are seen in the images are nuclei from the opposite side of the brain. Consequently, the data likely are an underestimate of cells with a higher nuclear number.

To assess the multinucleate SPG present in the VNC, both the dorsal and ventral sides of the VNC were imaged on the Nikon eclipse inverted microscope. Cells were scored as multinucleate only if the entire cell boundary was visible and consequently are likely an underestimate. An animal was scored as positive if any multinucleate cells were observed in the VNC.

To determine statistical significance the Kruskal-Wallis Test with Dunn's multiple comparisons or the Mann-Whitney, two-tailed test were applied using GraphPad Prism. A Chi-square test was performed to determine statistical significance for differential localization of mono versus multinucleate SPG proximal to the VNC.

DAPI staining/ploidy C value calculations

Samples were stained with DAPI at 50 ng/ml, the optimal concentration for quantification of DNA ploidy (Hamada and Fujita 1983), washed overnight, and imaged with a Nikon eclipse inverted microscope, using either 60X or 100X objectives. This low DAPI concentration was used so as not to oversaturate the signal. Although DAPI shows that nuclear size and staining intensity are proportional to DNA content, the nuclear GFP signal is not proportional to either nuclear size or DNA content. z-stacks that covered the entire nucleus were acquired. All images were deconvolved using NIS-Elements software (Nikon). An area was drawn around the diploid or polyploid nucleus of selected in focus stacks using the NIS Elements Draw Bezier ROI tool, and the adaptive background compensation function was used to decrease background signal until the DAPI pixel density measurement was between 0-100 around each nucleus. The area quantified was defined by the DAPI signal, as the nuclear-localized GFP signal was found to be sometimes broader than the DAPI-stained DNA. DNA content was

quantified for each nucleus by obtaining the sum intensity of the DAPI pixel density in NIS elements. For multinucleate SPG, the ploidy of each nucleus was measured, and the total cell ploidy was determined by summing the ploidy values for each nucleus within the cell. Ploidy was calculated by normalizing each SPG nucleus from wandering third instar larvae to diploid neuronal nuclei (average of 8-12 neurons per SPG cell). The diploid neurons were identified by staining with anti-ELAV (Robinow and White 1991). For salivary glands, ploidy was calculated by normalizing each salivary gland nucleus from wandering third instar larvae (average of 6 nuclei per salivary gland) to the diploid imaginal ring cells (average of 8 imaginal ring cells per gland). In both cases diploid reference cells and polyploid cells were collected from the same animal and imaged on the same slide with the same exposure settings.

Statistical significance was determined by the Kruskal-Wallis Test with Dunn's multiple comparisons or the Mann-Whitney, two-tailed test using GraphPad Prism. Where necessary, the Kruskal-Wallis Test was followed by a Bonferroni adjustment.

Dye penetration assay and septate junction analysis

The rhodamine-dextran dye penetration assay and the septate junction analyses were performed in wandering third instar larvae from all genotypes listed in Table 2-3 and Fig. 2-12M. The dye penetration assay was carried out as in (Unhavaithaya and Orr-Weaver 2012), with some modifications. Third-instar larvae were placed on molasses agar plates and, immediately prior to dye injection, gently rolled between Kimwipe sheets. The larvae were transferred to double-sided tape, which was placed on microscope slides, and gently pressed down to stick the larvae to the tape. The slide was placed on an inverted microscope and larvae were injected in the posterior body cavity with a machine-drawn capillary needle filled with

Tetramethylrhodamine dextran (ThermoFisher Scientific, D1816, 10 kDa, 2.5mM final concentration in water). Larvae were injected until the entire body turned the color of the dye. Injected larvae were covered with halocarbon oil for recovery and gently transferred to molasses plates after wiping off excess oil. After 10-15 minutes post injection, brains from live, injected larvae were dissected in unsupplemented Grace's medium, washed three times in the medium and mounted in Grace's medium along with some larval carcasses onto a microscope slide and coverslip. Brains were live imaged on a Nikon eclipse inverted microscope using a 10X objective. A brain was called positive for dye penetration when there was detectable signal inside of the brain lobes that was clearly higher than the background signal. In cases where dye clearly penetrated the brain, images of single frames in which the inside of the brain lobes were in focus were taken. In brains in which dye penetration was not as clear, Z-stacks of the brain were taken and several focal planes were analyzed. Brains in which dye penetration was ambiguous were not used in the quantification. Three independent researchers examined and scored the brains. Visible NRXIV::GFP and/or DLG breaks were scored using Z-stacks of deconvolved images taken with the Nikon eclipse microscope. Chi-squared tests were used to evaluate whether the differences in dye penetration or visible septate junctions breaks were significant between each of the control and experimental genotypes.

Fluorescence in situ hybridization (FISH) or alkaline phosphatase (AP) in situ hybridization

Salivary glands were dissected from third instar larvae (96-120 hrs AED) and fixed, pre-hybridized, hybridized, washed, and detected as described (Wolff 2000). Larval brains were dissected from third instar larvae (~120 hrs AED) and processed for FISH as described (Lecuyer et al. 2008). Sense and antisense probes were generated by amplifying the corresponding

cDNAs for all genes assayed from the Drosophila gene collection clones (*Myc*, LD32539; *eIF4E*, SD05406; *Su(H)*, GH10914; *N*, LD34134; *stg*, LD47579) following the Berkeley Drosophila genome project protocol. Amplified PCR fragments were purified and *in vitro* transcribed. All probes were size-reduced with 2X carbonate buffer (120mM Na₂CO₃, 80mM NaHCO₃, pH 10.2) for 15 minutes. AP detection time for *Myc* and *eIF4E* probes was 23 minutes. Both control *fkh-GAL4* alone and *Su(H)* RNAi salivary glands, distinguishable by their size, were hybridized and histochemically labeled in the same dish. Thus the intensity of the color stain can be compared between the two samples.

Anti-Cyclin B cytoplasmic fluorescence in both first and second instar larval brain SPG and salivary glands, *Myc* and *eIF4E* AP *in situ* signals in salivary glands or *N*, *Su(H)* and *stg in situ* hybridization fluorescence in brain lobes were all measured with Image J. For brain lobe or salivary gland protein or FISH transcript measurements, a single frame from Z-stacks taken with an LSM710 confocal microscope containing the SPG or the salivary gland nucleus in focus was used. For AP *in situ* measurements, a single scan of salivary glands taken with a Zeiss SteREO Discovery V8 microscope was used. For SPG, measurements were made from the signal from the entire circumference of whole half brain lobes. For salivary glands, measurements were made from the entire area from half salivary glands. All samples were imaged using the same exposure times between first and second instar stages (anti-Cyclin B fluorescence) or between the control and RNAi samples (AP signal and FISH fluorescence). Three independent background measurements were taken in areas without fluorescence or AP signal. Image J “area”, “integrated density”, and “mean gray value measurements” settings were selected for all measurements. Values were obtained from the following formula: *Corrected total fluorescence or AP signal* = *integrated density* - (*area of selected cell* X *mean fluorescence or AP signal of*

background readings). To determine the statistical significance between control and RNAi samples the Mann-Whitney, two-tailed test was applied using GraphPad Prism.

Cell Area

SPG cell area was measured (μm^2) by tracing the boundary of the cell, marked by NRXIV::GFP, using the NIS elements area tool. Area measurements were obtained in units of μm^2 . To determine statistical significance, Spearman's correlation was performed with linear regression.

Statistics

Sample sizes were calculated using the `pwr.t.test` (for 2 groups) and `pwr.anova.test` (for >2 groups) functions in the "pwr" R package, setting the power to 0.8 and the significance level to 0.05. Expected effect sizes were calculated from Cohen's d (using `cohen.d()` in the "effsize" R package) with preliminary data, and sample sizes were increased by 20% to account for the use of non-parametric tests. All data observations are independent and meet the assumptions of the (non-parametric) statistical tests.

EdU and Phospho-Histone H3 (PHH3) labeling

EdU labeling was performed in salivary glands from 96-120 hrs after egg deposition (AED) third instar larva or in brains from mid-late (30-40 hrs AED) first instar larvae. All tissues were dissected in unsupplemented Grace's medium and incubated in 50 μM EdU in Grace's medium for 1 hour at room temperature. EdU and PHH3 samples were fixed in 1X PBS/4% paraformaldehyde for 30 minutes at room temperature. After fixation, samples were

washed 4X for 10 min with 1X PBT (PBS + 0.3% TritonX-100). Larval brains were then blocked in 1X blocking solution (1X PBST-0.3%, 5% goat and donkey serum) for 1 hr, incubated with GFP-Booster nanobody [1:400] or anti-PHH3 [1:400] in blocking solution overnight at 4°C and washed 4X for 20 min with 1X PBT. Right before detection, both larval salivary glands and brain samples were rinsed 2X in 1X PBS, and incubated in Alexa Fluor 594 or 555 Click-it EdU (Invitrogen) reaction cocktail following the manufacture's instructions or with Alexa-647 anti-rabbit for 1 hour at room temperature in blocking solution. Samples were washed extensively with 1X PBT (6X for 20 min) and stained with DAPI [50 ng/ml] for 15 min at room temperature, washed with 1X PBT, and mounted in Vectashield (Vector laboratories).

Salivary glands chromosome squashes

Polytene chromosomes squashes were prepared following the protocol in (Cai et al. 2010). Squashed chromosomes were stained with DAPI [50 ng/ml].

ACKNOWLEDGMENTS

We are grateful to George Bell for expertise on statistical analysis and Wendy Salmon for microscopy advice. We thank the Bloomington Drosophila Stock Center (BDSC) and Vienna Resource Drosophila Stock Center (VDRC), Deborah Andrew, Don Fox, Anette Preiss, Christian Klämbt, Manzoor Bhat, and Matthew Rand for Drosophila stocks or reagents. Adam Martin, Sam LoCascio, Tony Mahowald, Jared Nordman, P. R. V. Satyaki, and Peter Reddien provided helpful comments on the manuscript. L.E.F. was supported by an NSF Predoctoral Fellowship and T.L.O.-W. is an American Cancer Society Research Professor. This research was supported by the Mathers Charitable Foundation and by grant NS092798 from the National Institutes of Health to T.L.O.-W.

REFERENCES

- Bailey AP, Koster G, Guillermier C, Hirst EM, MacRae JI, Lechene CP, Postle AD, Gould AP. 2015. Antioxidant role for lipid droplets in a stem cell niche of *Drosophila*. *Cell* **163**: 340-353.
- Bainton RJ, Tsai LT, Schwabe T, DeSalvo M, Gaul U, Heberlein U. 2005. *moody* encodes two GPCRs that regulate cocaine behaviors and blood-brain barrier permeability in *Drosophila*. *Cell* **123**: 145-156.
- Banerjee S, Blauth K, Peters K, Rogers SL, Fanning AS, Bhat MA. 2010. *Drosophila* Neurexin IV interacts with Roundabout and is required for repulsive midline axon guidance. *J. Neurosci.* **30**: 5653-5667.
- Bray SJ. 2006. Notch signalling: a simple pathway becomes complex. *Nat. Rev. Mol. Cell Biol.* **7**: 678-689.
- Cai W, Jin Y, Girton J, Johansen J, Johansen KM. 2010. Preparation of *Drosophila* polytene chromosome squashes for antibody labeling. *J. Vis. Exp.*: 1-4.
- Contrino S, Smith RN, Butano D, Carr A, Hu F, Lyne R, Rutherford K, Kalderimis A, Sullivan J, Carbon S, Kephart ET, Lloyd P, Stinson EO, Washington NL, Perry MD, Ruzanov P, Zha Z, Lewis SE, Stein LD, Micklem G. 2012. modMine: flexible access to modENCODE data. *Nucleic Acids Res.* **40**: D1082-1088.
- Cross JC. 2005. How to make a placenta: mechanisms of trophoblast cell differentiation in mice—a review. *Placenta* **26 Suppl A**: S3-9.
- Deng WM, Althausen C, Ruohola-Baker H. 2001. Notch-Delta signaling induces a transition from mitotic cell cycle to endocycle in *Drosophila* follicle cells. *Development* **128**: 4737-4746.
- Edgar BA, O'Farrell PH. 1990. The three postblastoderm cell cycles of *Drosophila* embryogenesis are regulated in G2 by string. *Cell* **62**: 469-480.
- Edgar BA, Orr-Weaver TL. 2001. Endoreplication cell cycles: more for less. *Cell* **105**: 297-306.
- Edgar BA, Zielke N, Gutierrez C. 2014. Endocycles: a recurrent evolutionary innovation for post-mitotic cell growth. *Nat. Rev. Mol. Cell Biol.* **15**: 197-210.
- Fox DT, Duronio RJ. 2013. Endoreplication and polyploidy: insights into development and disease. *Development* **140**: 3-12.
- Fox DT, Gall JG, Spradling AC. 2010. Error-prone polyploid mitosis during normal *Drosophila* development. *Genes Dev.* **24**: 2294-2302.
- Frawley LE, Orr-Weaver TL. 2015. Polyploidy. *Curr. Biol.* **25**: R353-358.
- Hamada S, Fujita S. 1983. DAPI staining improved for quantitative cytofluorometry. *Histochemistry* **79**: 219-226.
- Henderson KD, Andrew DJ. 2000. Regulation and function of *Scr*, *exd*, and *hth* in the *Drosophila* salivary gland. *Dev. Biol.* **217**: 362-374.
- Housden BE, Fu AQ, Krejci A, Bernard F, Fischer B, Tavares S, Russell S, Bray SJ. 2013. Transcriptional dynamics elicited by a short pulse of notch activation involves feed-forward regulation by *E(spl)/Hes* genes. *PLoS Genet.* **9**: e1003162.
- Lecuyer E, Necakov AS, Caceres L, Krause HM. 2008. High-resolution fluorescent in situ hybridization of *Drosophila* embryos and tissues. *CSH Protoc.* **2008**: pdb prot5019.
- Lee YU, Son M, Kim J, Shim YH, Kawasaki I. 2016. CDC-25.2, a *C. elegans* ortholog of *cdc25*, is essential for the progression of intestinal divisions. *Cell Cycle* **15**: 654-666.

- Li D, Liu Y, Pei C, Zhang P, Pan L, Xiao J, Meng S, Yuan Z, Bi X. 2017. miR-285-Yki/Mask double-negative feedback loop mediates blood-brain barrier integrity in *Drosophila*. *Proc. Natl. Acad. Sci. U S A* **114**: E2365-E2374.
- Limmer S, Weiler A, Volkenhoff A, Babatz F, Klambt C. 2014. The *Drosophila* blood-brain barrier: development and function of a glial endothelium. *Front. Neurosci.* **8**: 365.
- Lopez-Schier H, St Johnston D. 2001. Delta signaling from the germ line controls the proliferation and differentiation of the somatic follicle cells during *Drosophila* oogenesis. *Genes Dev.* **15**: 1393-1405.
- Micchelli CA, Perrimon N. 2006. Evidence that stem cells reside in the adult *Drosophila* midgut epithelium. *Nature* **439**: 475-479.
- Myer DL, Bahassi el M, Stambrook PJ. 2005. The Plk3-Cdc25 circuit. *Oncogene* **24**: 299-305.
- Nagl W. 1978. Endopolyploidy and polytene in differentiation and evolution: Towards and understanding of quantitative variation of nuclear DNA in ontogeny and phylogeny. North-Holland Publishing Company, Amsterdam, Netherlands.
- Ohlstein B, Spradling A. 2006. The adult *Drosophila* posterior midgut is maintained by pluripotent stem cells. *Nature* **439**: 470-474.
- Orr-Weaver TL. 2015. When bigger is better: the role of polyploidy in organogenesis. *Trends Genet.* **31**: 307-315.
- Pandit SK, Westendorp B, Nantasanti S, van Liere E, Tooten PC, Cornelissen PW, Toussaint MJ, Lamers WH, de Bruin A. 2012. E2F8 is essential for polyploidization in mammalian cells. *Nat. Cell. Biol.* **14**: 1181-1191.
- Ravid K, Lu J, Zimmet JM, Jones MR. 2002. Roads to polyploidy: the megakaryocyte example. *J. Cell Physiol.* **190**: 7-20.
- Robinow S, White K. 1991. Characterization and spatial distribution of the ELAV protein during *Drosophila melanogaster* development. *J. Neurobiol.* **22**: 443-461.
- Rossant J, Cross JC. 2001. Placental development: lessons from mouse mutants. *Nat. Rev. Genetics* **2**: 538-548.
- Salle J, Campbell SD, Gho M, Audibert A. 2012. CycA is involved in the control of endoreplication dynamics in the *Drosophila* bristle lineage. *Development* **139**: 547-557.
- Schoenfelder KP, Montague RA, Paramore SV, Lennox AL, Mahowald AP, Fox DT. 2014. Indispensable pre-mitotic endocycles promote aneuploidy in the *Drosophila* rectum. *Development* **141**: 3551-3560.
- Schulte J, Tepass U, Auld VJ. 2003. Gliotactin, a novel marker of tricellular junctions, is necessary for septate junction development in *Drosophila*. *J. Cell. Biol.* **161**: 991-1000.
- Schwabe T, Bainton RJ, Fetter RD, Heberlein U, Gaul U. 2005. GPCR signaling is required for blood-brain barrier formation in *Drosophila*. *Cell* **123**: 133-144.
- Skalska L, Stojnic R, Li J, Fischer B, Cerda-Moya G, Sakai H, Tajbakhsh S, Russell S, Adryan B, Bray SJ. 2015. Chromatin signatures at Notch-regulated enhancers reveal large-scale changes in H3K56ac upon activation. *EMBO J.* **34**: 1889-1904.
- Slattery M, Ma L, Spokony RF, Arthur RK, Kheradpour P, Kundaje A, Negre N, Crofts A, Ptashkin R, Zieba J, Ostapenko A, Suchy S, Victorsen A, Jameel N, Grundstad AJ, Gao W, Moran JR, Rehm EJ, Grossman RL, Kellis M, White KP. 2014. Diverse patterns of genomic targeting by transcriptional regulators in *Drosophila melanogaster*. *Genome Res.* **24**: 1224-1235.

- Song Y, Lu B. 2011. Regulation of cell growth by Notch signaling and its differential requirement in normal vs. tumor-forming stem cells in *Drosophila*. *Genes Dev.* **25**: 2644-2658.
- Speder P, Brand AH. 2014. Gap junction proteins in the blood-brain barrier control nutrient-dependent reactivation of *Drosophila* neural stem cells. *Dev. Cell* **30**: 309-321.
- Spradling AC. 1993. Developmental genetics of oogenesis in *The Development of Drosophila melanogaster* (eds. M. Bate and A. Martinez Arias), pp. 1-70. Cold Spring Harbor, NY: Cold Spring Harbor Laboratory Press.
- Stork T, Engelen D, Krudewig A, Silies M, Bainton RJ, Klambt C. 2008. Organization and function of the blood-brain barrier in *Drosophila*. *J. Neurosci.* **28**: 587-597.
- Taniguchi K, Kokuryo, A, Imano, T, Minami, R, Nakagoshi, H and Adachi-Yamada, T. 2012. Binucleation of *Drosophila* adult male accessory gland cells increases plasticity of organ size for effective reproduction. *Biological Systems: Open Access* **1**: 1-5.
- Terriente-Felix A, Li J, Collins S, Mulligan A, Reekie I, Bernard F, Krejci A, Bray S. 2013. Notch cooperates with Lozenge/Runx to lock haemocytes into a differentiation programme. *Development* **140**: 926-937.
- Trakala M, Rodriguez-Acebes S, Maroto M, Symonds CE, Santamaria D, Ortega S, Barbacid M, Mendez J, Malumbres M. 2015. Functional reprogramming of polyploidization in megakaryocytes. *Dev. Cell* **32**: 155-167.
- Unhavaithaya Y, Orr-Weaver TL. 2012. Polyploidization of glia in neural development links tissue growth to blood-brain barrier integrity. *Genes Dev.* **26**: 31-36.
- Volkenhoff A, Weiler A, Letzel M, Stehling M, Klambt C, Schirmeier S. 2015. Glial glycolysis is essential for neuronal survival in *Drosophila*. *Cell Metab.* **22**: 437-447.
- Watson ED, Cross JC. 2005. Development of structures and transport functions in the mouse placenta. *Physiology* **20**: 180-193.
- Wolff T. 2000. Histological Techniques for the *Drosophila* Eye Part I: Larva and Pupae in *Drosophila protocols* (eds. W. Sullivan, M. Ashburner and R.S. Hawley), pp. 216-220. Cold Spring Harbor, NY: Cold Spring Harbor Laboratory Press.

Chapter Three:

**The Role of Polyploidy in Wrapping Glia of the
Peripheral Nervous System**

Laura E. Frawley^{1,2}, and Terry L. Orr-Weaver^{1,2}

Whitehead Institute¹ and Dept. of Biology, Massachusetts Institute of Technology²,
Cambridge, MA 02142

Results in this chapter will be combined with work from Megan Corty and Marc Freeman in a collaborative paper.

Laura E. Frawley performed all experiments and analyses.

ABSTRACT

Development of an organ relies on the coordinated growth among different cell types within given tissues. Our lab has demonstrated that polyploidization is utilized to control glia cell size in the *Drosophila melanogaster* central nervous system (Unhavaithaya and Orr-Weaver, 2012). Here we expand our analysis and find that in the peripheral nervous system (PNS), wrapping glia (WG) are also polyploid. Wrapping glia function to ensheath sensory and motor axons in the peripheral nerves (Stork et al., 2008). Prior lineage-tracing analyses showed that there are only three WG per nerve, none of which divide during larval development (von Hilchen et al., 2013). Thus an important question is how, in the absence of increased cell number, these cells can compensate for a 10-fold increase in nerve length between the shortest and longest nerves during one larval instar, as well as up to a 50-fold increase in length of each nerve during larval development. We provide evidence that this hypertrophy is mediated by increased ploidy by showing there is a strong correlation between total WG ploidy and nerve length. We also investigated the function of polyploidization in WG and found that decreased ploidy leads to defective axonal ensheathment.

INTRODUCTION

Coordination amongst tissues layers within an organ is crucial for proper organ function. Cells can accommodate growth by either increasing in cell number or by increasing in cell size. Increases in cell size can be accomplished through polyploidization, the increase in genomic content. Throughout biology it is thought that ploidy dictates cell size (Cavalier-Smith, 1985). Additionally, polyploidy can lead to cells that are orders of magnitude larger in size than what is attainable from growth alone. One striking example is in *Aplysia* where single neurons are 200,000C (C value is defined as the haploid genome content) and visible to the naked eye (Lasek and Dower, 1971). In *Drosophila*, the enormous growth that takes place during larval development is due to larval tissues polyploidizing, as only imaginal tissues are divide mitotically. In most instances, polyploidy is driven by the endocycle, a variant cell cycle composed of oscillating rounds of G and S phases with no intervening mitosis, resulting in large mononucleate cells (Smith and Orr-Weaver, 1991).

Previously, our lab established that subperineurial glia (SPG) utilize polyploidy as a growth strategy to ensure proper blood-brain barrier (BBB) function (Unhavaithaya and Orr-Weaver, 2012). The SPG form this barrier through septate junctions and in order to maintain BBB integrity (Stork et al., 2008; Desalvo et al., 2011; Hatan et al., 2011), SPG do not increase in number, likely because cytokinesis would disrupt the BBB (Unhavaithaya and Orr-Weaver, 2012). Wrapping glia are a second glial cell type in the PNS that may also utilize polyploidy as a growth strategy. Wrapping glia function to ensheath axons throughout the peripheral nerves (Stork et al., 2008). During larval development there is a substantial increase in nerve length. In fact, between first and third larval instar, peripheral nerves can increase in length up to 50-fold (von Hilchen et al., 2013). Due to this extreme hypertrophy of the nerves, polyploidization may

be a good strategy for WG to use to ensure proper axonal ensheathment because it avoids cytokinesis and disruption of ensheathment. von Hilchen and colleagues determined that nerves A2-A7 each have only three wrapping glial cells throughout the larval stages (von Hilchen et al., 2008). Thus, we hypothesized that because WG number remains constant during larval development, WG may polyploidize to drastically increase in size to facilitate axonal ensheathment, particularly in the longer nerves.

The faithful transmission of neuronal signals is crucial to produce the desired response to a given stimulus in target cells. Ensheathment of axons by glial cells provides the insulation and metabolic support necessary to help ensure the integrity of these neuronal transmissions (Rodrigues et al., 2010). In *Drosophila*, wrapping glia ensheath axons in the PNS by extending their membranes around either individual or small bundles of axons (Stork et al., 2008), resembling mammalian non-myelinating Schwann cells, or Remak fibers (Griffin and Thompson, 2008). Recent studies have shown that wrapping glia ensheathment of axons is mediated by EGF signaling (Matzat et al., 2015). Specifically, the *Drosophila* neuregulin homolog encoded by *vein* is cell-autonomously required for proper WG differentiation (Matzat et al., 2015).

Here we show that WG are polyploid throughout the PNS and that total WG ploidy increases with increased nerve length. We also show that when WG ploidy is reduced, by knocking down expression of DNA replication components, axonal ensheathment becomes defective. Finally, we found that the three WG per nerve differentially contribute to overall WG nerve ploidy.

RESULTS

Wrapping glia are polyploid and total wrapping glia ploidy per nerve correlates with nerve length

Wrapping glia ensheath sensory and motor axons continuously and progressively throughout larval development (Matzat et al., 2015). To accommodate the massive increase in nerve length during larval development while not dividing mitotically, WG must increase in cell size to maintain axonal insulation. We hypothesized that increased ploidy may be responsible for this hypertrophy. To test this, we dissected larvae using the filet method, a dissection technique that allows for identification of the peripheral nerves, and measured WG ploidy in nerves A2-A7 (Figure 3-1C). The eight peripheral nerves that originate from the ventral nerve cord (VNC) are named for the abdominal segment they innervate (the A2 nerve innervates abdominal segment A2, etc.). To identify WG, we used the wrapping glia specific driver *nervana2 (nrv2)-GAL4* to drive expression of GFP under UAS control (Sun et al., 1999). We found that all wrapping glia nuclei were mononucleate and large in size (Figure 3-1A). The DNA content of each WG nucleus was calculated by measuring the DAPI fluorescence intensity of each WG nucleus and normalized against DAPI fluorescence intensity values from Elav-positive, post-mitotic, diploid neurons in the VNC (Robinow and White, 1991). We found wrapping glia from all nerves contain polyploid wrapping glia and that WG ploidy ranged from 2.5 to 76.2 C with a mean of 23.9C (Figure 3-1B).

Given that the number of WG per nerve is independent of nerve length and that nerve length increases through A8/9, we assessed whether WG ploidy increased with increasing nerve length (Figure 3-1C). To this end we summed the three WG for each nerve within an animal. We

did this for five animals, averaged them and found that the average total C value per nerve significantly correlated with nerve length (Fig 3-1D).

Reduction of WG ploidy correlates with defective axonal ensheathment

An important question to address is what is the function of WG ploidy. When either of the DNA replication machinery components Double Parked (DUP) or Proliferating Cell Nuclear Antigen (PCNA) was reduced specifically in SPG cells, not only did SPG ploidy decrease, but the BBB function of SPG cells was also defective (Unhavaithaya and Orr-Weaver, 2012). Similarly, we examined WG ploidy function by knocking down expression of genes encoding DNA replication proteins. If polyploid WG are required to ensheath axons, reduction in WG ploidy and thus cell size should effectively decrease the extent to which WG can ensheath axons. Therefore, we assessed whether WG expressing RNAi against several DNA replication and cell cycle genes had decreased ploidy. The genes we analyzed for effects on ploidy included: *cyclin A (cycA)*, *cyclin E (cycE)*, *dup*, *minichromosome maintenance 2 (mcm2)*, *origin of replication complex (orc)1*, *orc2*, *orc5*, *orc6*, *pcna*, and *partner of SLD five 1 (psf1)*. For each of these genes, we drove RNAi against the gene specifically in WG with the *nrv2-GAL4* driver and assessed ploidy. We found that when knocked down, all genes except *orc1* and one RNAi line of *orc2* resulted in significantly decreased ploidy levels (Figure 3-2). As a negative control, *laminin beta-1 (lanB1)* was used, as it has no known roles in DNA replication or the cell cycle.

We evaluated axonal ensheathment by immunofluorescence to determine if axonal ensheathment was defective upon reduction of WG ploidy. The axons were visualized by staining with antibodies against horseradish peroxidase (HRP) (Jan and Jan, 1982) and the WG cytoplasm was labeled by driving GFP with the *nrv2-GAL4* driver. *lanB1* was a positive control because it has been shown to have ensheathment defects (Corty personal communication). We

Figure 3-1. Wrapping glia are polyploid and total WG ploidy correlates with nerve length.

(A) Wrapping glia nuclei were labeled with *UAS-GFP* driven by *nrv2-GAL4* and are shown in white. Image is a peripheral nerve from a third instar larva containing a mononucleate, polyploid wrapping glia nucleus stained with DAPI, GFP nanobody, and merge. Inset shows the nucleus of a diploid nucleus outlined with white dashed lines. Scale bars: 5 μ m (B) Scatter plot showing DNA ploidy C values per WG from wandering third instar larvae, n=232 WG, 28 larvae. Scatter plot shows mean \pm 95% confidence interval (c.i.). (C) Schematic of a larval nervous system with peripheral nerves A1-A8/9 labeled. Nerves A2-A7, the nerves used for all filet dissection based experiments, are highlighted in blue. (D) Average total WG C value per nerve of 5 larvae. Spearman's rank correlation two-tailed test: $P=8.2 \times 10^8$, n= 79 WG, 29 nerves, 5 larvae.

Figure 3-1

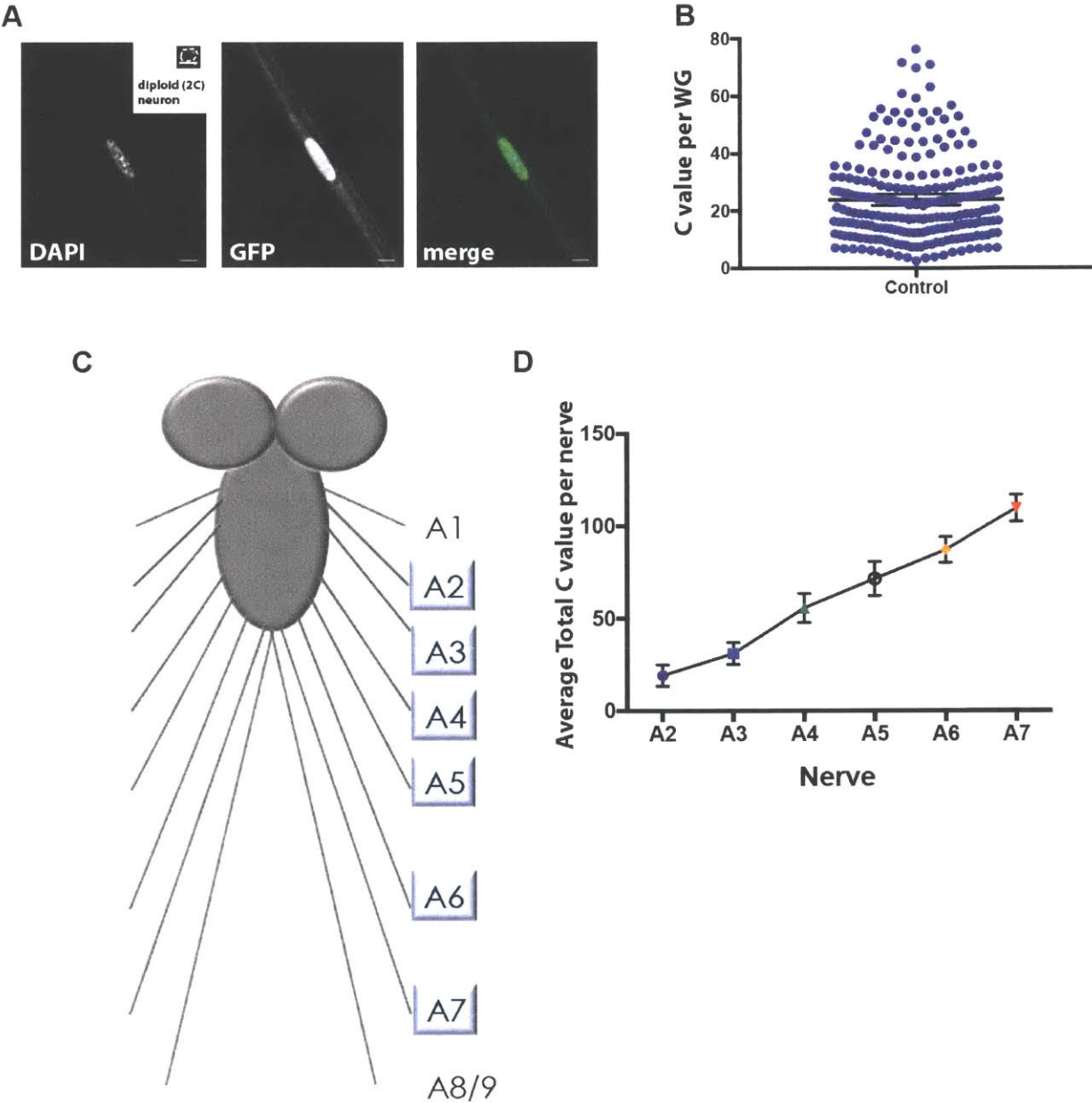
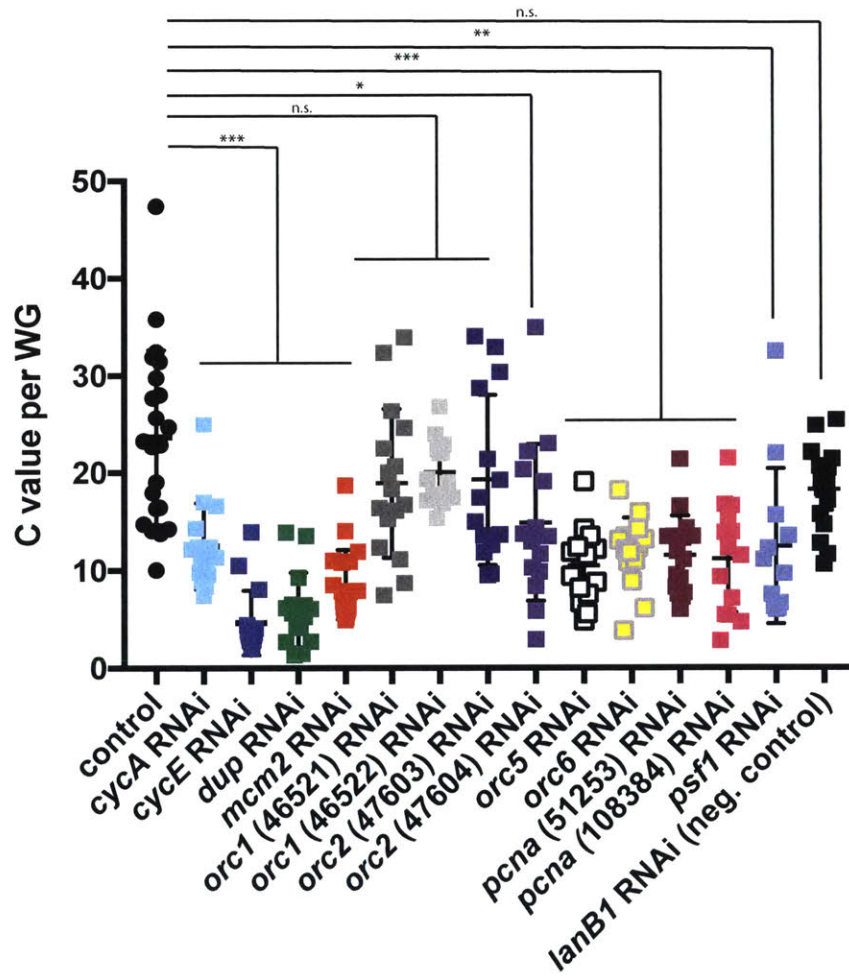


Figure 3-2. Wrapping glia ploidy is reduced when levels of DNA replication machinery

components are reduced. (A) Scatter plot showing DNA ploidy per WG from wandering third instar larvae. Mean ploidy control: 23.6C, n= 22 WG, 9 larvae; *cycA* RNAi: 12.5C, n=15 WG, 8 larvae, *** $P < 0.0001$; *cycE* RNAi: 4.63C, n=16 WG, 8 larvae, *** $P < 0.0001$; *dup* RNAi: 5.96C, n=15 WG, 10 larvae, *** $P < 0.0001$; *mcm2* RNAi: 8.56C, n=19 WG, 7 larvae, *** $P < 0.0001$; *orc1* RNAi (46521): 18.93C, n=16 WG, 8 larvae, n.s. $P = 0.95$; *orc1* RNAi (46522): 20.05C, n=14 WG, 7 larvae, n.s. $P = 0.30$; *orc2* RNAi (47603): 19.3C, n=14 WG, 8 larvae, n.s. $P = 0.13$; *orc2* RNAi (47604): 14.87C, n=15 WG, 8 larvae, * $P = 0.0019$; *orc5* RNAi: 10.48C, n=15 WG, 8 larvae, *** $P < 0.0001$; *orc6* RNAi: 11.81C, n=15 WG, 8 larvae, *** $P < 0.0001$; *pcna* RNAi (51253): 11.5C, n=16 WG, 8 larvae, *** $P < 0.0001$; *pcna* RNAi (108384): 11.2C, n=14 WG, 8 larvae, *** $P < 0.0001$; *psfl* RNAi: 12.43C, n=12 WG, 6 larvae, ** $P = 0.0003$; negative control *lanB1* RNAi: 18.2C, n=17 WG, 8 larvae, n.s. $P = 0.067$. Statistical significance was determined using the Mann–Whitney two-tailed test. Scatter plot shows mean \pm 95% c.i..

Figure 3-2

A



imaged axonal ensheathment in the peripheral nerves just above or below each WG nucleus. We found that axons were not as effectively ensheathed in animals where WG ploidy levels were significantly reduced (Figure 3-3). Ensheathment was called defective if qualitatively, the relative area of HRP signal marking the axons was greater than the relative area of GFP signal marking the WG cytoplasm.

An *in vivo* RNAi screen to identify glial genes required for ensheathment was conducted by Megan Corty in Marc Freeman's lab (current collaboration). Interestingly, several DNA replication or cell cycle genes we found have decreased ploidy when knocked down were also determined to have defects in axonal ensheathment in Corty's screen. Specifically, *cycA*, *cycE*, *mcm2*, *orc5*, *orc6*, and *psf1* affected ensheathment. The additional genes we found that resulted in decreased ploidy when down-regulated were not examined in her screen. Our collaborator will perform more in depth analyses by electron microscopy when these genes are targeted by RNAi.

WG1 is the main contributor to total increased wrapping glia ploidy in the longer peripheral nerves

Each peripheral nerve contains two regions, the nerve extension region (NER) and the muscle field area (MFA). The increased nerve length of A7 relative to A2 is achieved by drastic increases in the NER, whereas the MFA remains relatively constant (von Hilchen et al., 2013). The three wrapping glia have been named WG1, WG5, and WG9 based on their stereotypic location along the nerve (von Hilchen et al., 2008; von Hilchen et al., 2013). WG1 is present in the NER, and both WG5 and WG9 are present in the MFA (Figure 3-4A). Given our findings that total WG ploidy per nerve increases with increasing nerve length, we questioned whether the contribution of increased ploidy in the longer nerves was due to the WG present in the NER, WG1. To test this, we quantified the ploidy of each individual WG in nerves A2 and A3. The

Figure 3-3. WG with reduced ploidy do not effectively ensheath axons.

Orthographic views of axonal ensheathment in control and RNAi lines. Control (A), *cycA* RNAi, Chi-squared test, $P=1.3 \times 10^{-5}$ (B), *cycE* RNAi, Chi-squared test, $P=1.3 \times 10^{-4}$ (C), *dup* RNAi, Chi-squared test, $P=5.8 \times 10^{-5}$ (D), *mcm2* RNAi, Chi-squared test, $P=2.4 \times 10^{-5}$ (E), *orc1* (46522) RNAi, Chi-squared test, $P=0.13$ (F), *orc2* (47603) RNAi, Chi-squared test, $P=0.13$ (G), *orc2* (47604) RNAi, Chi-squared test, $P=1.3 \times 10^{-5}$ (H), *orc5* RNAi, Chi-squared test, $P=5.8 \times 10^{-5}$ (I), *orc6* RNAi, Chi-squared test, $P=5.8 \times 10^{-5}$ (J), *pcna* (108384) RNAi, Chi-squared test, $P=2.3 \times 10^{-5}$ (K), *psf1* RNAi, Chi-squared test, $P=8.6 \times 10^{-5}$ (L), *lanB1* RNAi, Chi-squared test, $P=1.3 \times 10^{-7}$ (positive control) (M). All images were taken from WG whose ploidy level was close to the mean ploidy level in order to show representative ensheathment defects. WG cytoplasm is marked by *UAS-GFP* driven by *nrv2-GAL4* (green) and axons by anti-HRP (red). Scale bars: 5 μ m. The status of ensheathment of each orthograph is indicated as defective (yes) or normal (no). The ploidy quantification results are indicated as significantly reduced (yes) or not significantly reduced (no).

Figure 3-3



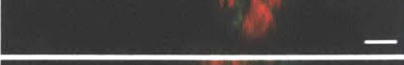










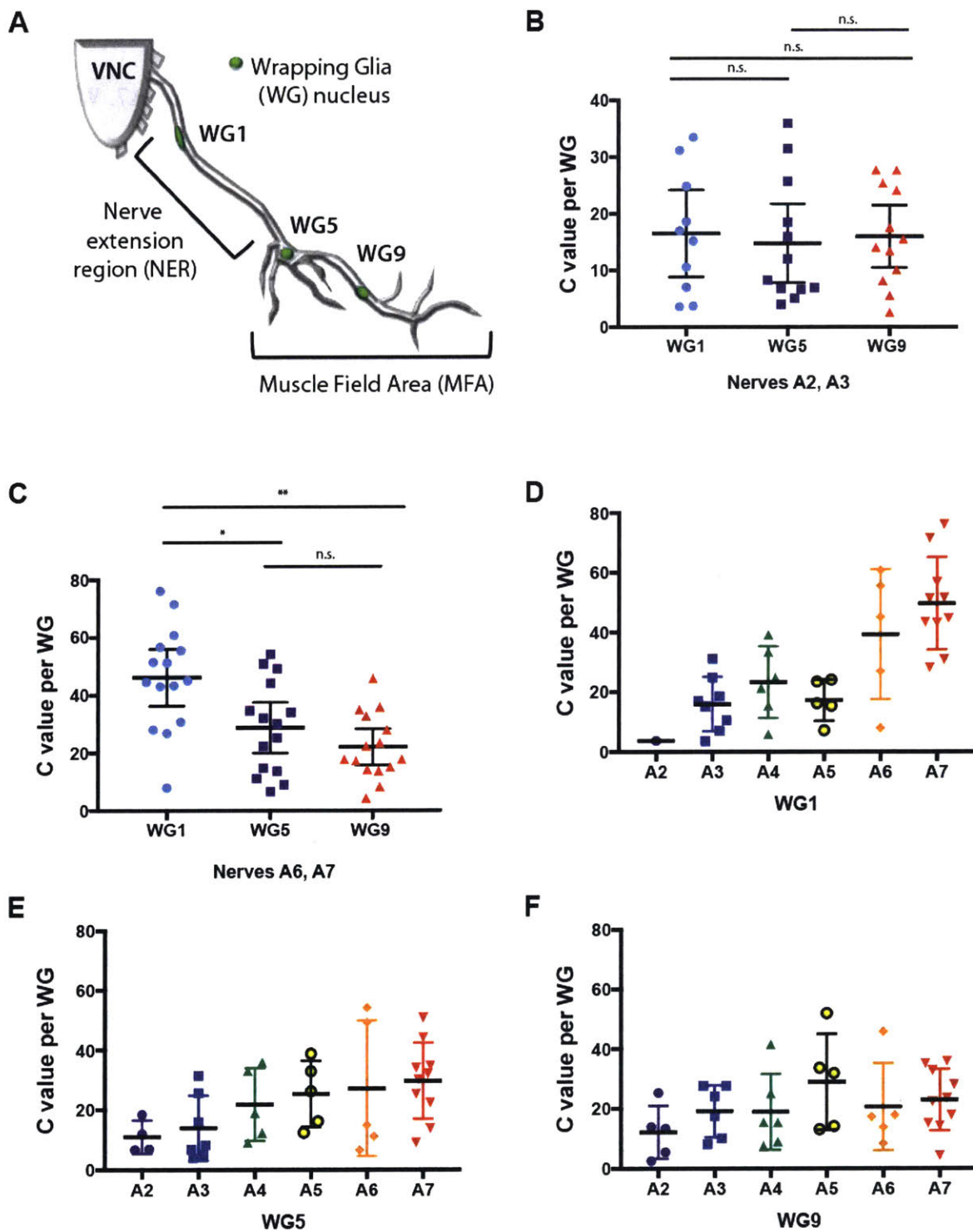
		HRP	Defective ensheathment?	Significantly reduced ploidy?
control	A		no	no
<i>cycA</i> RNAi	B		yes	yes
<i>cycE</i> RNAi	C		yes	yes
<i>dup</i> RNAi	D		yes	yes
<i>mcm2</i> RNAi	E		yes	yes
<i>orc1</i> (46522) RNAi	F		no	no
<i>orc2</i> (47603) RNAi	G		no	no
<i>orc2</i> (47604) RNAi	H		yes	yes
<i>orc5</i> RNAi	I		yes	yes
<i>orc6</i> RNAi	J		yes	yes
<i>pcna</i> (108384) RNAi	K		yes	yes
<i>psf1</i> RNAi	L		yes	yes
<i>lanB1</i> RNAi (positive control)	M		yes	no

Figure 3-4. WG1 is primarily responsible for the increase in total WG ploidy with increasing nerve length. (A) Schematic of a peripheral nerve with WG nuclei in green. WG1 is present in the nerve extension region (NER) while WG5 and WG9 are in the muscle field area (MFA). VNC= ventral nerve cord. (B) Scatter plot showing DNA ploidy per WG from nerves A2 and A3 from 10 larvae. WG1: mean ploidy=16.5C, n=10 WG, nerves, and larvae; WG5: mean ploidy= 14.8C, n=12 WG and nerves, 10 larvae; WG9: mean ploidy= 15.9C, n=12 WG and nerves, 10 larvae. Mann-Whitney two-tailed test. *P* value between: WG1 and WG5 = 0.77; WG1 and WG9 = 0.92; WG5 and WG9= 0.67. n.s.= not significant. (C) Scatter plot showing DNA ploidy per WG from nerves A6 and A7. These data are a subset of the data presented in B. WG1: mean ploidy= 46.2C, n= 15 WG and nerves, 10 larvae; WG5: mean ploidy= 28.8C, n=15 WG and nerves, 10 larvae; WG9: mean ploidy= 22.1C, n=15 WG and nerves, 10 larvae. Mann-Whitney two-tailed test, between WG1 and WG5, **P*= 0.01; WG1 and WG9 ***P*= 0.0004; WG5 and WG9 n.s., *P*= 0.35. (D-F) Scatter plots showing DNA ploidy C values of WG1, WG5, or WG9 per nerve for all larvae. (D) WG1: A2, n= 1 WG, nerve, and larva; A3, n= 8 WG, nerves, and larvae; A4, n= 6 WG, nerves, and larvae; A5, n= 5 WG, nerves, and larvae; A6, n= 5 WG, nerves, and larvae; A7, n= 10 WG, nerves, and larvae. Spearman correlation two-tailed test, *P*= 1.6×10^{-6} . (E) WG5: A2, n= 4 WG, nerves, and larvae; A3, n= 7 WG, nerves, and larvae; A4, n= 5 WG, nerves, and larvae; A5, n= 5 WG, nerves, and larvae; A6, n= 5 WG, nerves, and larvae; A7, n= 10 WG, nerves, and larvae. Spearman correlation two-tailed test, *P*= 0.0028. (F) WG9: A2, n= 5 WG, nerves, and larvae; A3, n= 6 WG, nerves, and larvae; A4, n= 6 WG, nerves, and larvae; A5, n= 5 WG, nerves, and larvae; A6, n= 5 WG, nerves, and larvae; A7, n= 10 WG, nerves, and larvae. Spearman correlation two-tailed test, n.s. *P*= 0.07. Scatter plots show mean \pm 95% c.i..

Figure 3-4



mean ploidy of WG1 from was higher than the mean ploidies of WG5 and WG9, but the differences were not significant (Figure 3-4B). If our hypothesis that WG1 ploidy increases in the larger nerves is correct, the difference in the mean WG ploidy of WG1 relative to WG5 and WG9 should be significantly greater if we look only at the longer nerves A6 and A7. We found this to be the case: the mean ploidy of WG1 was significantly higher than both the means of WG5 and WG9, whereas the means of WG5 and WG9 were not significantly different from one another (Figure 3-4C). This indicates that the total wrapping glia ploidy and nerve length is mainly due to WG1, but WG5 and WG9 both have a similar capacity to contribute to the observed total increased ploidy.

Additionally, we hypothesized that only WG1 ploidy would increase with increasing nerve length because it is the only WG present in the NER. To this end, we plotted the ploidy of each WG1, WG5, or WG9 per nerve from all larvae. Surprisingly we found both WG1 and WG5 significantly correlated with nerve length (Figure 3-4D,E). However, this relationship is absent for WG9 (Figure 3-4F). Thus, WG1 and WG5 ploidy correlates with nerve length, whereas WG9 does not correlate with nerve length.

Axonal ensheathment in the distal NER and MFA is less than in the proximal NER

We examined whether axonal ensheathment was constant throughout the entire peripheral nerve. Previously, axonal wrapping in the proximal NER was found to be relatively constant at 2 μ m, 5 μ m, 200 μ m and 400 μ m from the VNC (Matzat et al., 2015). However, axonal ensheathment of the distal NER and MFA had not been examined. To assess ensheathment, we drove a membrane fused GFP marker under UAS control, *UAS-mCD8::GFP*, to visualize all the WG membrane extensions and we visualized both sensory and motor axons by immunofluorescence against HRP. We dissected control larvae via the filet method and

examined ensheathment in the distal NER, and in the MFA by both the WG5 and WG9 nuclei. We consistently saw that the distal NER as well as the segmental nerves (SNs) and the intersegmental nerve (ISN) of the MFA had visibly less wrapping of axons than in the proximal NER (Figure 3-5).

Reduction of DNA replication components causes significant reduction of WG ploidy in longer nerves

Given our findings that total ploidy increases with nerve length we hypothesized that when ploidy is reduced, the longer nerves would have dramatically reduced ploidy relative to shorter nerves. Thus, we evaluated the total ploidy per nerve for either A2 or A3 and A6 or A7 for animals expressing driver alone, *dup* RNAi or *psfl* RNAi. We found that in animals expressing *dup* RNAi and *psfl* RNAi, relative to control, there was not a significant reduction in ploidy within nerves A2 or A3, but there was a significant reduction in ploidy in A6 or A7 (Figure 3-6A).

Additionally, because WG1 is the main contributor to increased ploidy in control animals, we questioned whether all three of the wrapping glia had decreased ploidy values or just WG1. To this end we quantified the ploidy of WG1, WG5, and WG9 in animals expressing *dup* RNAi and *psfl* RNAi in WG cells and compared them to control animals. WG1 ploidy was significantly reduced in animals expressing either *dup* RNAi or *psfl* RNAi (Figure 3-6B). Interestingly, although there was no significant reduction in ploidy for WG5, WG9 had significantly reduced ploidy in animals expressing either *dup* RNAi or *psfl* RNAi (Figure 3-6B).

Figure 3-5. Axonal ensheathment is decreased in the distal NER and MFA relative to the proximal NER. Orthographic views of peripheral nerves from control larvae. The axons of the proximal NER are extensively ensheathed (A,B). Axons within the distal NER (C,D), segmental nerves (SNs) (white arrows) (E), and intersegmental nerves (ISNs) (F) are more exposed. White arrows in E point to two SNs. Wrapping glia membranes are marked by *UAS-mCD8::GFP* driven by *nrv2-GAL4* (green) and axons by anti-HRP (red). These images are representative of five animals. Scale bars: 5 μ m.

Figure 3-5

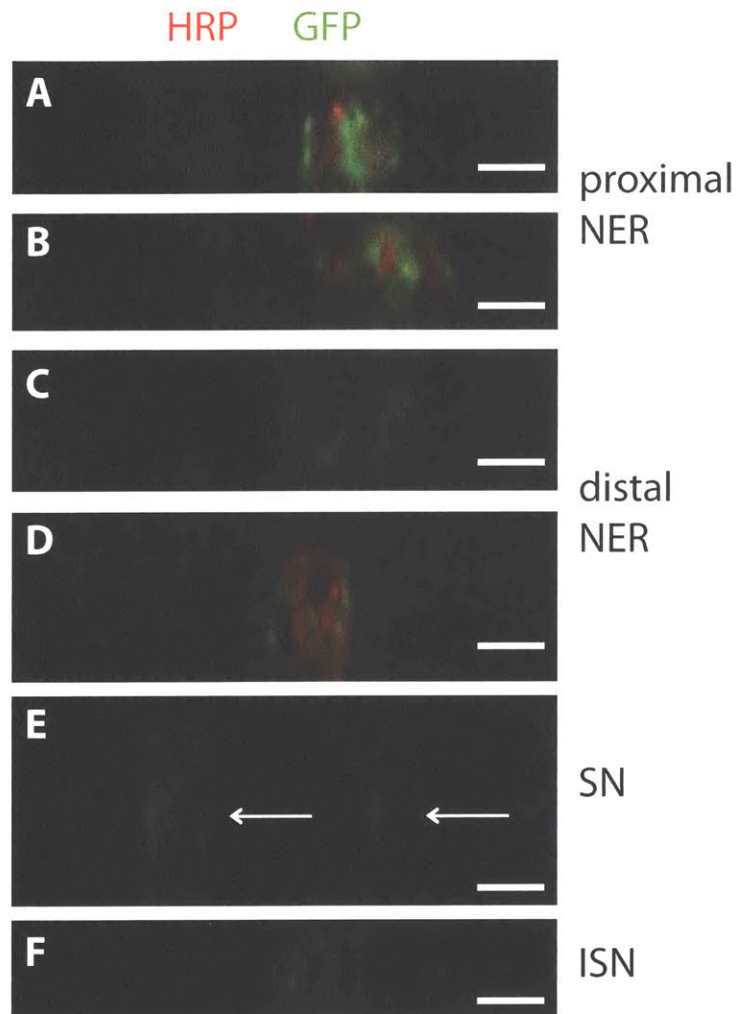
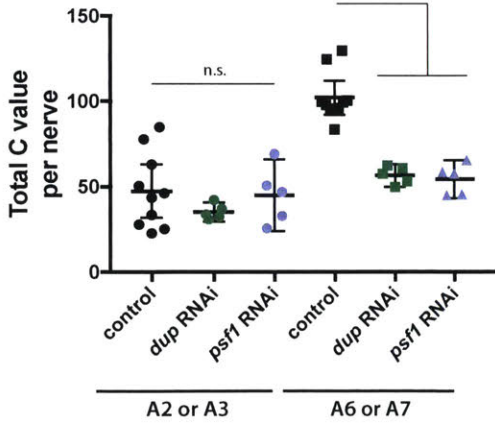


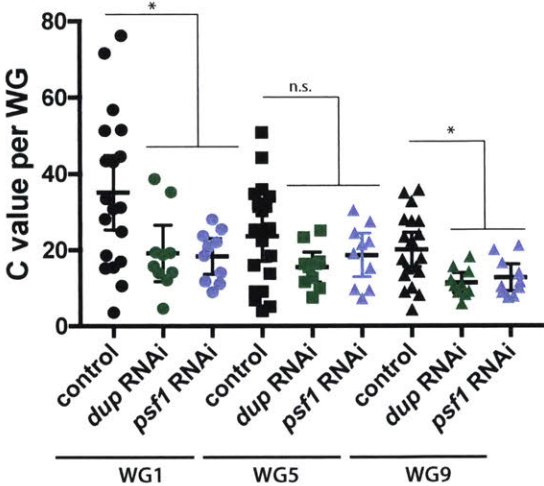
Figure 3-6. Reduction of DNA replication machinery components leads to significantly reduced WG ploidy only in longer nerves. (A) Scatter plot showing total DNA ploidy per nerve from wandering third instar larvae from either nerve A2 or A3 and A6 or A7. Control: A2 or A3, n= 10 WG, nerves, and larvae; A6 or A7, n=10 WG, nerves, and larvae; *dup* RNAi: A2 or A3, n=5 WG, nerves, and larvae, not significant (n.s.) $P=0.44$; A6 or A7, n=5 WG, nerves, and larvae, $**P=0.0007$; *psfl* RNAi: A2 or A3, n=WG, nerves, 10 larvae, n.s. $P=0.95$; A6 or A7, n=WG, nerves, 10 larvae, $**P=0.0007$. Statistical significance was determined by Mann-Whitney two-tailed test. (B) Scatter plot showing DNA ploidy per WG from nerves A2 or A3 and A6 or A7. Control: WG1: mean ploidy=35.1C, n=19 WG and nerves, 10 larvae; WG5: mean ploidy= 23.6C, n=19 WG and nerves, 10 larvae; WG9: mean ploidy= 20.1C, n=19 WG and nerves, 10 larvae; *dup* RNAi: WG1: mean ploidy=19.2C, n=10 WG and nerves, 5 larvae; WG5: mean ploidy= 15.5C, n=10 WG and nerves, 5 larvae; WG9: mean ploidy= 11.4C, n=10 WG and nerves, 5 larvae; *psfl* RNAi: WG1: mean ploidy=18.4C, n=10 WG and nerves, 5 larvae; WG5: mean ploidy= 18.6C, n=10 WG and nerves, 5 larvae; WG9: mean ploidy= 12.8C, n=10 WG and nerves, 5 larvae. Scatter plots show mean \pm 95% c.i.. Mann-Whitney two-tailed test, between control and *dup* RNAi: WG1, $*P=0.044$, WG5, n.s. $P=0.15$, WG9, $*P=0.019$; between control and *psfl* RNAi: WG1, $*P=0.019$, WG5, n.s. $P=0.38$, WG9, $*P=0.035$.

Figure 3-6

A



B



DISCUSSION

Here we show that wrapping glia are polyploid, WG ploidy is correlated with nerve length, reduced WG ploidy correlates with defective axonal ensheathment, WG1 primarily contributes to increased total ploidy per nerve, and longer nerves are more susceptible to reduction in WG ploidy than shorter nerves.

Our lab has previously shown that the nervous system, similar to other tissues in *Drosophila* larvae, exploit polyploidy for cell growth (Orr-Weaver, 2015). The function of wrapping glia ensheathment is hypothesized to provide trophic, metabolic, and/or homeostatic support to axons and to increase conduction velocity (von Hilchen and Altenhein, 2014). One advantage to utilizing polyploidization is to generate large cells (Orr-Weaver, 2015). This strategy also seems to be utilized by WG. The large size of wrapping glia is required to sufficiently wrap around the 42-44 sensory axons and 34-36 motor axons along the nerves by the end of larval development (Matzat et al., 2015).

Additionally, the large WG cell size required for ensheathment of axons may be necessary to maintain increased conduction velocity required for sophisticated larval locomotion later in larval development. It has been hypothesized that wrapping glia may speed up conduction velocity later in larval development once wrapping glial membranes start to ensheath individual axons (Stork et al., 2008). Uninterrupted ensheathment of axons by wrapping glia may be crucial during late larval development. Specifically, by mid-third instar, larvae must migrate out of the food in a short timeframe in preparation for pupation. This migration requires more sophisticated locomotion than what is required earlier in larval development and may result from increased membrane resistance provided by WG (Stork et al., 2008). Disruptions in this insulation if the wrapping glia were instead to mitotically divide to achieve increased cell mass

could decrease conduction velocity, inhibiting reliable neuronal signals and thus be detrimental to larval development.

Reduction of DNA replication machinery components in WG led to significantly reduced ploidy values with the exception of *orc1* and *orc2*. It is not unexpected that reduction in *orc1* expression did not significantly reduce ploidy because *orc1* is transcribed during each S phase of the endocycle (Narbonne-Reveau et al., 2008). Thus, RNAi may not be able to effectively decrease *orc1* expression in this time window. Our lab and others have demonstrated that *orc1* and *orc2* null mutants have between a two and four-fold reduction in ploidy in salivary gland cells (Park and Asano, 2008; Sher et al., 2012), thus the most likely explanation for why both *orc2* RNAi lines did not significantly decrease WG ploidy is that the *orc2* VDRC #47603 RNAi line did not effectively reduce *orc2* with the *nrv2-GAL4* WG driver.

Our finding that axonal ensheathment is defective following ploidy reduction raises the question of whether there is a functional requirement for WG ploidy. To date, the existing wrapping glia drivers are also expressed in other glial subtypes making whole body functional studies such as larval locomotion impossible. It will be beneficial for the field to generate a peripheral nerve WG only driver so functional analysis of WG ploidy can be carried out.

The use of polyploidy to increase metabolic capacity has also been proposed. It is hypothesized that the increase in gene copy number subsequently increases the rates of biosynthesis and metabolism. Thus, it is possible that the huge metabolic demands of axons may be more easily met by polyploid wrapping glia than by mitotic cells.

Our analysis of ploidy contribution by the three WG per nerve provides further insight into the differences between individual WG within a nerve. First, WG1 is mainly responsible for the observed increased total WG ploidy. The mean WG1 ploidy increases as the NER lengthens

in the longer nerves, whereas WG5 and WG9 present in the MFA both contribute about equally to ploidy across all nerves. Further, we were surprised to find that WG1 and WG5 both correlate with nerve length. WG5 encompasses the SNs a, b, c, and d as well as the ISN (von Hilchen et al., 2013) and thus should be independent of nerve length. However, Matzat and colleagues have recently observed that the cell membranes of WG1 and WG5 can overlap in the distal region of the NER (Matzat et al., 2015). The fact that WG9 ploidy does not correlate with nerve length is likely because WG9 is exclusively present in the MFA, which is relatively constant in nerves A2-A7. The result that only WG1 had significantly reduced ploidy when dup RNAi or psf1 RNAi was expressed suggests that the timing of S phase for each WG may not be synchronous. Specifically, it is possible that S phase in WG1 occurs later in larval development after the RNAi has taken effect, whereas WG5 and WG9 replicate its DNA earlier in larval developmental before the RNAi has taken effect. A comprehensive analysis of the developmental timing of S phase in the WG would be beneficial.

The Klambt lab has coined the term wrapping index, which is defined as the percent of axons that are individually ensheathed by WG. Analysis of the NER between 2-400 μ m from the VNC has shown that the average wrapping index is 19 (Matzat et al., 2015). The wrapping index of the more distal NER and the entire MFA had previously not been studied. Our immunofluorescence data showing axonal ensheathment throughout the entire nerve starts to shed light on how wrapping index varies in the distal NER and MFA. Specifically, the distal NER and MFA appear to have a lower wrapping index. This suggests that axonal wrapping is dependent on the position along the anterior-posterior larval body axis. More comprehensive ensheathment studies, including electron microscopy, are necessary to determine precisely how the wrapping index varies based on location.

There are many parallels between *Drosophila* and mammalian peripheral nerves. In mammals, immature Schwann cells can differentiate into either myelinating or non-myelinating Schwann cells to ensheath axons (Nave and Trapp, 2008). *Drosophila* WG resemble non-myelinating Schwann cells, which surround more than one axon into Remak bundles (Griffin and Thompson, 2008). Despite the absence of myelination in *Drosophila*, WG's intimate association with axons as well as the outer perineurial glia and SPG layers sufficiently provide the support and insulation required by the axons. Further, the axonal ensheathment by glial membranes in both systems is dependent on receptor tyrosine kinase activity. Axonal ensheathment in the *Drosophila* PNS has been recently elucidated. Wrapping glia differentiation is dependent on EGFR activation by the neuregulin-like molecule Vein in a cell-autonomous manner (Matzat et al., 2015). In mammals, the correct differentiation of immature Schwann cells into either myelinating or non-myelinating Schwann cells is dependent on the activation of the ErbB receptor by axonal expression of Neuregulin1 (Nrg1) (Michailov et al., 2004; Taveggia et al., 2005; Nave and Trapp, 2008). Interestingly, the autocrine activation mechanism used in *Drosophila* may represent an evolutionary conserved mechanism of axonal ensheathment because when Schwann cells become injured they express Nrg1 to initiate remyelination (Stassart et al., 2012; Matzat et al., 2015). Given the striking similarity in function and wrapping mechanism between *Drosophila* and mammals, it would be interesting to investigate whether polyploidy is also present in Schwann cells, and if so, what function it plays.

MATERIALS AND METHODS

Fly strains

Drosophila strains used were: Oregon R; *nrv2-GAL4 (II)* and *nrv2-GAL4, UAS-GFP(II)* (provided by Paul Salvaterra, City of Hope National Medical Center), *UAS-mCD8::GFP(II)*

(Bloomington Stock Center #5137), *UAS-cycA* RNAi (II) (Vienna *Drosophila* Resource Center (VDRC), #103595), *UAS-cycE* RNAi (II) (VDRC, #110204), *UAS-dup* RNAi (III) (VDRC, #23131), *UAS-LanB1* RNAi (III) (VDRC #23119), *UAS-mcm2* RNAi (II) (VDRC, #103619), *UAS-orc1* RNAi (II) (VDRC, #46521), *UAS-orc1* RNAi (II) (VDRC, #46522), *UAS-orc2* RNAi (II) (VDRC, #47603), *UAS-orc2* RNAi (III) (VDRC, #47604), *UAS-orc5* RNAi (II) (VDRC, #108885), *UAS-orc6* RNAi (II) (VDRC, #101728), *UAS-pcna* RNAi (II) (VDRC, #51253), *UAS-pcna* RNAi (II) (VDRC, #108384), *UAS-psf1* RNAi (II) (VDRC, #102009).

Antibodies

Primary antibodies were rat anti-ELAV (DSHB, 7E8A10; 1:15) and Rhodamine Red-X AffiniPure Goat Anti-Horseradish Peroxidase (1:50; Jackson ImmunoResearch). The GFP-Booster nanobody (Chromotek, #gba488) was used at 1:400. Secondary antibodies were Alexa Fluor 568 goat anti-mouse or anti-rabbit (1:1000; Life Technologies), Alexa Fluor 647 goat anti-rabbit (1:1000; Life Technologies), and RRX- and Cy5-conjugated to donkey/goat anti-rabbit or anti-rat (1:250; Jackson ImmunoResearch).

Dissection, fixation and antibody staining of larval tissues

Larval brains were dissected in unsupplemented Grace's medium, fixed in 4% formaldehyde in PBS for 30 min, washed in PBST (0.3% Triton X-100) and blocked for 1 h at room temperature with blocking solution (PBST, 2.5% goat and donkey serum). In the initial screen of DNA replication genes required for ploidy and ensheathment, brains were dissected without the filet preparation. In all other experiments assessing ploidy and ensheathment of specific peripheral nerves, the filet dissection technique was used. Data used to generate Figure

3-1D were dissected during a four-hour developmental window to minimize ploidy variability with age.

DAPI staining/ploidy C value calculations

Samples were stained with DAPI at 50 ng/ml, the optimal concentration for quantification of DNA ploidy (Hamada and Fujita, 1983), washed overnight, and imaged using the Nikon Eclipse inverted microscope with a 60x or 100x objective. This low DAPI concentration was used so as not to oversaturate the signal. Although DAPI shows that nuclear size and staining intensity are proportional to DNA content, the nuclear GFP signal is not proportional to either nuclear size or DNA content. z-stacks that covered the entire nucleus were acquired. All images were deconvolved using NIS Elements software (Nikon). An area was drawn around the diploid or polyploid nucleus of selected in-focus stacks using the NIS Elements draw bezier ROI tool, and the adaptive background compensation function was used to decrease background signal until the DAPI pixel density measurement was between 0 and 100 around each nucleus. The area quantified was defined by the DAPI signal, as the nuclear GFP signal was found to be sometimes broader than the DAPI-stained DNA. DNA content was quantified for each nucleus by obtaining the sum intensity of the DAPI pixel density in NIS Elements. Ploidy was calculated by normalizing each WG nucleus from wandering third instar larvae to diploid neuronal nuclei (average of 8-12 neurons per SPG cell). The diploid neurons were identified by staining with anti-ELAV (Robinow and White, 1991). Diploid reference cells and polyploid cells were collected from the same animal and imaged using the same exposure settings. Statistical significance was determined by the Mann–Whitney two-tailed test using GraphPad Prism and Spearman correlation two-tailed test or Spearman’s rank correlation two-

tailed test in R.

Ensheathment Studies

To evaluate axonal ensheathment, orthographic views were acquired using NIS Elements. In our initial screen of DNA replication genes, WG were visualized using *nrv2-GAL4, UAS-GFP*. However, in all other experiments assessing ensheathment *UAS-mCD8::GFP* was driven by *nrv2-GAL4, UAS-GFP*. To assess ensheathment, regions above or below each nucleus we quantified for ploidy was viewed. Ensheathment was called defective if qualitatively, the relative area of HRP signal marking the axons was greater than the relative area of GFP signal marking the WG cytoplasm. A Chi-square test was performed to determine statistical significance for defective axonal ensheathment.

ACKNOWLEDGEMENTS

We thank George Bell for critical advice on statistical analysis and Helena Kashevsky for assistance with genetic crosses. This work was supported by a National Science Foundation Predoctoral Fellowship to L.E.F. and the National Institute of Health grant NS092798 to T.L.O-W.

REFERENCES

- Cavalier-Smith, T. 1985. Cell volume and the evolution of eukaryotic genome size in *The Evolution of Genome Size* (ed. T. Cavalier-Smith), pp. 105-185. John Wiley and Sons.
- Desalvo MK, Mayer N, Mayer F, Bainton RJ. 2011. Physiologic and Anatomic Characterization of the Brain Surface Glia Barrier of *Drosophila*. *Glia* **59**: 1322-1340.
- Griffin JW, Thompson WJ. 2008. Biology and Pathology of Nonmyelinating Schwann Cells. *Glia* **56**: 1518-1531.
- Hamada S, Fujita S. 1983. Dapi Staining Improved for Quantitative Cytofluorometry. *Histochemistry* **79**: 219-226.
- Hatan M, Shinder V, Israeli D, Schnorrer F, Volk T. 2011. The *Drosophila* Blood Brain Barrier Is Maintained by GPCR-Dependent Dynamic Actin Structures. *J. Cell Biol.* **192**: 307-319.

- Jan LY, Jan YN. 1982. Antibodies to Horseradish Peroxidase as Specific Neuronal Markers in *Drosophila* and in Grasshopper Embryos. *Proc. Natl. Acad. Sci. USA* **79**: 2700-2704.
- Lasek RJ, Dower WJ. 1971. *Aplysia californica*: Analysis of Nuclear DNA in Individual Nuclei of Giant Neurons *Science* **172**: 278-280.
- Matzat T, Sieglitz F, Kottmeier R, Babatz F, Engelen D, Klambt C. 2015. Axonal Wrapping in the *Drosophila* PNS Is Controlled by Glia-Derived Neuregulin Homolog Vein. *Development* **142**: 1336-1345.
- Michailov GV, Sereda MW, Brinkmann BG, M FT, Haug B, Birchmeier C, Role L, Lai C, Schwab MH, Nave K-A. 2004. Axonal Neuregulin-1 Regulated Myelin Sheath Thickness. *Science* **304**: 700-703.
- Narbonne-Reveau K, Senger S, Pal M, Herr A, Richardson HE, Asano M, Deak P, Lilly MA. 2008. APC/CFzr/Cdh1 Promotes Cell Cycle Progression During the *Drosophila* Endocycle. *Development* **135**: 1451-1461.
- Nave K-A, Trapp BD. 2008. Axon-Glial Signaling and the Glial Support of Axon Function. *Annu. Rev. Neurosci.* **31**: 535-561.
- Orr-Weaver TL. 2015. When Bigger Is Better: The Role of Polyploidy in Organogenesis. *Trends Genet.* **31**: 307-315.
- Park SY, Asano M. 2008. The Origin Recognition Complex Is Dispensable for Endoreplication in *Drosophila*. *Proc. Natl. Acad. Sci. USA* **105**: 12343-12348.
- Robinow S, White K. 1991. Characterization and Spatial Distribution of the Elav Protein During *Drosophila melanogaster* Development. *J. Neurobiol.* **22**: 443-461.
- Rodrigues F, Schmidt I, Klambt C. 2010. Comparing Peripheral Glial Cell Differentiation in *Drosophila* and Vertebrates. *Cell. Mol. Life Sci.* **68**: 55-69.
- Sher N, Bell GW, Li S, Nordman J, Eng T, Eaton ML, MacAlpine DM, Orr-Weaver TL. 2012. Developmental Control of Gene Copy Number by Repression of Replication Initiation and Fork Progression. *Genome Res.* **22**: 64-75.
- Smith AV, Orr-Weaver TL. 1991. The Regulation of the Cell Cycle During *Drosophila* Embryogenesis: The Transition to Polyteny. *Development* **112**: 997-1008.
- Stassart RM, Fledrich R, Velanac V, Brinkmann BG, Schwab MH, Meijer D, Sereda MW, Nave K-A. 2012. A Role for Schwann Cell-Derived Neuregulin-1 in Remyelination. *Nat. Neurosci.* **16**: 48-54.
- Stork T, Engelen D, Krudewig A, Silies M, Bainton RJ, Klambt C. 2008. Organization and Function of the Blood-Brain Barrier in *Drosophila*. *J. Neurosci.* **28**: 587-597.
- Sun B, Xu P, Salvaterra PM. 1999. Dynamic Visualization of Nervous System in Live *Drosophila*. *Proc. Natl. Acad. Sci. USA* **96**: 110438-110443.
- Taveggia C, Zanazzi G, Petrylak A, Yano H, Rosenbluth J, Einheber S, Xu X, Esper RM, Loeb JA, Shrager P et al. 2005. Neuregulin-1 Type III Determines the Ensheathment Fate of Axons. *Neuron* **47**: 681-694.
- Unhavaithaya Y, Orr-Weaver TL. 2012. Polyploidization of Glia in Neural Development Links Tissue Growth to Blood-Brain Barrier Integrity. *Genes Dev.* **26**: 31-36.
- von Hilchen C, Altenhein B. 2014. Tracing Cells Throughout Development: Insights into Single Glial Cell Differentiation. *Fly* **8**: 7-6.
- von Hilchen CM, Beckervordersandforth RM, Rickert C, Technau GM, Altenhein B. 2008. Identity, Origin, and Migration of Peripheral Glial Cells in the *Drosophila* Embryo. *Mech. Dev.* **125**: 337-352.

von Hilchen CM, Bustos AE, Giangrande A, Technau GM, Altenhein B. 2013. Predetermined Embryonic Glial Cells Form the Distinct Glial Sheaths of the *Drosophila* Peripheral Nervous System. *Development* **140**: 3657-3668.

Chapter Four:
Conclusions, Perspectives, and Future Directions

Collectively, we determined key differences in endocycling versus endomitotic subperineurial glia (SPG) as well as identified an additional polyploid glia cell type. We established that the Notch signaling pathway developmentally regulates endocycling and endomitotic SPG in the brain lobes, and the String Cdc25 phosphatase is required for endomitosis in the SPG. We also found that both SPG cell cycle variants are required for blood-brain barrier (BBB) function. These data on SPG cells suggest key differences in the properties and regulation of endocycling and endomitotic SPG. Our characterization of wrapping glia (WG) polyploidization and its link to proper axonal ensheathment adds to the repertoire of polyploid cell types. We also identified key differences in the contribution to overall ploidy as well as ensheathment differences among the three wrapping glia cells present in each nerve.

Differential properties of endocycling and endomitotic SPG

Our findings that both endocycling and endomitotic SPG are required for a functional BBB and that ploidy and nuclear number regulation is mediated by Notch signaling and cell cycle changes leaves us with a plethora of unanswered questions. Specifically, how are endomitotic SPG different from endocycling SPG? What advantages does endomitosis provide to SPG biology and function? Do multiple nuclei in endomitotic SPG spread throughout the cell to increase growth capacity? Do multiple nuclei allow for better gene product dispersion? How are the variant cell cycles actively regulated? And what signaling pathways are differentially activated or repressed in endocycling versus endomitotic SPG?

The finding that endomitotic SPG are required for a functional blood-brain barrier and are capable of reaching a higher ploidy and larger cell area than endocycling SPG was surprising. Given that SPG is one of two cell types in *Drosophila* to utilize endomitosis and the only *Drosophila* cell type that uses both variant cell cycles in the same tissue, it is critical to

understand what makes endomitotic SPG unique from their endocycling neighbors. One way to test whether endomitotic SPG have an increased growth capacity is to experimentally prevent nuclear dispersion and measure both cell size and ploidy compared to control endomitotic SPG. It may be possible to do this if cytoskeletal elements are required for active dispersal of the nuclei in endomitotic SPG. When nuclei are forced to clump in the middle of endomitotic SPG cells, if the consequence is that these cells are unable to reach the ploidy and cell area values of control endomitotic SPG, the relative location of the nuclei to the cell membrane may provide an advantage over a single large nucleus present in the middle of endocycling cells. Assessing the integrity of the BBB by dye injection assays in brains with clumped SPG nuclei would indicate whether nuclear dispersion is required to preserve the BBB.

One possible advantage of having multiple nuclei per cell is that the mRNA can be more dispersed throughout the cell cytoplasm. We could examine if there is a difference in mRNA distribution throughout endomitotic SPG by performing single molecule fluorescent *in situ* hybridization (FISH) in wild-type brains on mRNAs that are highly expressed in SPG, such as those encoding septate junction components, and compare the transcript distribution throughout the cell between endocycling and endomitotic SPG.

There are approximately 13 SPG per brain lobe, each of which is large and no more than 1 μm in thickness; thus manually isolating SPG cells is extremely difficult. Despite intensive efforts to isolate intact SPG cells, Unhavaithaya was only able to isolate SPG nuclei (Unhavaithaya personal communication). The transcriptome of SPG from wild-type third instar larvae has been profiled using the cell isolation-independent technique Targeted DNA Methyltransferase Identification (TaDa) (Jessica Von Stetina unpublished data). TaDa enables genome-wide cell-specific transcriptome profiling without cell isolation by the UAS/GAL4

system to temporally drive expression of Dam (control) or Dam-RNA Polymerase II in a cell-type of interest, in our case SPG using the *moody-GAL4* driver (Southall et al., 2013). We can use this established transcriptomic profiling technique to provide further insight into the developmental regulation of variant cell cycles. Specifically, the developmental regulation of the cell cycle is not entirely accounted for by CycB and Stg, as protein levels were equivalent by immunofluorescence in endocycling and endomitotic SPG. Because we determined that the transition from endocycling to endomitosis occurs by second larval instar, we could perform TaDa on first and second instar larvae and compare these transcriptomes. Differentially expressed transcripts between these two developmental stages could reflect differences in regulation of endocycling versus endomitotic SPG.

We were able to experimentally manipulate brain lobes to contain almost entirely endocycling or entirely endomitotic SPG cells by downregulating or overexpressing Stg in SPG cells, respectively. This provides us with an opportunity to profile expression differences in endocycling versus endomitotic SPG. Unfortunately, TaDa cannot be used to identify transcripts that are downregulated in response to RNAi knockdown, because the DNA methylation resulting from the binding of Dam-RNA Polymerase II is very stable, and once the genome is methylated, it takes many cell generations for the mark to be removed. Transcripts that are induced can be identified, but these will represent only a subset of the transcription changes that could account for the differences between the endocycle and endomitosis. In our system, *moody* is expressed in late embryogenesis, so the RNAi-induced changes in transcription likely will not have not taken effect before methylation occurs.

Rather than identifying transcriptomes, an alternative approach we could employ would be to infer which proteins are likely to be present in the SPG by measuring translated mRNAs by

Translating Ribosome Affinity Purification (TRAP)-RNAseq. This technique has been adapted for use with the UAS/GAL4 system (Thomas et al., 2012), and TRAP-RNAseq has been shown to successfully profile actively translated mRNAs in *Drosophila* astrocyte glia (Huang et al., 2015). In our system, we would use the SPG driver *moody-GAL4* to drive expression of the EGFP tagged L10a, a 60S ribosomal protein, under *UAS* control in wild-type brains, brains containing only endocycling SPG (*stg* RNAi) and brains containing only endomitotic SPG (*stg* OE). Because this strategy requires isolating mRNAs from the tagged ribosomes on polysomes, it may be difficult to recover sufficient amounts of material from the SPG cells to do the polysome gradients. If sufficient material can be recovered, then TRAP and RNAseq could make it possible to determine which mRNAs are undergoing translation in the two different SPG populations, suggesting differences in protein levels.

Identification of other polyploid central nervous system glial subtypes

To our knowledge, the only *Drosophila* glial cell types where DNA content has been analyzed are the SPG and WG. It would be informative to investigate whether other glial cell types of the CNS are polyploid. During our studies on the brain lobes, we noticed that the glia cells just below the SPG, the cortex glia, have large nuclei relative to neurons by DAPI fluorescence. A comprehensive study analyzing if cortex glia as well as other CNS glia are polyploid, by what mechanism they become polyploid, and the functional consequence of ploidy would be beneficial to the field. To answer these questions, the well-characterized drivers for each glial cell type can be used to drive expression of nuclear GFP to allow for identification of the glia nucleus, followed by ploidy quantification by DAPI fluorescence using diploid neurons for normalization. Demonstrating the incorporation of a nucleotide analog such as EdU in the

absence of mitosis or mitotic chromosome condensation (by staining with antibodies to phosphorylated Histone H3) would provide definitive evidence for polyploidization arising by the endocycle. Finally, downregulation of ploidy using RNAi against DNA replication components in glial subtypes that are polyploid would provide a means to evaluate the functional requirement for polyploidy.

Polyploidization in wrapping glia of the peripheral nervous system

We found that all WG are mononucleate and polyploid. Although WG clearly do not undergo nuclear division, it is possible they undergo other aspects of mitosis. It will be important to determine if WG nuclei become polyploid by endomitosis, as there are currently no *Drosophila* cell types that undergo endomitosis in the absence of nuclear division (Taniguchi, 2012; Unhavaithaya and Orr-Weaver, 2012). To test this, we could stain WG for phosphorylated Histone H3.

Further, we found that WG are polyploid throughout the PNS and that the overall WG ploidy increases with increasing nerve length. The numerous examples of ploidy scaling with cell size (Orr-Weaver, 2015) would suggest that WG ploidy also correlates with cell size. However, finding a correlation between total WG ploidy and nerve length does not tell us if a correlation exists between individual WG ploidy and cell size. We attempted to mark single WG cells by using a modified FRT system. Specifically, we crossed *nrv2-gal4(II); UAS-mCherry-nls(III)* to *UAS>CD2y+>CD8GFP/CyO Dfd::YFP (II); UAS-flp/TM6, Tb (III)*. Theoretically, we could identify wrapping glia by nuclear mCherry expression, recombinant WG by GFP expression, and non-recombinant WG by CD2 expression. The frequency of this

intrachromosomal recombination event was rare in WG, however, and we were not able to find single-labeled WG.

We identified key properties of the three WG, including differences in ploidy contribution and extent of axonal wrapping. A study asking if developmental control of polyploidization differs between the three WG and between nerves would be insightful. We could address this by looking to see if there is synchrony of when S versus G phase occur in each of the three WG as well as between the peripheral nerves. We could not visualize S phase in WG by EdU nucleotide incorporation, however. It is possible that we missed the developmental time window during which WG are actively replicating their DNA because we did not perform a detailed time course study. An alternative approach would be to stain with antibodies against dE2F1 or Cyclin E as markers of G1 and S phase and Cyclin B, a marker of G2 and M. In the endocycle Cyclin B protein will be absent, and levels of dE2F1 and Cyclin E proteins oscillate, decreasing in S phase and rising near the G to S transition (Zielke et al., 2011). Therefore, it may be possible to identify developmental time points with high versus low levels of dE2F1 and Cyclin E to monitor endocycle progression. Should antibody staining prove problematic, another method we can use to identify periods of DNA synthesis in WG is the Fly-FUCCI (fluorescent ubiquitination-based cell cycle indicator) system. This technique harnesses the activity of the two temporally regulated ubiquitin E3 ligases APC/C and CRL4^{Cdt2} (Zielke et al., 2014). A fragment of the CRL4^{Cdt2} that targets E2F1 fused to GFP is used as a marker for G2, M, and G1 phases, whereas a fragment of the APC/C target CycB fused to mRFP is used as a marker for G1, S, and G2 phases (Zielke et al., 2014). The E2F1 and CycB fragments only contain the functional degron domains so will be degraded depending on the cell cycle phase (Zielke et al., 2014). Thus, in WG, we would identify S phase by the presence of mRFP and absence of GFP.

Our studies of axonal wrapping in the distal nerve extension region (NER) and muscle field area (MFA) suggest that the extent of ensheathment may be dependent upon location of the nerve region. It will be enlightening to assess wrapping index by electron microscopy along the distal NER, in the segmental nerves and the intersegmental nerves and compare them to the wrapping index of the proximal NER from the Klambt lab (Matzat et al., 2015). Furthermore, our results showing defective ensheathment upon decreased WG ploidy lead us to question whether there is a functional requirement for proper axon wrapping. The current WG driver *nervana2 (nrv2)-GAL4* does not express GAL4 specifically in the WG of the PNS. *nrv2-GAL4* is also expressed in the cortex glia and SPG of the CNS. Therefore, we would not be able to determine whether defects we observe are due to reduction of WG ploidy versus reduction of cortex glia and/or SPG ploidy. Generation of a driver specific to WG in the PNS is crucial to discern the functional consequence of WG ploidy.

Finally, determining what signaling pathways are involved in WG polyploidization would be beneficial to both the cell cycle and glial fields. Given our findings on Notch's involvement in SPG polyploidization, Notch signaling may also be involved in WG polyploidization. As in the SPG, we could decrease Notch signaling and assess ploidy levels.

Growth coordination among the glial layers of the peripheral nerves

The proper development of the peripheral nerves requires growth coordination among the three glial layers and axons. It was previously determined that SPG are polyploid, but perineurial glia proliferate extensively during larval development (Unhavaithaya and Orr-Weaver, 2012; von Hilchen et al., 2013). Our finding that WG are polyploid completes the picture of how each of

the three types of peripheral nerve glia grow. Importantly, we can now probe any compensatory interactions that may exist between the three glial cell types.

Throughout larval development, direct contact between the SPG and axons decreases as WG extend their cell membranes around axons, but this direct contact is still present in late third instar larvae (Stork et al., 2008). This poses an important question: if WG ploidy is reduced, are the SPG able to compensate for the loss of wrapping glia ploidy and cell area? To address this question we can reduce WG ploidy by driving RNAi against one of the DNA replication machinery components we found to have decreased ploidy in the WG and marking SPG using the direct reporter we generated (See Appendix One). Because we know the longer nerves have significantly reduced ploidy when we drive RNAi against *dup* or *psfl*, we would calculate the ploidy of both WG and SPG in these nerves to see if SPG compensate for decreased WG ploidy. If the SPG are able to compensate, we would expect the ploidy and thus cell size of SPG cells to be larger than the SPG ploidy in control larvae. This would first require characterization of the four SPG cells in the longer peripheral nerves. Because WG function to ensheath axons, and we know decreased WG ploidy leads to decreased axonal wrapping, a requirement for compensation by the SPG would also require them to ensheath axons. Given that the SPG reporter is nuclear and GAL4 independent, the only way to assess this given our current tools is by electron microscopy.

Additionally, it would be productive to ask how the mitotic perineurial glial cells respond to ploidy deficiencies in either of the other two glial layers. Of particular interest would be to reduce SPG ploidy by driving RNAi against *dup* (Unhavaithaya and Orr-Weaver, 2012) and ask how perineurial glia respond. Studies from the Altenhein lab showed that in the nerve extension region of nerve A8/9, there are approximately 78 perineurial glia compared to the 10 perineurial

glia in nerve A2 (von Hilchen et al., 2013). Therefore, it is possible that in all the nerves the number of perineurial glia would increase dramatically upon reduction of SPG ploidy. If we find perineurial glia increase in cell number upon SPG ploidy reduction, it would be useful to assess the blood-nerve barrier, to which the SPG are the main contributor. This work would require a direct reporter for larval perineurial glia cells to positively mark them, however, one is not currently available.

Conclusion

As studies continue to reveal new cell types that are polyploid, it will be exciting to identify the advantage polyploidy provides as well as elucidate the developmental regulation of polyploidization in these cell types. The identification of two polyploid *Drosophila* glial cell types serves as a catalyst for the mammalian neurobiology field to systematically explore nervous system cell types for polyploidization.

ACKNOWLEDGEMENTS

We thank Christian Klämbt for providing us with the *Drosophila* stock *UAS>CD2y+>CD8GFP/CyO Dfd::YFP (II); UAS-flp/TM6, Tb (III)*.

REFERENCES

- Huang Y, Ng FS, Jackson FR. 2015. Comparison of larval and adult *Drosophila* astrocytes reveal stage-specific gene expression profiles. *G3 (Bethesda)* **5**: 551-558.
- Matzat T, Sieglitz F, Kottmeier R, Babatz F, Engelen D, Klämbt C. 2015. Axonal Wrapping in the *Drosophila* PNS Is Controlled by Glia-Derived Neuregulin Homolog Vein. *Development* **142**: 1336-1345.
- Orr-Weaver TL. 2015. When Bigger Is Better: The Role of Polyploidy in Organogenesis. *Trends Genet.* **31**: 307-315.

- Southall TD, Gold KS, Egger B, Davidson CM, Caygill EE, Marshall OJ, Brand AH. 2013. Cell-Type-Specific Profiling of Gene Expression and Chromatin Binding without Cell Isolation: Assaying RNA Pol II Occupancy in Neural Stem Cells. *Dev. Cell* **26**: 101-112.
- Stork T, Engelen D, Krudewig A, Silies M, Bainton RJ, Klambt C. 2008. Organization and Function of the Blood-Brain Barrier in *Drosophila*. *J. Neurosci.* **28**: 587-597.
- Taniguchi K, Kokuryo, A, Imano, T, Minami, R, Nakagoshi, H and Adachi-Yamada, T. 2012. Binucleation of *Drosophila* Adult Male Accessory Gland Cells Increases Plasticity of Organ Size for Effective Reproduction. *Biological Systems: Open Access* **1**: 1-5.
- Thomas A, Lee PJ, Dalton JE, Nomie KJ, Stoica L, Costa-Mattioli M, Chang P, Nuzhdin S, Arbeitman MN, Dierick HA. 2012. A versatile method for cell-specific profiling of translated mRNAs in *Drosophila*. *PLoS One* **7**: e40276.
- Unhavaithaya Y, Orr-Weaver TL. 2012. Polyploidization of Glia in Neural Development Links Tissue Growth to Blood-Brain Barrier Integrity. *Genes Dev.* **26**: 31-36.
- von Hilchen CM, Bustos AE, Giangrande A, Technau GM, Altenhein B. 2013. Predetermined Embryonic Glial Cells Form the Distinct Glial Sheaths of the *Drosophila* Peripheral Nervous System. *Development* **140**: 3657-3668.
- Zielke N, Kim KJ, Tran V, Shibutani ST, Bravo MJ, Nagarajan S, van Straaten M, Woods B, von Dassow G, Rottig C et al. 2011. Control of *Drosophila* Endocycles by E2F and CRL4(CDT2). *Nature* **480**: 123-127.
- Zielke N, Korzelius J, van Straaten M, Bender K, Schuhknecht GFP, Dutta D, Xiang J, Edgar BA. 2014. Fly-Fucci: A Versatile Tool for Studying Cell Proliferation in Complex Tissues. *Cell Reports* **7**: 588-598.

Appendix One:
Generation of a Direct Subperineurial Glia Reporter

Currently, the *Drosophila* community visualizes subperineurial glia (SPG) by using the GAL4 system. Specifically, we drive GFP expression under control of the upstream activating sequence (UAS) using the SPG driver *moody-GAL4* (Bainton et al., 2005; Schwabe et al., 2005). However, having to rely on the GAL4 system for positive labeling of the SPG prevents independent manipulation with a second GAL4 driver. For example, if we wanted to downregulate wrapping glia (WG) ploidy using RNAi driven under UAS control, the RNAi would also be driven in SPG cells.

We created a direct SPG reporter construct that is independent of the GAL4 system. We used the Gateway™ Cloning Kit (Invitrogen™) to generate a construct that expresses a nuclear localized mCherry reporter under the 2.4kb *moody* promoter region (the same region used in the *moody-GAL4* construct). The following two vectors were used: destination vector, pBPGUw plasmid #17575 from Addgene, and the donor vector, pENTR™/D-TOPO® containing the PCR-amplified 2.4kb fragment of the *moody* promoter. pQC NLS mCherry IX plasmid #37354 from Addgene was used as the source of the nuclear localized mCherry. Refer to Figure A1-1 for the final direct SPG reporter construct and sequence. To confirm the structure of this plasmid, we sequenced the entire plasmid using the primers in Table A1.

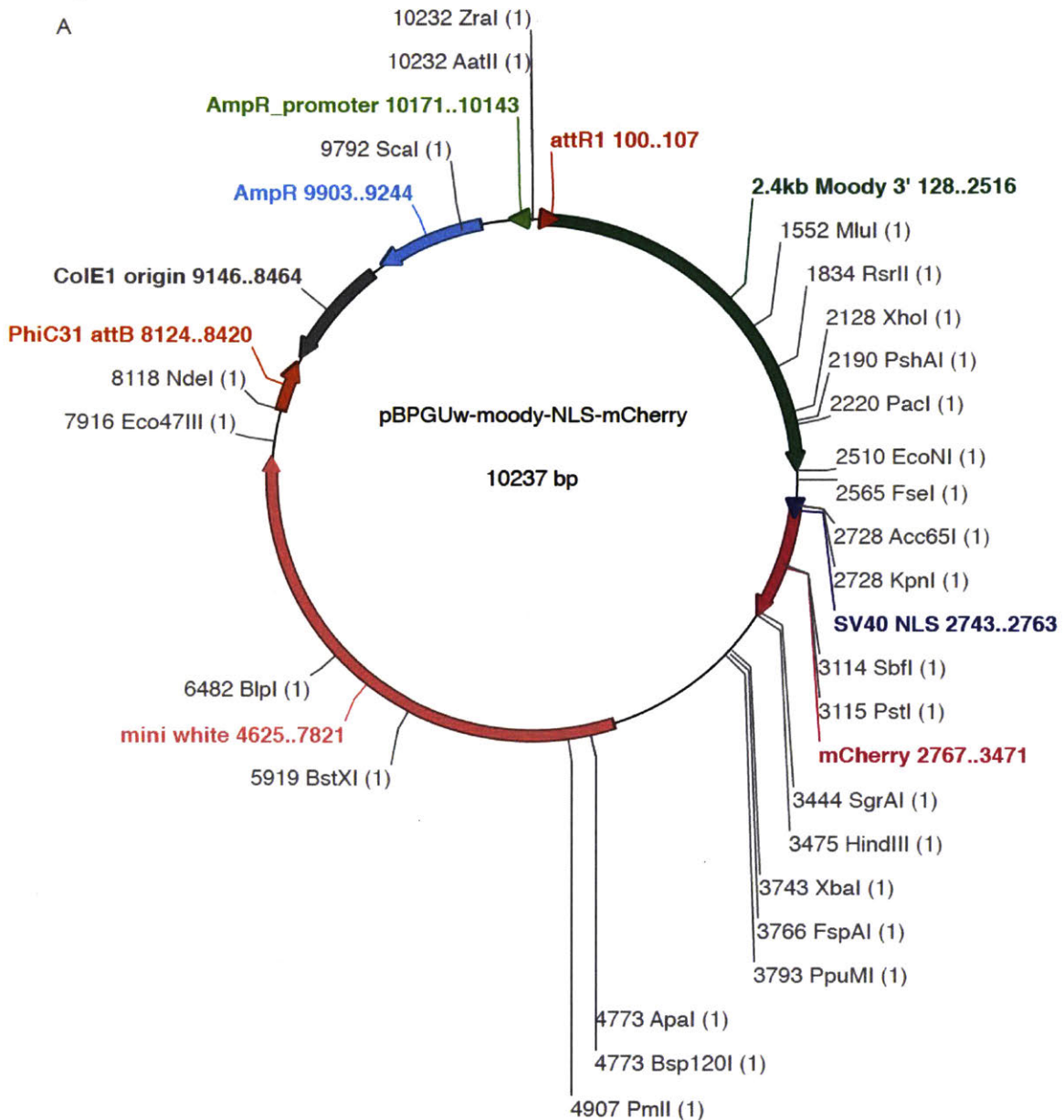
The complete SPG construct was sent to BestGene for injection into two injection stocks with ATT recipient sites on the X and third chromosomes: 9753(X) and 9750(III). BestGene generated four fly stocks with the direct *moody* construct on the X (#1-4) and five on the III (#5-9). Two stocks with the SPG reporter on the III, #6 and 8, were tested via immunofluorescence to confirm that it recapitulated the expression pattern of *moody-GAL4* (Figure A1-2). The inherent fluorescence was not bright enough for imaging so the RFP-Booster (Chromotek, rba594) that also binds to mCherry was used to enhance fluorescence intensity. In both stocks, the SPG

Figure A1-1. Plasmid map and sequence of the SPG reporter construct.

(A) The pBPGUw-moody-NLS-mCherry construct where the 2.4kb *moody* promoter region (dark green) drives expression of the SV40 nuclear localization sequence (NLS) and mCherry (pink). (B) Complete sequence of the SPG reporter construct.

Figure A1-1

A



B

```

TAAGAAACCATTATTATCATGACATTAACCTATAAAAATAGGCGTATCACGAGGCCCTT
TCGTCTTCAAGAATTCGTTTATCACAAGTTTGTACAAAAAAGCAGGCTCCGCGGCCGCC
CCTTACCCTACGTCTTCAGTTCGATATCTGCACCGAAAACATTTATTACCAGGTACAG
TTCCTAATGCGATATGTGCGGTAGCTCCAACCATCAGTTCCTTACCATGCGACAGACCGT
TTTTCCAGTGCAGCCATGTTGGATCGCCTCGATCGATGTCGAATGTCCAATTGTGTA
  
```


CATTAGAATGCAGACACATGAAGCCTTATCATTGCACATTTGCTTCAGTGGAGAGAGGA
AGCAGAAGCGGCGTATCTGCGATATGCATCTGATCGATCGGCAACCATTTAGCGGCCTCC
ACCCACACCCGCCCTCGGTTCGGTACCAGATGGCCGATGGCTGATCGCCGATCTCCGCCT
CTCTGTCTGTCCCTGTCTGTCTTCTGCGCTGTCTCCGGCCGGCGGGCGAGAGTGGGGAG
TGCGAGCGAGCAAGAGAGCAGAAGAGAGCGCCAAGTCGTGGGGGCAGTAACAGGGGGCGC
GCCAATGAGGGGAAACCTGACTAACATGGAGCGCAACTGACGTGCGTTCAGACGGAAT
ATCTAACGAACGGAGTATACCCTCCCTCAATCAGTTCCTACGCCACTGGCCGGCGGGCGG
AGAGTCATTTAGACACTAGTTGAGAGTGAGAGTAAAGAGTGAGAGGGGGCTGCCGATTG
TCAACTGGCAATATCGCGACTCGCTCTACGCTGCCCGCACTCGACGAACTGCACTCGATC
CGGCAGTTATAGACGATCCAATACGATCCGGCACGAGAACGCAGGCGCTACGCAATTTGT
CCGTTACATTTCAACCAGTACGGATAATAAACAACGAAAAGTAACTACGATTTTCAGTTCCG
ACTTGAGTGACATTCGATACGATACCGTTGAAGCAGTCGCGAGCGTGTGCCTATTTGTTA
GATATTTAATTCGACTGTTCCCTTTTTGTTTTTTGTGATTATGTCAAGTGCTGAGTTAGGGC
AACCTGTAACCTTTTTATTCTCTACCTGATCTCGCGATTCAAAGCATTAGTCATGAAAG
CTGGTGCGACTTTTGAATCACCGACAGCAGCAAGCAATAACAAAAACAAAAAGCAATGC
TCCAGTGGCGTCCCCAGAGCAACAATAAAAAACACAGCGATTTCATGAATAACCCAGCAA
ATGCCGAATGCCGTAACCTGTTTACATTTGCTAACAGCATTACTCACTCACTCTTTCACCT
CGCTCAACCTGAGCGAAAAAGAGGAAGTGGTGGAGTAAGAGTTGGAGAGGAGTGGAGTG
GAGATCGGAGTTGGAGAGAGTGGAGAGAGGAGCACGACAGGGGAGCAAAGAAGAGAAG
ATCGCAACCGCACTAGTTTCCATTACGTGAGCAGAAAGCAAATAAACAAGCGATTTTCCA
TTTTCCCATACCCAGTTCCCAAGTCCCGCCACTGTCCATCCTCTCCTCCTGACCACTGATA
ACGCGTCCGTCAGTGTGGTGCGGCACACGACTTAGAGGGAAGAGGAGAGGTTGAGGAGA
GTAGAGGAGACCTAGACACGGAGAAAGCAATCAGGCCAAGAGGAAGGAGAGAGCGAGAG
CGAGCCCAGCGATCGTTAGAATTAAGAAATCGCAGAGGATTACCAATAGCGAAACCA
AATTCAGCTAGGTAAGTGCTTTTTTGATAAGATAAGGAAATATTCTAAATTCGTATGTG
TATGTGTATGTGTAAGCGAGCCAGACACATTTGCGTATACGCCCCGTCCGACCGTGCTAAG
TGGCGGCCGTGACCTGGTTCGGGGTTAAGGGGAACGAGGGCAGCTGAGGGCCACAGAGGG
CAGAGCAGAGGCATATCAATGCATGTACACAGAAAACAAATGCGTTGCACAACGAATTC
GAAAACGTTTTAGGCATAGGCTAACGATTGCGTTAAAGATTCCCATACTTAATATAAGG
CCAAACCACACCTGACTGCGTTGCACAGAAATCGAAACAGCGACATTTCCGACCAGTGCA
GAGAATGTTACAAGAACATAACACTTGTCTCGATTAGCGGCCACTCGAGCGGGAACAGA
GAATTACCATCGCATCACATCACATCACGATTAGAGACGCCCCGAGACGACCGTCTCCG
CCAAACAGTCACTCAATTAATTAAGGTTGACGCTGATCTTTCACCCCCGAGTGGTGCAA
ACTGCTGAGGCAGTAGCCACCACTGAACTACTACCGCCGAGCAACTGAAACCGAAACAG
AGGCGATTGTGACCTCTTTAAATTAATTAATTTGACACTAATTTATCATAGTCCCGAGGA
AGCAGAAGGGGTGCCACGCCCCATGCCGGGTTACGGGCCTCGGACTCCGGCTGCCGGGCT
ACGGCTACGAGCGTTGCGTTCGGCGCGAAGTGCAGTCAGCGCCAGCGGTTTTTTATTTCTT
ACCAGAGCCTGAGCAAGGGTGGGCGCGCCGACCCAGCTTTCTTGTACAAAGTGGTGATAA
ACGGCCGGCCGAGCTCGCCCCGGGATCGAGCGCAGCGGTATAAAAGGGCGCGGGGTGGCT
GAGAGCATCAGTTGTGAATGAATGTTGAGCCGAGCAGACGTGCCGCTGCCTTCGTTAAT
ATCCTTTGAATAAGCCAACCTTTGAATCACAAGACGCATACCAAACGGTACCATGACTGCT
CCAAAGAAGAAGCGTAAGGTAATGGTGAAGCAAGGGCGAGGAGGATAACATGGCCATCAT
CAAGGAGTTCATGCGCTTCAAGGTGCACATGGAGGGCTCCGTGAACGGCCACGAGTTCGA
GATCGAGGGCGAGGGCGAGGGCCGCCCTACGAGGGCACCCAGACCCGAAGCTGAAGGT
GACCAAGGGTGGCCCCCTGCCCTTCGCCTGGGACATCCTGTCCCCTCAGTTCATGTACGGC
TCCAAGGCCTACGTGAAGCACCCCGCCGACATCCCCGACTACTTGAAGCTGTCTTCCCCG

AGGGCTTCAAGTGGGAGCGCGTGATGAACTTCGAGGACGGCGGCGTGGTGACCGTGACCC
AGGACTCCTCCCTGCAGGACGGCGAGTTCATCTACAAGGTGAAGCTGCGCGGCACCAACT
TCCCCTCCGACGGCCCCGTAATGCAGAAGAAGACCATGGGCTGGGAGGCCTCCTCCGAGC
GGATGTACCCCGAGGACGGCGCCCTGAAGGGCGAGATCAAGCAGAGGCTGAAGCTGAAG
GACGGCGGCCACTACGACGCTGAGGTCAAGACCACCTACAAGGCCAAGAAGCCCGTGCAG
CTGCCCGGCGCTACAACGTCAACATCAAGTTGGACATCACCTCCCACAACGAGGACTAC
ACCATCGTGGAACAGTACGAACGCGCCGAGGGCCGCACTCCACCGGCGGCATGGACGAG
CTGTACAAGTAAAAGCTTATCGATACCGTGCCTAAAGCCAAATAGAAAATTATTCAGT
TCCTGGCTTAAGTTTTTAAAAGTGATATTATTTATTTGGTTGTAACCAACCAAAGAAT
GTAAATAACTAATACATAATTATGTTAGTTTTAAGTTAGCAACAAATTGATTTTAGCTA
TATTAGCTACTTGGTTAATAAATAGAATATATTTATTTAAAGATAATTGCGTTTTTATT
GTCAGGGAGTGAGTTTGTCTAAAACTCGTTTAGATCCACTAGTCTAGAGCGGCCGCTG
GCCACGGGTGCGCATGATCGTGCTCCTGTGCTGAGGACCCGGCTAGGCTGGCGGGGTTG
CCTTACTGGTTAGCAGAATGAATCACCGATACGCGAGCGAACGTGAAGCGACTGCTGCTG
CAAAACGTCTGCGACCTGAGCAACAACATGAATGGTCTTCGGTTTCCGTGTTTCGTAAAG
TCTGGAACGCGGAAGTCAGCGCCCTGCACCATTATGTTCCGGAGGCGCGCCCTAGTTCC
AGTGAAATCCAAGCATTTCCTAAATTAATGTATTCTTATTATTATAGTTGTTATTTTT
GATATATATAAACAACACTATTATGCCACCATTTTTTTGAGATGCATCTACACAAGGA
ACAAACACTGGATGTCACCTTCAGTTCAAATTGTAACGCTAATCACTCCGAACAGGTCAC
AAAAAATTACCTTAAAAGTCATAATATTAATTAGAATAAATATAGCTGTGAGGGAAA
TATATACAAATATATTGGAGCAAATAAATTGTACATACAAATATTTATTACTAATTTCT
ATTGAGACGAAATGAACCACTCGGAACCATTTGAGCGAACCGAATCGCGCGGAACAAAC
GACAGTCGCTCCAAGGTGCTCGAACAAAAGGTGAATGTGTTGCGGAGAGCGGGTGGGAG
ACAGCGAAAGAGCAACTACGAAACGTGGTGTGGTGGAGGTGAATTATGAAGAGGGCGCG
CGATTTGAAAAGTATGTATATAAAAAATATATCCCGGTGTTTTATGTAGCGATAAACGA
GTTTTTGATGTAAGGTATGCAGGTGTGTAAGTCTTTTGGTTAGAAGACAAATCCAAGT
CTACTTGTGGGGATGTTCGAAGGGGAAATACTTGTATTCTATAGGTCATATCTTGTTTT
TATTGGCACAAATATAATTACATTAGCTTTTTGAGGGGGCAATAAACAGTAAACACGAT
GGTAATAATGGTAAAAAAAAAAAAACAAGCAGTTATTTCCGATATATGTCGGCTACTCCT
TGCGTCGGGCCCCGAAGTCTTAGAGCCAGATATGCGAGCACCCGGAAGCTCACGATGAGAA
TGGCCAGACCCACGTAGTCCAGCGGCAGATCGGCGGCGGAGAAGTTAAGCGTCTCCAGGA
TGACCTTGCCCGAACTGGGGCACGTGGTGTTCGACGATGTGCAGCTAATTTGCCCGGCT
CCACGTCCGCCCATTGGTTAATCAGCAGACCCCTCGTTGGCGTAACGGAACCATGAGAGGT
ACGACAACCATTGAGGTATACTGGCACCGAGCCCGAGTTCAAGAAGAAGCCGCCAAAGA
GCAGGAATGGTATGATAACCGGCGGACCCACAGACAGCGCCATCGAGGTCGAGGAGCTGG
CGCAGGATATTAGATATCCGAAGGACGTTGACACATTGGCCACCAGAGTGACCAGCGCCA
GGCAGTTGAAGAAGTGCAGCACTCCGGCCCGCAGTCCGATCATCGGATAGGCAATCGCCG
TGAAGACCAGTGGCACTGTGAGAAAAAGCGGCAATTCGGCAATCGTTTTGCCAGAAAG
TATGTGTCACAGCGATAAAGTCGACTTCGGGCCCTCCCTCATAAAAACTGGCAGCTCTGAG
GTGAACACCTAAATCGAATCGATTATTAGAAAGTTAGTAAATTATTGAAATGCAAATG
TATTCTAAACATGACTTACATTTATCGTGGCAAAGACGTTTTGAAAGGTCATGTTGGTC
AGGAAGAGGAAGATGGCTCCGTTGATATTCATCACACCCACTTGGCTGAGTTGTTGGCCC
AAAAAGATGAGGCCAATCAAGATGGCAACCATCTGCAAATTAATGTTACTCGCATCT
CATTAATATTCGCGAGTTAAATGAAATTTATTTATCTTCTGCAAAACTATAAACTATAC
ATCTCATTGAAAAAACTAAGAAGGGTGTGGAATCAGGCAATTCTATCTAAAATCTAGC
GAATTTGTTTCCAAGAATTGTAAGCGTTATATCATTTGTTTCCACTGGAACCACTCACCG

TTGTCTGAATAAGTCGCACTTTTACGAGGAGTGGTTCCTTGAGCACCGACAGCCAGGATC
GCCACAGGACCGCCCGAACTGCATGAACCAGGTGGCCTTGTAGGTGTACCCATTCTCCG
GCTGCTCCAGTGGCTTCTCCAGATTTTTGGTGGCCAACAACCTGCTCCATATCCCGGGCTA
CTTTGCTAATGGCAAATTTGTCGCATATCTTGGCGATCCGATCACGGGACTCGATCTCCC
GTCCGGGCACAACGGCCAACACCTGTACGTAAGTCCGCCGATTGTAGTTGGTAGGAC
ACTGGGCACCCACGCTGGATAGGAGTTGAGATGTTATGTAATACTAGATACCTTAATA
AACACATCGAACTCACTAGGAAAAGAAGTCGACGGCTTCGCTGGGAGTGCCCAAGAAAG
CTACCCTGCCCTCGGCCATCAGAAGGATCTTGTCAAAGAGCTCAAACAGCTCGGAAGACG
GCTGATGAATGGTCAGGATGACGGTCTTGCCTTCTGCGACAGCTTCTCAGCACCTGGA
CGACGCTGTGGGCGGTAAGGAGTCCAGTCCGGAGGTGGGCTCATCGCAGATCAGAAGCG
GCGGATCGTTAGAGCCTCGGAGGCGAATGCCAGACGCTTCCTTTCTCCGCCGGACAGAC
CTTTCACCTGCCGGGCACACCGATGATCGTGTGCTGACATTTGCTGAGCGAAAGCTCCT
GGATCACCTGATCCACGCGGGCCACTCGCTGCCGATAGGTCAGATGTGCTGGCATCCGCA
CCATGGCTTGAAAATCAGGTGTTCCCTGGCCGTTAGGGAGCCGATAAAGAGGTCATCCT
GCTGGACATAGGCGCACCTGGCCTGCATCTCCTTGGCGTCCACAGGTTGGCCATTGAGCA
GTCGCATCCCGGATGGCGATACTTGGATGCCCTGCCGGCATCGAAAGGCAAGGGCATTCA
GCAGGGTCGTCTTTCGGCACCGGAACTGCCCATCACGGCCAAAAGTTCGCCCGGATAGG
CCACGCCGAAACTGAGTTTCAAATTTGGTAATTTGGACCCTTTATTAAGATTTACACAGA
TCAGCCGACTGCGAATAGAACTCACCGTTCCTTGAGCAAATGTTTCCTGGGCGCCGGTAT
GTGTCGCTCGTTGCAGAATAGTCCGCGTGTCCGTTGACCAGCTGCCGCCATCCGGAGCC
CGGTGATTGACCGCCCCAAAGATGTCCATATTGTGCCAGGCATAGGTGAGGTTCTCGGC
TAGTTGGCCGCTCCCTGAACCGGAGTCTCCGGCGGACTGGGTGGCCGGAGCGTGCCGTA
GTTTTTGGCCTGCCCGAAGCCCTGGTTAATGCAGCTCTGCGAAGCCGCTCCGCTGTCACC
CTGCAATGATAGGGGATCTCAAATATCAACTACTAGCGTTATGCTCATCTAACCCCGAAC
AAAAAGTACCCCGAAGTATCCTACGAAGTAGGTTTATACTTTTATTTATTTTTTGTGCA
TCTAGGATCAGCTTAAAATATCTGGTTGTTATATTTTTTGTAAAAAAGAATATAGTCGA
AAATGAATGCCTTTAGATGTCTTGATCATGATATGATCTCAAAAATTTGCTTATATAGC
GAGAACAGCTACCAGAATAATCTGTTTCGTGTCACTATTTGTTTGTGCAATTGCGGTTTG
GGATTTTTTGTGGGTGCGAGTTCTCACGCCGATACAATTTGATGTTGCAATCGCAGTTCC
TATAGATCAAGTGAACCTAAGATGTATGCACATGTACTACTCACATTGTTTCCAGATGCTC
GGCAGATGGGTGTTTGTGCTGCCTCCGCGAATTAATAGCTCCTGATCCTCTTGGCCCATTGC
CGGGATTTTTTACACTTTCCCCTGCTTACCCACCCAAAACCAATCACCCCCAATCACTC
AAAAACAAACAAAATAAGAAGCGAGAGGAGTTTTTGGCACAGCACTTTGTGTTAATT
GATGGCGTAAACCGCTTGGAGCTTCGTACGAAACCGCTGACAAAATGCAACTGAAGGCG
GACATTGACGCTACGTAACGCTACAAACGGTGGCGAAAGAGATAGCGGACGCAGCGGCG
AAAGAGACGGCGATATTTCTGTGGACAGAGAAGGAGGCAAACAGCGCTGACTTTGAGTG
GAATGTCATTTTGTAGTGAGAGGTAATCGAAAGAACCTGGTACATCAAATACCCTTGAT
CGAAGTAAATTTAAAACCTGATCAGATAAGTTCAATGATATCCAGTGCAGTAAAAAAA
AAATGTTTTTTTTATCTACTTTCCGCAAAAATGGGTTTTTATTAACCTACATACTACTAG
GCGCGCCCATATGTTCCGGCTTGTGACATGCCCGCCGTGACCGTCGAGAACCCGCTGACG
CTGCCCGCGTATCCGCACCCGCCGACCCGTGCGACGTCCCGTGCTCACCGTGACCACCG
CGCCAGCGGTTTCGAGGGCGAGGGCTTCCCGGTGCGCCGCGGTTTCGCCGGGATCAACT
ACCGCCACCTCGACCCGTTTCATCATGATGGACCAGATGGGTGAGGTGGAGTACGCGCCCG
GGGAGCCCAAGGGCACGCCCTGGCACCCGCACCGCGGCTTCGAGACCGTGACCTACATCG
TCGACGGTAACATGTGAGCAAAGGCCAGCAAAGGCCAGGAACCGTAAAAAGGCCCGG
TTGCTGGCGTTTTTCCATAGGCTCCGCCCCCTGACGAGCATCACAAAATCGACGCTCA

AGTCAGAGGTGGCGAAACCCGACAGGACTATAAAGATACCAGGCGTTTCCCCCTGGAAGC
TCCCTCGTGCGCTCTCCTGTTCCGACCCTGCCGCTTACCGGATACCTGTCCGCTTTCTCC
CTTCGGGAAGCGTGGCGCTTTCTCATAGCTCACGCTGTAGGTATCTCAGTTCGGTGTAGG
TCGTTTCGCTCCAAGCTGGGCTGTGTGCACGAACCCCCGTTTCAGCCCAGCGCTGCGCCTT
ATCCGGTAACTATCGTCTTGAGTCCAACCCGGTAAGACACGACTTATCGCCACTGGCAGC
AGCCACTGGTAACAGGATTAGCAGAGCGAGGTATGTAGGCGGTGCTACAGAGTTCTTGA
AGTGGTGGCCTAACTACGGCTACACTAGAAGAACAGTATTTGGTATCTGCGCTCTGCTGA
AGCCAGTTACCTTCGGAAAAAGAGTTGGTAGCTCTTGATCCGGCAAACAAACCACCGCTG
GTAGCGGTGGTTTTTTTTGTTTGCAAGCAGCAGATTACGCGCAGAAAAAAGGATCTCAA
GAAGATCCTTTGATCTTTTTCTACGGGGTCTGACGCTCAGTGGAACGAAAACCTCACGTTAA
GGGATTTTGGTCATGAGATTATCAAAAAGGATCTTACCTAGATCCTTTTAAATTA
ATGAAGTTTTAAATCAATCTAAAGTATATATGAGTAAACTTGGTCTGACAGTTACCAAT
GCTTAATCAGTGAGGCACCTATCTCAGCGATCTGTCTATTTTCGTTTCATCCATAGTTGCCT
GACTCCCCGTCGTGTAGATAACTACGATACGGGAGGGCTTACCATCTGGCCCCAGTGCTG
CAATGATACCGCGAGACCCACGCTCACCGGCTCCAGATTTATCAGCAATAAACCAGCCAG
CCGGAAGGGCCGAGCGCAGAAGTGGTCTGCAACTTTATCCGCCTCCATCCAGTCTATTA
ATTGTTGCCGGGAAGCTAGAGTAAGTAGTTCGCCAGTTAATAGTTTTCGCAACGTTGTT
GCCATTGCTACAGGCATCGTGGTGTACGCTCGTTCGTTTGGTATGGCTTCATTCAGCTCC
GGTTCCCAACGATCAAGGCGAGTTACATGATCCCCATGTTGTGCAAAAAAGCGGTTAGC
TCCTTCGGTCCTCCGATCGTTGTCAGAAGTAAGTTGGCCGCAGTGTTATCACTCATGGTT
ATGGCAGCACTGCATAATTCTCTTACTGTCATGCCATCCGTAAGATGCTTTTTCTGTGACT
GGTGAGTACTCAACCAAGTCATTCTGAGAATAGTGTATGCGGCGACCGAGTTGCTCTTGC
CCGGCGTCAATACGGGATAATAACCGCGCCACATAGCAGAACTTTAAAAGTGCTCATCATT
GGAAAACGTTCTTCGGGGCGAAAACCTCTCAAGGATCTTACCGCTGTTGAGATCCAGTTCC
ATGTAACCCACTCGTGCACCCAACCTGATCTTCAGCATCTTTTACTTTACCAGCGTTTCT
GGGTGAGCAAAAACAGGAAGGCAAAATGCCGCAAAAAAGGGAATAAGGGCGACACGGAA
ATGTTGAATACTCATACTCTTCCTTTTTCAATATTATTGAAGCATTATCAGGGTTATTG
TCTCATGAGCGGATACATATTTGAATGTATTTAGAAAAATAAACAAATAGGGGTTCCGC
GCACATTTCCCCGAAAAGTGCCACCTGACGTC

Table A1-1

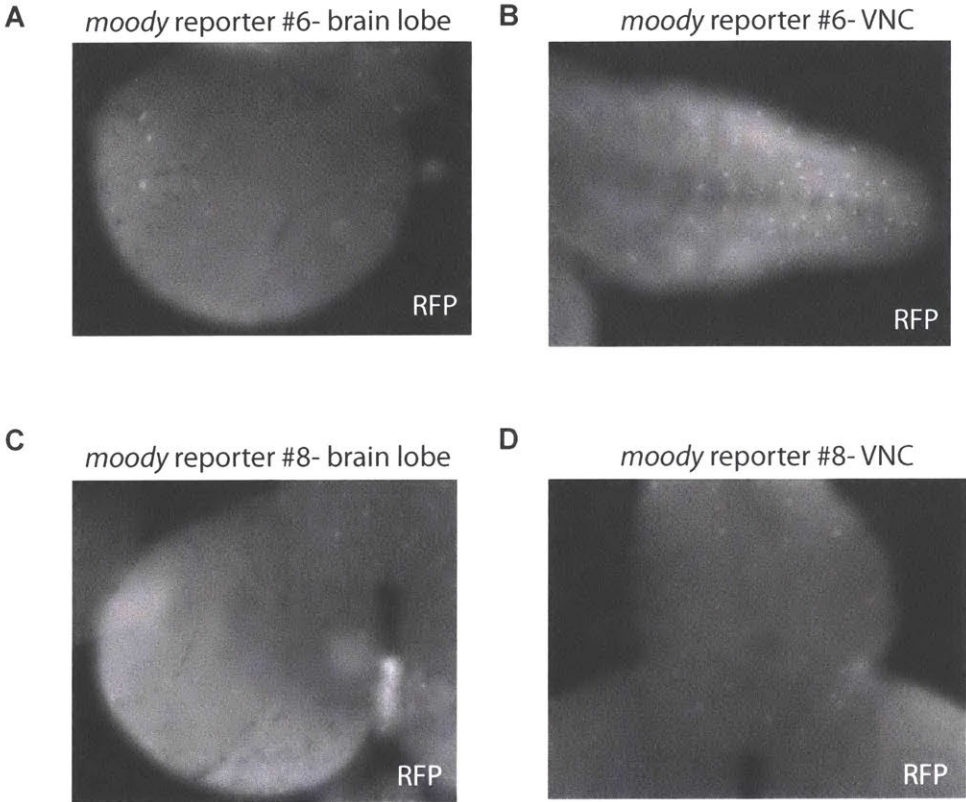
Forward/Reverse	Sequence 5' to 3'
Forward	CAGTTCTCACGCCGCAGAC
Forward	GCTCCCTGAACCGGAGTCCTC
Forward	GACAGCTTCTTCAGCACCTG
Forward	GGTCATGTTGGTCAGGAAGAG
Forward	GCAACTGAAGGCGGACATTG
Forward	CTGAAACCGAAACAGAGGCG
Forward	GGAGCGCGTGATGAACTTCG
Forward	CCTCACTGATTAAGCATTGG
Forward	GAATGAATGTTTCGAGCCGAG
Reverse	CGAAGTTCATCACGCGCTCC
Reverse	CAACGACAGGAGCACGATCATG
Reverse	CTCTTCCTGACCAACATGACC
Reverse	GATATCGAACTGAAGACGTAG
Reverse	CTTGTACAGCTCGTCCATGC

Primer sequences used to sequence the pBPGUw-moody-NLS-mCherry reporter construct.

Figure A1-2. Immunofluorescence of the direct moody reporter.

Two fly stocks containing the pBPGUw-moody-NLS-mCherry construct were dissected and stained with an RFP nanobody. (A-B) *moody* reporter construct #6 in the brain lobe (A) and ventral nerve cord (VNC) (B). (C-D) *moody* reporter construct #8 in the brain lobe (C) and VNC (D). Images were taken by Jessica Von Stetina.

Figure A1-2



reporter is more strongly expressed in the ventral nerve cord than in the brain lobe. It is unclear if all of the brain lobe SPG nuclei have signal from the SPG reporter. To test this, we could dissect brains expressing both the SPG direct reporter as well as *moody-GAL4*, *UAS-GFP-nls* and look for coexpression in every nucleus.

ACKNOWLEDGEMENTS

We thank Boryana Petrova for guidance in designing the construct and Helena Kashevsky for help with cloning and stock generation. Christian Klambt graciously shared us with the pENTR™/D-TOPO® vector with the PCR-amplified 2.4kb fragment of *moody*.

REFERENCES

- Bainton RJ, Tsai LT, Schwabe T, DeSalvo M, Gaul U, Heberlein U. 2005. *Moody* Encodes Two GPCRs That Regulate Cocaine Behaviors and Blood-Brain Barrier Permeability in *Drosophila*. *Cell* **123**: 145-156.
- Schwabe T, Bainton RJ, Fetter RD, Heberlein U, Gaul U. 2005. GPCR Signaling Is Required for Blood-Brain Barrier Formation in *Drosophila*. *Cell* **123**: 133-144.

Appendix Two:
Endomitosis in the Peripheral Nerve SPG

Our finding that ventral nerve cord (VNC) subperineurial glia (SPG) cells retain the capability of undergoing endomitosis upon Cyclin/CDK activation led us to examine if SPG in the peripheral nervous system (PNS) also retain endomitotic potential. The Altenhein lab has established that there are four SPG cells found in stereotypic locations in each peripheral nerve (von Hilchen et al., 2013). Therefore, we examined the peripheral nerves by immunofluorescence of GFP after overexpression of the mitosis-activating Cdc25 phosphatase String (Stg) under the SPG driver, *moody-GAL4* to determine if there were additional SPG nuclei present. We found that overexpression of *stg* does cause an increased number of SPG nuclei in a given nerve, suggesting SPG in the PNS become polyploid by endomitosis rather than endocycling upon *stg* overexpression (Figure A2-1A). We also found an increased number of SPG nuclei when we reduced levels of the Notch effector *Su(H)* by RNAi, suggesting SPG utilize endomitosis upon decreased Notch signaling (Figure A2-1B). In the future, staining for the mitotic marker phospho-Histone H3 should be used to confirm that the SPG become endomitotic under these conditions.

To determine whether the ability to retain mitotic potential is unique to SPG or if other polyploid glial cells have a similar capability, we overexpressed *stg* and reduced *Su(H)* using the wrapping glia (WG) driver *nervana2-GAL4*. When *Su(H)* RNAi is expressed in WG, a number of concentrated regions of GFP signal were apparent (Figure A2-1C). However, they did not have any detectable corresponding DAPI signal. These regions of concentrated GFP signal were very small, so it is possible that they are small nuclei with corresponding DAPI signals that are not above background staining intensity. When the *stg* gene was overexpressed, the WG were thin (Figure A2-1D). It is possible

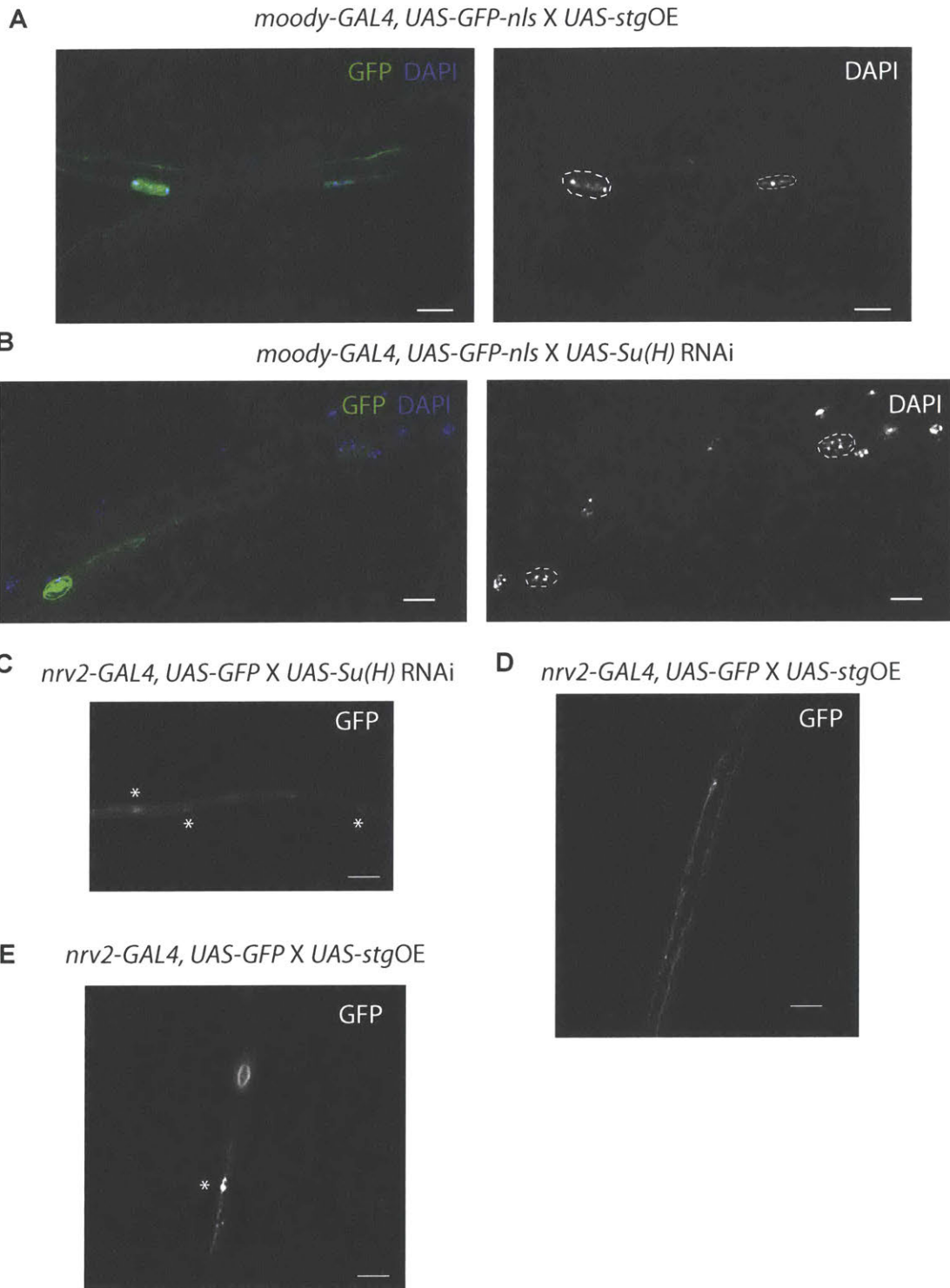
Figure A2-1. Perturbing the Notch signaling pathway or the Stg phosphatase leads to additional SPG nuclei in the PNS.

(A-B) Images of *moody-GAL4* driving expression of GFP^{nls} in the peripheral nerves when *stg* is overexpressed (A) or *Su(H)* is downregulated (B) in SPG. SPG nuclei are outlined.

(C-E) Images of *nervana2 (nrv2)-GAL4* driving expression of GFP in the peripheral nerves when *Su(H)* is downregulated (C) or *stg* is overexpressed (D,E) in WG. Asterisks mark concentrated regions of GFP signal that do not have corresponding DAPI signal.

Scale bars: 10 μ m.

Figure A2-1



that the membranes or ensheathment were affected. There also were regions of concentrated GFP signal lacking DAPI staining (Figure A2-1E). These WG experiments were performed using the filet preparation, a technique that keeps both the larval nervous system and muscle field intact. The DAPI signal from the muscle field increases the overall DAPI background signal, so repeating these experiments by dissecting the nervous system without the filet preparation would isolate only the nervous system, making it more feasible to score if altering Notch signaling or String phosphatase levels increases the number of WG nuclei.

REFERENCES

von Hilchen CM, Bustos AE, Giangrande A, Technau GM, Altenhein B. 2013. Predetermined Embryonic Glial Cells Form the Distinct Glial Sheaths of the *Drosophila* Peripheral Nervous System. *Development* **140**: 3657-3668.